Precambrian Research 292 (2017) 350–377

Contents lists available at ScienceDirect

Precambrian Research

journal homepage: www.elsevier.com/locate/precamres

Geochemistry and isotopic signatures of metavolcanic and metaplutonic rocks of the Faina and Serra de Santa Rita greenstone belts, Central Brazil: Evidences for a Mesoarchean intraoceanic arc

Caio César Aguiar Borges [a,*], Catarina Labouré Bemfica Toledo [a], Adalene Moreira Silva [a], Farid Chemale Junior [b], Hardy Jost [a], Cristiano de Carvalho Lana [c]

[a] Universidade de Brasília, Instituto de Geociências, 70910-900 Brasília, DF, Brazil
[b] Universidade do Vale do Rio dos Sinos, Departamento de Geologia, 93022-000 São Leopoldo, RS, Brazil
[c] Escola de Minas de Ouro Preto, Departamento de Geologia, 35400-000 Ouro Preto, MG, Brazil

ARTICLE INFO

Article history:
Received 23 May 2016
Revised 20 February 2017
Accepted 22 February 2017
Available online 24 February 2017

Keywords:
Tocantins Province
Archean-Paleoproterozoic Terrane of Goiás
Faina greenstone belt
Serra de Santa Rita greenstone belt
Nb-enriched basalts
Adakites

ABSTRACT

The Archean-Paleoproterozoic Terrane of Goiás, Central Brazil, is an allochthonous block within the Neoproterozoic Tocatins Province and consists of an association of Archean TTG complexes and gold-bearing Archean-Paleoproterozoic greenstone belts. The Faina and Serra Santa Rita greenstone belts, located in the southern portion of the terrane, are investigated using geochemistry and isotope geology to establish the time of magmatism and tectonic environment. Our data show that the ultramafic rocks have some chemical characteristics similar to modern boninites, whereas the amphibolites are subdivided into two groups: the type 1 basalts group are tholeiites with flat REE patterns and are similar to back-arc basin basalts; the type 2 basalts group have high Nb contents and are comparable to Nb-enriched basalts. Felsic to intermediate rocks present some of the main chemical diagnostic features of adakites, in which the metandesites and metatonalites are comparable to high-SiO_2 adakites, and the metadiorites, characterized by very high MgO, Cr and Ni contents, are comparable to low-SiO_2 adakites or high-Mg andesites. Metavolcanic and metaplutonic rocks show two main periods of magmatic crystallization ages with juvenile and slightly crustal contaminated rocks. The first occurred at 2.96–2.92 Ga with positive ε_{Nd} (t) values of +2.16 to +2.77, while the second formed at 2.8 Ga with slightly negative ε_{Nd} (t) value of −0.15. The volcanic and plutonic protoliths of the two greenstone belts were formed in an intraoceanic forearc-arc-back-arc system. The initial stage corresponds to ultramafic lava eruption in the forearc region of a proto-island arc, at 2.96 Ga. The evolution of the island arc and subduction progression led to oceanic slab-melting and generation of adakites. At 2.92 Ga, the adakitic melt was totally consumed by peridotite mantle and the subsequent melting of these hybridized mantle wedge generated high-Mg andesites that lodged in the crust as dioritic intrusions with high MgO, Cr and Ni contents. The late-stage corresponds to a continental arc formation at 2.8 Ga, marked by tonalitic magmatism and amalgamation with other island arcs and continental arcs of the TTG complexes of the Archean-Paleoproterozoic Terrane of Goiás.

1. Introduction

Archean greenstone belts are components of several cratons and present a wide variety of igneous and sedimentary rocks that carry the imprint of different tectonic environments, magmatic episodes and stages of metamorphism, deformation, metasomatism and mineralization (Anhaeusser, 2014; Pearce, 2014). The geochemical studies on metavolcanic rocks of greenstone belts have revealed two main types of associations: (1) a plume-related association composed of komatiites and tholeiitic basalts in oceanic and continental plateaus (*e.g.* Campbell et al., 1989; Herzberg, 1992; Xie et al., 1993; Arndt, 1994; Dostal and Mueller, 1997, 2004; Puchtel et al., 1998; Polat, 2009); and (2) a subduction-related association composed of calc-alkaline basalts, andesites, dacites and rhyolites, with minor occurrences of boninites, picrites, adakites, high-Mg andesites and Nb-enriched basalts. (*e.g.* Kerrich et al., 1998; Hollings and Kerrich, 2000; Wyman et al., 2000; Polat and Kerrich, 2004; Hollings, 2002; Percival et al., 2003; Polat and Hofmann, 2003; Shchinpasky

* Corresponding author.
E-mail address: caioaguiar0@gmail.com (C.C.A. Borges).

http://dx.doi.org/10.1016/j.precamres.2017.02.017
0301-9268/

et al., 2004; Polat and Kerrich, 2006; Ujike et al., 2007; Manikyamba et al., 2009; Khanna et al., 2015).

The Archean-Paleoproterozoic Terrane of Goiás, located in Central Brazil, is an allochthonous part of the Neoproterozoic Tocantins Province, a large Brasiliano/Pan-African orogen of the South American Platform formed during the Brasiliano orogeny. The terrane amalgamated to the province during the late stages of the orogeny and consists of an association of six Archean TTG complexes (tonalite-trondhjemite-granodiorite orthogneisses) and five Archean to Paleoproterozoic (Rhyacian) greenstone belts (Jost et al., 2013). The greenstone belts comprise lower units of metakomatiites overlain by metabasalts and upper units of metasedimentary rocks and host diverse types of gold deposits (Jost et al. 2014). The available data regarding the region are currently not sufficient for a detailed reconstruction of the magmatism and the different periods of crustal accretion, and to outline the tectonic environment in which the different units were formed.

The main purpose of this study is to provide an interpretation of the tectonic setting of the Faina and Serra de Santa Rita greenstone belts, located in the southern portion of the Archean-Paleoproterozoic Terrane of Goiás, based on new geochemical and isotopic data of metavolcanic and metaplutonic rocks. We suggest that these rocks constitute an association generated in subduction zone settings, which include adakite-like rocks, high-Mg andesites and Nb-enriched basalts occurrences. We intent to contribute to the different juvenile crustal accretion characterization, which preceded the formation of the Archean orogenic systems, and to comprehend the mechanism of crustal growth involved in the formation of the southern portion of the Archean-Paleoproterozoic Terrane of Goiás.

2. Geological setting

The Tocantins Province (Almeida et al., 1981) represents a large Brasiliano/Pan-African orogen of the South American Platform formed by the collision of the Amazonian, São Francisco-Congo and Paranapanema cratons (the latter is currently covered by Cenozoic rocks of the Paraná Basin) that led to the amalgamation of the supercontinent Western Gondwana in the Neoproterozoic. The province consists of three fold belts: the Paraguai Belt, on the southwestern portion, the Araguaia Belt, on the northern portion, and the Brasilia Belt, that borders the western edge of the São Francisco Craton (Pimentel et al., 2000).

The Brasilia Belt is divided into a NE-SW northern branch and a NW-SE southern branch. The separation of these two branches is established by the Pirineus Syntaxis that marks the change of the structural directions and configures the juxtaposing of the northern structures onto the southern counterparts by a large set of E-W shear sones (Araújo Filho, 2000). Both branches are divided into the External and Internal zones (Fig. 1). The External Zone includes thick sequences of low-grade metasedimentary rocks and their basements structured in fold-and-thrust belts verging towards the São Francisco Craton. The Internal Zone comprises: (1) the metamorphic core of the orogen, known as Anápolis-Itauçu Granulitic Complex (Piuzana et al., 2003) and Uruaçu Complex (DellaGiustina et al., 2009), distal metasedimentary rocks of the Araxá Group (Seer et al., 2001) and ophiolitic fragments (Strieder and Nilson, 1992); (2) the Goiás Massif, composed of allochthonous cratonic fragments that constitute the Archean-Paleoproterozoic Terrane of Goiás (Jost et al., 2013), a Paleoproterozoic metasedimentary cover and Meso- to Neoproterozoic mafic-ultramafic layered complexes associated with metavolcanosedimentary sequences (Ferreira Filho et al., 1992, 1994; Moraes et al., 2000); and (3) the Neoproterozoic Goiás Magmatic Arc, composed of metavolcanosedimentary sequences and orthogneisses disposed on a broad area of juvenile and continental crust generated during plate convergence between 990 and 630 Ma (Pimentel et al., 1991, 1997; Pimentel and Fuck, 1992; Pimentel et al., 2000, 2004; Junges et al., 2002, 2003; Laux et al., 2005) (Fig. 1).

2.1. The Archean-Paleoproterozoic Terrane of Goiás

The Archean-Paleoproterozoic Terrane of Goiás is located in the midwestern portion of the Brasilia Belt (Fig. 2A), Central Brazil, and is composed of an association of six Archean TTG complexes (orthogneisses) and five Archean to Paleoproterozoic greenstone belts (Fig. 2B). The cratonization of the Archean substrate occurred at around 2.7 Ga and the region was also subject to Paleoproterozoic magmatic activity related to crustal extension during the Siderian and closing of the orogen in the Rhyacian (Danni et al., 1986; Jost et al., 1992, 1993, 2010, 2014; Queiroz, 2000; Corrêa da Costa, 2003). The amalgamation of the Archean-Paleoproterozoic Terrane of Goiás to the Brasilia Belt during the Brasiliano orogeny in the Neoproterozoic resulted in broadly distributed granitic intrusions, partial anatexis of Archean orthogneisses and hydrothermal alteration (Fortes, 1996; Fortes et al., 2003; Pimentel et al., 2003; Jost et al., 2005, 2008, 2014; Tassinari et al., 2006; Queiroz et al., 2008; Rodrigues, 2011).

2.1.1. The TTG complexes

The TTG complexes comprise tonalitic to granodioritic and minor granitic orthogneisses that differ in the structural framework, lithology associations and magmatic crystallization ages. In the northern portion of the terrane, are located the Anta, Caiamar, Moquém and Hidrolina complexes, and in the southern portion, the Caiçara and Uvá complexes (Fig. 2B). Two stages of magmatism were recognized in the northern complexes. The first stage corresponds to juvenile poly-deformed tonalitic, granodioritic and granitic orthogneisses of the Hidrolina and Caiamar complexes and part of the Anta Complex, with U-Pb zircon crystallization ages between 2845 and 2785 Ma and initial $_{\varepsilon Nd}$ values of −1.0 to +2.41. Inherited zircon crystals of 3.3–3.15 Ga and Sm-Nd model age of 3.0 Ga indicate that these magmas were contaminated by older continental crust (Queiroz et al., 2008). The second stage, restricted to the Moquém Complex and part of the Anta Complex, corresponds to sheet-like granitic to granodioritic intrusions of crustal derivation with U-Pb zircon crystallization ages between 2792 and 2707 Ma and initial $_{\varepsilon Nd}$ value of −2.2 (Queiroz et al., 2008).

The Caiçara Complex, located in the southern portion of the terrane, is composed predominantly of tonalitic orthogneisses with U-Pb zircon crystallization age of 3.14 Ga and minimum Sm-Nd model age of 3.1 Ga (Beghelli Junior, 2012). The tonalitic orthogneisses are intruded by smaller granodiorites, granites and charnockites with U-Pb crystallization ages of 2.8 Ga and Sm-Nd model ages of 2.9 Ga (Beghelli Junior, 2012). The Uvá Complex is located in the southernmost portion of the terrane and consists of two groups of orthogneisses (Jost et al., 2005, 2013). The dominant group is the oldest and includes poly-deformed tonalitic to granodioritic orthogneisses and a diorite stock. The tonalitic orthogneisses present U-Pb zircon crystallization ages between 3040 and 2930 Ma (Jost et al., 2013) and the diorite stock presents U-Pb zircon crystallization age of 2934 ± 5 Ma (Pimentel et al., 2003). The second group corresponds to sheet-like tonalite and monzogranite intrusions with U-Pb zircon crystallization age of 2846 and 2764 Ma (Jost et al., 2005, 2013). Therefore, the Archean substrate of the region is polyphase and the TTG complexes of the southern portion of the Archean-Paleoproterozoic Terrane of Goiás are older than the northern counterparts.

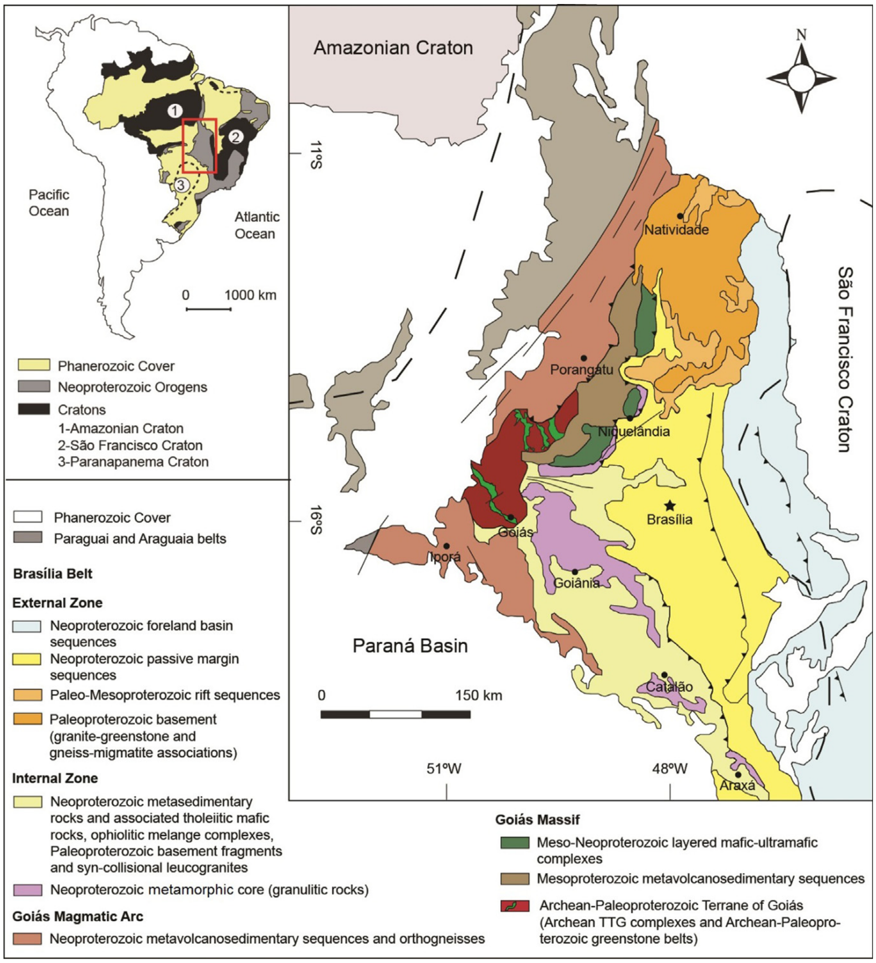

Fig. 1. Location of the Brasilia Belt and its main components. The Archean-Paleoproterozoic Terrane of Goiás is located in the midwestern portion of the belt (Modified after Pimentel et al., 2004).

2.1.2. The greenstone belts

The greenstone belts occur as five elongated and irregularly shaped sequences situated between the TTG complexes. It the northern portion, are located the Crixás, Guarinos and Pilar de Goiás greenstone belts, and in the southern portion, the Faina and Serra de Santa Rita greenstone belts (Fig. 2B). Their contacts with the adjacent TTG rocks are tectonic and marked by northwest-verging thrust faults (Jost et al., 2005, 2013). The stratigraphy of the greenstone belts comprises lower metavolcanic sequences of metakomatiites overlain by metabasalts and upper metasedimentary sequences. The rocks underwent a greenschist to amphibolite facies metamorphism and the stratigraphic reconstruction is complex due to the fragmentary state, polycyclic deformation, thinning, thickening and the rarity of marker horizons, which hinders the correlation through the structural and igneous discontinuities (Jost et al., 2014).

Primary volcanic features are locally preserved and include pillow lavas, spinifex and cumulate textures, polyhedral joints, flux breccia and vesicles (Danni et al., 1981, 1986; Teixeira, 1981; Teixeira et al., 1981; Kuyumjian and Teixeira, 1982; Profumo, 1993; Jost et al., 1995). Intercalation of banded iron formation, gondite and metachert occur in different proportions among the metavolcanic rocks. The crystallization ages of the volcanic protoliths of the five greenstone belts range from Archean to Paleoproterozoic. The metakomatiites of the Crixás greenstone belt presented Sm-Nd isochron age of 3.00 ± 0.07 Ga (Fortes et al., 2003). On the other hand, U-Pb zircon data for the Guarinos and Pilar de Goiás greenstone belts suggest that the metabasalts are from the Rhyacian, with ages at around 2.1 Ga (Jost et al., 2012, 2014). New LA-ICP-MS U-Pb zircon data for the Faina and Serra de Santa Rita greenstone belts are presented here and indicate a Mesoarchean age for their metavolcanic sequences (2.96 Ga).

The metasedimentary sequences of the five greenstone belts are markedly contrasting (Danni and Ribeiro, 1978; Jost and Oliveira, 1991; Resende and Jost, 1994, 1995a, 1995b; Jost et al., 1995, 2012; Resende et al., 1998). Several isotopic data have shown provenance of the clastic load from the Archean to the Paleoproterozoic (Rhyacian) (Resende et al., 1999; Fortes et al., 2003; Tassinari et al., 2006; Jost et al., 2008, 2012, 2014; Brant et al., 2015). Isotopic data of metadolomites of the northern greenstone belts and of the first sedimentary cycle of the southern greenstone belts revealed highly positive δ13C values, variable from +10 to +14‰ (Fortes, 1996; Resende et al., 1998; Jost et al., 2008; Santos et al., 2008). These values are comparable to the first δ13C positive anomaly in Earth's dolomites that is worldwide distributed between 2.2 and 2.06 Ga, known as Lomagundi-Jatuli positive δ13C excursion (Melezhik et al., 2007). These data suggest that the deposition of the dolomites of these greenstone belts occurred due to the Huronian glaciation (Snowball Earth) decay, between the end of the Siderian and the beginning of the Rhyacian (Jost et al., 2014). In the Faina greenstone belt, the δ13C values in metadolomites of the second sedimentary cycle fell between −0.66 and +0.66‰, suggesting that the deposition occurred at the end of the Lomagundi-Jatuli anomaly, but still during the Rhyacian, with

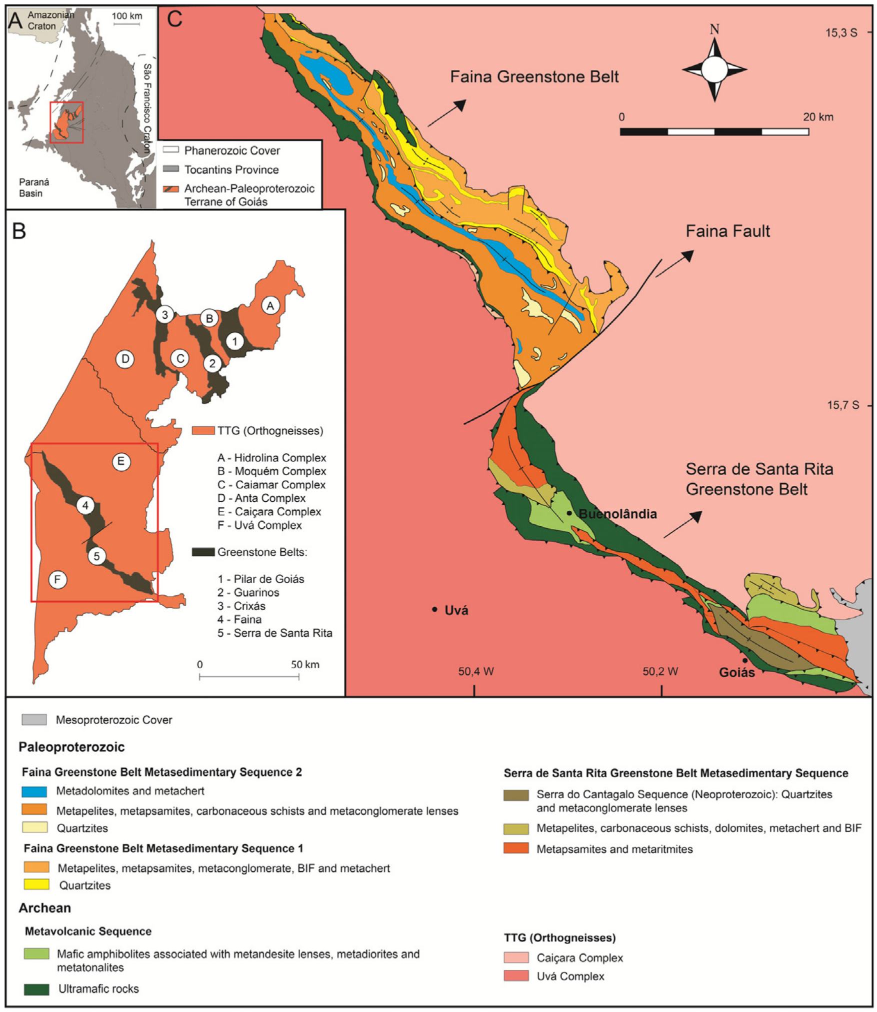

Fig. 2. The Archean-Paleoproterozoic Terrane of Goiás and the Faina and Serra de Santa Rita greenstone belts, located in the southern portion of the terrane. (A) Location of the Archean-Paleoproterozoic Terrane of Goiás in the Brasilia Belt. (B) Distribution of the TTG complexes and greenstone belts that constitute the Archean-Paleoproterozoic Terrane of Goiás; the Faina and Serra de Santa Rita greenstone belts are highlighted. (C) Geological map of the Faina and Serra de Santa Rita greenstone belts (Modified after Baêta Júnior et al., 2000 and Toledo et al., 2014).

likely extension into the early Orosirian (Resende et al., 1999; Jost et al., 2014).

In summary, the available isotopic data indicate that the metasedimentary rocks of the five greenstone belts of the Archean-Paleoproterozoic Terrane of Goiás and the metavolcanic rocks of the Guarinos and Pilar de Goiás greenstone belts have Paleoproterozoic (Rhyacian) ages, whereas the metavolcanic rocks of the Crixás, Faina and Serra de Santa Rita greenstone belts have Mesoarchean ages.

2.1.3. The Faina and Serra de Santa Rita greenstone belts

The Faina and Serra de Santa Rita greenstone belts, located in the southern portion of the Archean-Paleoproterozoic Terrane of Goiás, are disposed in a NW-SE synform and are separated by the Faina Fault (Fig. 2C). These greenstone belts are located between the Caiçara and Uvá complexes and their contacts are tectonic and marked by high-angle northeast-verging shear zones that completely obliterate their original architecture (Resende et al., 1998; Jost et al., 2005). Both greenstone belts comprise lower metavolcanic sequences unconformably overlain by metasedimentary rocks. The metavolcanic rocks predominate in the Serra de Santa Rita greenstone belt and in the northern portion of the Faina greenstone belt and are mainly ultramafic in composition (Fig. 2C). The mafic metavolcanic rocks correspond to amphibolites restricted to the Serra de Santa Rita greenstone belt and are associated with lenses of metandesites and metavolcanoclastic rocks. Dioritic to tonalitic poly-deformed intrusions also occur among these rocks. The metavolcanic sequences were affected by at least two greenschist to amphibolite facies metamorphic events. The overlying metasedimentary sequences record only the greenschist facies metamorphism. As described by Jost et al. (2005), the metavolcanic rocks, mostly ultramafics, of both *greenstone belts* extend towards south until the southern limit of the terrane as klippen that cover about 60% of the Uvá Complex orthogneisses.

The metasedimentary sequences of the Faina and Serra de Santa Rita greenstone belts differ from each other in several aspects and were probably developed under different conditions and sedimentary environments. Two metasedimentary sequences separated by a thrust fault occur in the Faina greenstone belt (metasedimentary sequences 1 and 2) (Fig. 2C). These two sequences represent two transgressive cycles of increasing depth (Resende et al., 1998). The base of both sequences is composed of metaconglomerates, followed by metarenites, thick packages of metapelites and metadolomites overlain by banded iron formation. The basal metaconglomerate of the first sedimentary cycle is in contact with the lower metavolcanic unit by an erosive unconformity and occurs as metadiamictite lenses with clasts of metabasalt, metakomatiite and milky quartz. This conglomerate protolith was fed with clasts from a mafic-ultramafic source area, possibly the underlying metavolcanic rocks (Resende et al., 1998). The basal metaconglomerate of the second cycle is associated with impure metarenites and metapelites. The nature of the clasts indicates that this conglomerate protolith was formed by the erosion of rocks from the first sedimentary cycle and cratonic source areas (Resende et al., 1998; Carvalho et al., 2013).

The sedimentation in the Serra de Santa Rita greenstone belt occurred in a deep marine environment progressing to a shallow water. The metasedimentary sequence is composed of lower carbonaceous schists overlain by metachert, banded iron formation and metadolomites. These rocks are overlain by metaturbidites that are interpreted as an "extravasation" of the second sedimentary cycle of the Faina greenstone belt through a continental break towards the deeper marine environment of the Serra de Santa Rita greenstone belt (Resende et al., 1998).

3. Sampling and analytical methods

3.1. Sampling

The studied samples were collected during two field seasons of geological mapping of the Faina greenstone belt and part of the Serra de Santa Rita greenstone belt on a 1:25,000 scale. The samples of ultramafic rocks were collected from outcrops along the Faina and Serra de Santa Rita greenstone belts. The samples of amphibolites, metandesites, metadiorites and metatonalites were collected from outcrops in specific areas of the Serra de Santa Rita greenstone belt. In addition to the rocks collected from outcrops, this study includes data of four metandesite samples from drilling cores located in the southern portion of the Serra de Santa Rita greenstone belt. The most representative and preserved samples were selected for petrographic, geochemical and isotopic studies. The coordinates of the samples are listed in Table 1.

3.2. Whole-rock geochemistry

The samples selected for whole rock geochemical analyses were pulverized and analyzed at the ALS Geochemistry Laboratory in Goiânia, Brazil, following standard laboratory procedures. Major elements were determined by X-ray Fluorescence (XRF) and are presented in weight oxides percentages. The rare earth elements (REE), high field strength elements (HFSE) and large ion lithophile elements (LILE) were determined by ICP-MS and the metals Ag, As, Cd, Co, Cu, Li, Mo, Ni, Pb, Sc, Tl and Zn were determined by ICP-AES. Major element analyses were recalculated to 100 wt.% anhydrous basis for inter-comparisons. Chondrite and primitive mantle compositions, used for normalizations, and the N-MORB composition are those of Sun and McDonough (1989). Europium (Eu/Eu*) and cerium (Ce/Ce*) anomalies were calculated with respect to the neighboring elements on chondrite-normalized REE diagrams, following method of Taylor and McLennan (1985). Mg-numbers (Mg#) were calculated as the molecular ratios of $Mg/(Mg + Fe^{2+}) \times 100$. Major and trace elements data are listed in Table 2.

3.3. U-Pb geochronology

The initial preparation of five selected samples for U-Pb zircon dating was conducted at the Geochronology Laboratory of the Universidade de Brasilia (UnB) by traditional methods of crushing, milling and sieving. The concentration of non-magnetic grains was conducted using a Frantz isodynamic magnetic separator. The individual zircon crystals were manually separated from the non-magnetic concentrate under a binocular microscope. All zircon grains were mounted in epoxy mounts and polished to expose the core. Images of zircon were obtained using optical, cathodolu-

Table 1
Coordinates of the studied samples of metavolcanic and metaplutonic rocks of the Faina and Serra de Santa Rita greenstone belts. Datum: WGS 84/UTM zone 22S.

Sample	Rock type	Location	E	N
TF14-0	Pillowed komatiite	Serra de Santa Rita GB	595604	8242442
TF14-I-003	Ultrumafic cumulate	Faina GB	550838	8301340
TF14-I-004A	Ultrumafic cumulate	Faina GB	550624	8301244
TF14-I-075B	Ultramafic schist	Faina GB	550113	8301266
TF14-I-098A	Ultramafic schist	Faina GB	543998	8304892
TF14-I-099	Chloritite	Faina GB	544033	8304924
TF14-II-125A	Ultramafic schist	Faina GB	574611	8255516
TF14-V-133	Ultramafic schist	Faina GB	563256	8287986
TF14-VII-012B	Chloritite	Faina GB	563806	8279585
TF14-XI-016	Chloritite	Serra de Santa Rita GB	568539	8260278
TF14-XII-079B	Mafic schist	Serra de Santa Rita GB	569280	8260068
TF14-XII-015A	Mylonitized diorite	Serra de Santa Rita GB	574116	8252818
TF14-XII-015B	Amphibolite (type 2 basalts)	Serra de Santa Rita GB	574116	8252818
TF14-XII-093	Ultramafic schist	Serra de Santa Rita GB	568419	8253089
TF14-XII-167	Ultramafic schist	Serra de Santa Rita GB	577167	8252313
TF14-XII-178	Amphibolite (type 2 basalts)	Serra de Santa Rita GB	574505	8252410
TF14-XII-183	Metatonalite	Serra de Santa Rita GB	572842	8253857
PFG-CA-004A	Metadiorite	Serra de Santa Rita GB	572842	8253857
PFG-CA-004B	Metadiorite	Serra de Santa Rita GB	573802	8252860
PFG-CA-004D	Metadiorite	Serra de Santa Rita GB	573802	8252860
PFG-CA-004E	Metadiorite	Serra de Santa Rita GB	573802	8252860
PFG-CA-004G	Metadiorite	Serra de Santa Rita GB	573802	8252860
PFG-CA-016A	Amphibolite (type 1 basalts)	Serra de Santa Rita GB	574121	8252906
PFG-CA-016B	Mylonitized diorite	Serra de Santa Rita GB	574121	8252906
PFG-CA-017A	Amphibolite (type 1 basalts)	Serra de Santa Rita GB	573838	8253571
PFG-CA-019A	Amphibolite (type 1 basalts)	Serra de Santa Rita GB	573757	8253538
PFG-CA-019B	Amphibolite (type 1 basalts)	Serra de Santa Rita GB	573757	8253538
PFG-CA-030	Metandesite	Serra de Santa Rita GB	596209	8240176
D22	Metandesite (Drill hole sample)	Serra de Santa Rita GB	596209	8240176
D23	Metandesite (Drill hole sample)	Serra de Santa Rita GB	596209	8240176
D24	Metandesite (Drill hole sample)	Serra de Santa Rita GB	596209	8240176
D26	Metandesite (Drill hole sample)	Serra de Santa Rita GB	596209	8240176

Table 2
Major element (wt.%) and trace-element (ppm) data for metavolcanic and metaplutonic rocks of the Faina and Serra de Santa Rita greenstone belts.

Samples	Ultramafic rocks							Chloritites	
	TF14-000	TF14-I-003	TF14-I-004A	TF14-I-075B	TF14-II-125A	TF14-V-133	TF14-XII-093	TF14-XII-167	TF14-VII-12B
SiO_2	51.5	45.5	45.1	46.9	46.7	54.9	48.7	31.2	32.3
TiO_2	0.2	0.3	0.4	0.2	0.2	0.1	0.6	1.4	1.2
Al_2O_3	2.9	5.8	4.4	5.7	6.8	6.2	7.7	22.9	21.7
Fe_2O_3	10.1	15.1	15.9	14.4	10.2	8.5	13.5	15.5	13.5
MnO	0.1	0.2	0.2	0.2	0.1	0.1	0.2	0.1	0.1
MgO	32.5	27.9	30.9	27.9	31.9	29.8	20.3	28.8	31.1
CaO	1.8	5.1	2.9	5.0	4.1	0.01	8.4	0.5	0.5
Na_2O	LDL	0.1	0.1	0.04	0.1	0.01	0.3	0.03	LDL
K_2O	LDL	0.02	0.01	0.01	0.01	0.04	0.04	LDL	LDL
P_2O_5	0.02	0.02	0.03	0.01	0.01	LDL	0.1	0.4	0.4
LOI	8.9	6.9	8.3	6.8	8.0	6.4	4.3	10.9	11.2
#Mg	86	79	79	79	86	87	75	79	82
Sc	13.4	24.0	21.7	25.3	20.0	18.9	28.0	19.3	11.0
V	62	124	116	105	89	85	141	213	174
Cr	2910	1680	1990	1700	2550	1320	2220	164	80
Co	127	113	121	113	82.0	91.0	93.0	76.0	51.0
Ni	2460	1105	1475	1275	1630	1590	905	352	110
Rb	0.2	0.3	0.2	0.1	0.6	1.7	2.4	0.3	0.4
Sr	9.1	4.4	2.9	3.4	19.3	2.2	28.5	32.3	13.0
Y	1.3	9.5	9.6	4.4	5.2	5.7	17.3	21.7	18.2
Zr	LDL	8.2	8.4	1.9	9.0	2.9	34.0	175	424
Hf	LDL	0.3	0.3	0.1	LDL	0.1	0.9	3.9	8.7
Nb	0.6	0.6	0.8	0.4	1.2	0.1	1.5	3.4	22.1
Cs	0.1	LDL	LDL	LDL	0.1	0.2	0.2	LDL	0.03
Ba	LDL	10.0	LDL	LDL	3.6	20.0	5.7	30.0	6.9
Ta	0.2	0.1	0.1	LDL	LDL	LDL	0.1	0.3	0.9
Samples	Ultramafic rocks							Chloritites	
	TF14-000	TF14-I-003	TF14-I-004A	TF14-I-075B	TF14-II-125A	TF14-V-133	TF14-XII-093	TF14-XII-167	TF14-VII-012B
Pb	1.4	0.5	LDL	0.5	LDL	5.1	LDL	1.1	LDL
Th	LDL	LDL	LDL	LDL	0.1	LDL	0.4	4.7	6.4
U	0.1	0.1	LDL	LDL	LDL	0.3	0.1	0.7	1.2
La	0.8	1.1	3.0	0.6	0.7	3.9	10.8	53.4	69.5
Ce	1.6	2.2	2.2	1.4	1.4	2.4	5.1	105	137
Pr	0.2	0.4	0.9	0.2	0.2	0.7	2.6	13.0	14.7
Nd	1.0	2.2	4.0	1.1	0.9	2.8	10.7	52.0	55.0
Sm	0.3	0.7	1.1	0.4	0.2	0.6	2.3	8.8	9.0
Eu	0.1	0.2	0.3	0.1	0.1	0.2	0.9	3.5	1.8
Gd	0.3	1.0	1.4	0.5	0.5	0.7	3.3	6.7	6.0
Tb	0.1	0.2	0.3	0.1	0.1	0.1	0.5	0.8	0.8
Dy	0.3	1.6	1.9	0.9	0.7	0.8	3.1	4.2	3.8
Ho	0.1	0.4	0.4	0.2	0.2	0.2	0.6	0.8	0.7
Er	0.2	1.1	1.0	0.6	0.6	0.5	1.7	1.9	1.9
Tm	0.02	0.2	0.2	0.1	0.1	0.1	0.2	0.3	0.3
Yb	0.2	1.1	1.0	0.7	0.6	0.4	1.4	1.6	1.8
Lu	0.03	0.2	0.2	0.1	0.1	0.1	0.2	0.2	0.3
La/Yb_{cn}	3.38	0.70	2.22	0.61	0.84	6.36	5.53	24.71	27.09
La/Sm_{cn}	1.91	1.01	1.76	1.05	1.88	4.27	3.02	3.91	4.97
Gd/Yb_{cn}	1.41	0.75	1.17	0.59	0.73	1.37	1.94	3.58	2.69
$(Eu/Eu)*$	0.55	0.86	0.80	0.84	0.94	0.93	0.96	1.40	0.73
$(Ce/Ce)*$	0.98	0.77	0.34	0.96	0.97	0.35	0.24	0.98	1.05
Nb/Th_{pm}	–	–	–	–	1.19	–	0.51	0.09	0.41
Ti/Sm_{pm}	1.58	0.78	0.61	0.99	1.18	0.45	0.49	0.28	0.24
Zr/Sm_{pm}	0.00	0.46	0.30	0.20	1.49	0.19	0.58	0.79	1.86
$\sum$REE	9	13	18	8	8	20	38	214	250
Samples	Chloritites	Amphibolites (Type 1 basalts)				Amphibolites (Type 2 basalts)			Metandesites
	TF14-XI-016	PFG-CA-017A	PFG-CA-019A	PFG-CA-019B	TF14-XI-079B	TF14-XII-178	TF14-XII-015B	PFG-CA-016A	PFG-CA-030
SiO_2	31.5	54.3	53.7	53.6	52.6	55.0	52.5	54.3	67.6
TiO_2	1.0	0.9	0.7	0.7	0.4	0.9	1.2	1.2	0.5
Al_2O_3	21.4	11.1	8.8	10.1	10.7	15.6	14.5	13.4	15.8
Fe_2O_3	17.1	11.7	11.2	11.8	11.6	8.9	9.2	11.3	5.1
MnO	0.2	0.2	0.2	0.2	0.2	0.1	0.2	0.2	0.04
MgO	28.4	8.8	12.2	11.4	15.1	9.0	6.9	7.2	2.7
CaO	0.2	9.5	11.2	11.0	7.6	5.9	13.5	9.7	2.7
Na_2O	LDL	3.5	1.8	1.8	2.2	4.5	2.5	2.6	4.0
K_2O	LDL	0.1	0.1	0.1	0.1	0.1	0.1	0.3	1.5
P_2O_5	0.2	0.1	0.1	0.1	0.02	0.3	0.2	0.2	0.2
LOI	10.8	1.0	1.6	1.7	3.1	2.8	1.3	1.7	3.8
#Mg	77	60	68	66	72	67	60	56	51
Sc	23.0	37.0	41.0	41.0	35.0	18.9	34.0	32.0	8.0
V	164	302	272	280	186	134	235	245	75

(continued on next page)

Table 2 (*continued*)

Samples	Chloritites	Amphibolites (Type 1 basalts)				Amphibolites (Type 2 basalts)			Metandesites
	TF14-XI-016	PFG-CA-017A	PFG-CA-019A	PFG-CA-019B	TF14-XI-079B	TF14-XII-178	TF14-XII-015B	PFG-CA-016A	PFG-CA-030
Cr	940	570	870	600	1280	430	350	340	110
Co	71.0	52.0	57.0	58.0	63.0	37.3	23.0	49.0	13.0
Ni	410	191	275	256	384	237	128	110	51
Rb	0.3	1.3	1.0	0.8	0.8	2.1	1.3	7.6	38.5
Sr	11.1	342	177	143	114.5	474	422	331	186
Y	12.0	17.7	14.1	14.6	10.4	16.7	28.4	25.8	14.9
Zr	163	47	36	38	20	106	97	90	170
Hf	3.6	2.5	2.7	2.6	1.3	1.1	1.1	0.3	4.5
Nb	8.8	2.1	1.5	1.4	0.8	12.2	5.3	8.6	7.0
Cs	0.02	0.03	0.02	0.01	0.04	0.1	0.1	0.3	0.3
Ba	8.8	19.0	13.9	20.2	29.5	43.3	18.9	51.3	168
Ta	0.4	0.2	0.2	0.2	LDL	0.5	0.3	0.4	0.5

Samples	Chloritites	Amphibolites (Type 1 basalts)				Amphibolites (Type 2 basalts)			Metandesites
	TF14-XI-016	PFG-CA-017A	PFG-CA-019A	PFG-CA-019B	TF14-XI-079B	TF14-XII-178	TF14-XII-015B	PFG-CA-016A	PFG-CA-030
Pb	LDL	3.0	LDL	6.0	LDL	LDL	LDL	2.0	8.0
Th	3.8	0.2	0.2	0.2	0.1	1.2	0.9	0.8	3.2
U	0.8	0.1	0.1	0.1	LDL	0.3	0.4	0.2	0.8
La	20.0	2.6	2.2	2.5	1.3	15.1	9.5	7.7	25.2
Ce	40.1	6.4	4.6	4.9	3.4	31.5	15.4	18.6	47.5
Pr	4.3	1.0	0.9	0.8	0.5	3.8	2.5	2.6	5.9
Nd	16.2	4.9	3.7	4.1	2.5	15.4	10.9	11.6	21.9
Sm	3.0	1.7	1.3	1.4	0.9	3.6	2.9	3.1	4.0
Eu	0.7	0.7	0.7	0.6	0.4	1.2	1.0	1.2	1.3
Gd	2.5	2.6	2.3	2.4	1.4	3.7	4.4	4.3	3.5
Tb	0.4	0.5	0.4	0.4	0.2	0.5	0.8	0.7	0.6
Dy	2.3	3.2	2.6	2.7	1.6	3.0	4.7	4.8	3.1
Ho	0.4	0.7	0.5	0.5	0.4	0.6	1.0	1.0	0.6
Er	1.3	2.0	1.6	1.4	1.2	1.5	3.1	2.9	1.4
Tm	0.2	0.3	0.2	0.2	0.2	0.3	0.5	0.4	0.2
Yb	1.3	1.6	1.4	1.2	1.2	1.6	2.7	2.7	1.2
Lu	0.2	0.3	0.2	0.2	0.2	0.3	0.5	0.4	0.2
La/Yb_{cn}	11.12	1.17	1.14	1.53	0.79	6.90	2.51	2.04	14.58
La/Sm_{cn}	4.28	1.01	1.09	1.14	0.94	2.73	2.11	1.62	4.12
Gd/Yb_{cn}	1.60	1.35	1.37	1.67	1.00	1.95	1.34	1.31	2.34
$(Eu/Eu)*$	0.72	1.04	1.24	0.92	0.98	1.04	0.89	1.04	1.07
$(Ce/Ce)*$	1.06	0.99	0.82	0.84	1.01	1.03	0.78	1.02	0.96
Nb/Th_{pm}	0.28	1.04	0.99	0.88	0.95	1.17	0.68	1.27	0.26
Ti/Sm_{pm}	0.61	1.06	1.12	1.04	0.94	0.49	0.84	0.79	0.27
Zr/Sm_{pm}	2.14	1.12	1.10	1.06	0.89	1.18	1.33	1.16	1.71
$\sum$REE	84	27	22	23	15	73	52	55	104

Samples	Metandesites				Metadiorites				
	D22	D23	D24	D26	PFG-CA-004A	PFG-CA-004B	PFG-CA-004D	PFG-CA-004E	PFG-CA-004G
SiO_2	63.2	57.5	61.3	56.0	58.2	55.6	56.2	54.4	55.4
TiO_2	0.7	0.8	0.7	1.1	0.6	1.2	0.3	0.6	1.1
Al_2O_3	15.9	16.2	16.7	20.5	15.1	13.1	14.5	12.6	14.6
Fe_2O_3	5.3	7.3	6.3	7.7	7.6	8.0	9.8	9.4	7.1
MnO	0.1	0.1	0.1	0.1	0.1	0.1	0.2	0.2	0.1
MgO	4.2	5.8	4.9	4.6	8.8	11.9	11.2	12.5	9.9
CaO	5.6	6.4	5.8	5.6	5.3	6.3	4.7	6.2	5.5
Na_2O	5.0	5.2	5.1	6.0	5.1	4.3	4.1	3.6	5.3
K_2O	0.3	0.3	0.3	0.1	0.1	0.1	0.1	0.1	0.2
P_2O_5	0.2	0.2	0.2	0.2	0.2	0.5	0.1	0.3	0.6
LOI	2.4	2.5	2.1	2.8	2.4	2.6	3.1	2.9	2.4
#Mg	61	61	61	54	70	75	69	72	74
Sc	–	–	–	–	16.0	21.0	13.0	14.0	21.0
V	104	140	119	167	97	134	80	99	145
Cr	180	230	240	60	440	910	780	840	710
Co	21.4	30.1	22.9	23.4	37.0	43.0	44.0	45.0	40.0
Ni	99	128	110	78	231	247	347	473	200
Rb	8.2	7.7	6.8	1.6	1.7	3.9	1.6	2.0	4.0
Sr	584	606	616	494	485	309	264	200	481
Y	14.3	14.7	14.1	27.4	12.4	17.0	8.4	11.4	16.8
Zr	164	126	114	171	82	136	54	153	252
Hf	4.3	3.5	2.9	4.5	2.2	3.5	1.4	3.5	5.2
Nb	7.9	5.5	5.5	7.2	4.9	10.3	2.6	4.7	11.0
Cs	0.1	0.2	0.1	0.03	0.1	0.2	0.03	0.1	0.2
Ba	97.9	43.5	88.3	15.4	53.7	38.3	17.6	30.7	59.5
Ta	0.4	0.3	0.4	0.5	0.3	0.6	0.2	0.3	0.6

Table 2 (*continued*)

Samples	Metandesites				Metadiorites				
	D22	D23	D24	D26	PFG-CA-004A	PFG-CA-004B	PFG-CA-004D	PFG-CA-004E	PFG-CA-004G
Pb	8.0	10.0	10.0	7.0	LDL	3.0	LDL	LDL	LDL
Th	3.6	2.3	2.4	2.4	1.5	1.8	0.4	0.9	1.7
U	0.7	0.6	0.6	0.7	0.5	0.5	0.1	0.3	0.6
La	22.4	15.7	17.3	16.5	14.8	29.4	10.8	17.9	31.4
Ce	46.8	33.3	35.5	37.8	30.5	66.7	22.5	38.0	67.2
Pr	5.1	3.8	4.0	4.3	3.8	8.6	2.8	4.9	8.4
Nd	19.1	16.3	15.9	18.2	13.6	34.3	11.4	19.3	33.2
Sm	3.8	3.5	3.3	4.2	2.9	6.5	2.2	3.3	6.3
Eu	1.3	1.3	1.1	1.5	1.0	1.9	1.0	1.1	2.0
Gd	3.5	3.4	3.7	5.1	2.7	5.5	2.2	3.1	5.4
Tb	0.4	0.5	0.4	0.8	0.4	0.7	0.3	0.4	0.7
Dy	2.6	2.9	2.5	4.9	2.3	3.7	1.7	2.3	3.7
Ho	0.5	0.5	0.6	0.9	0.4	0.6	0.3	0.4	0.7
Er	1.3	1.3	1.5	2.3	1.3	1.7	0.9	1.1	1.6
Tm	0.2	0.2	0.2	0.4	0.2	0.2	0.1	0.2	0.2
Yb	1.5	1.6	1.4	2.5	1.3	1.2	0.7	1.0	1.2
Lu	0.2	0.2	0.2	0.3	0.2	0.2	0.1	0.2	0.2
La/Yb_{cn}	10.43	7.08	9.06	4.70	8.49	18.34	11.07	12.84	18.61
La/Sm_{cn}	3.79	2.87	3.34	2.55	3.34	2.93	3.24	3.47	3.24
Gd/Yb_{cn}	1.86	1.75	2.24	1.66	1.81	3.93	2.58	2.59	3.69
$(Eu/Eu)*$	1.09	1.12	0.96	1.02	1.07	0.98	1.37	1.05	1.05
$(Ce/Ce)*$	1.08	1.06	1.05	1.11	1.00	1.03	1.00	0.99	1.01
Nb/Th_{pm}	0.26	0.28	0.28	0.35	0.39	0.67	0.84	0.63	0.77
Ti/Sm_{pm}	0.36	0.45	0.41	0.53	0.41	0.35	0.24	0.38	0.35
Zr/Sm_{pm}	1.70	1.42	1.35	1.62	1.14	0.83	1.00	1.82	1.60
$\sum REE$	96	75	79	86	69	144	58	87	144

Samples	Metadiorites		Metatonalite
	TF14-XII-015A	PFG-CA-016B	TF14-XII-183
SiO_2	56.7	54.8	66.0
TiO_2	0.4	0.8	0.7
Al_2O_3	12.6	12.7	15.0
Fe_2O_3	6.8	8.8	4.8
MnO	0.1	0.2	0.1
MgO	14.6	12.5	1.7
CaO	5.7	7.4	7.3
Na_2O	1.2	3.2	4.9
K_2O	1.4	0.5	0.1
P_2O_5	0.1	0.3	0.1
LOI	3.9	2.5	0.6
#Mg	81	74	42
Sc	18.0	13.0	12.2
V	111	99	96
Cr	1060	1000	330
Co	43.0	48.0	16.4
Ni	456	378	120
Rb	30.6	14.6	1.0
Sr	44.1	167.0	925.0
Y	9.7	13.5	8.1
Zr	67	140	145
Hf	1.5	3.6	3.3
Nb	2.6	12.8	5.0
Cs	0.4	0.4	0.1
Ba	618	230	16.2
Ta	LDL	0.8	0.3
Pb	LDL	LDL	LDL
Th	1.4	2.6	1.7
U	0.5	0.6	0.6
La	11.9	26.2	13.5
Ce	17.5	53.7	27.6
Pr	2.5	6.2	3.2
Nd	9.1	23.1	13.7
Sm	1.9	4.1	3.0
Eu	0.5	1.2	1.1
Gd	1.8	3.5	2.1
Tb	0.3	0.5	0.3
Dy	1.8	2.7	1.5
Ho	0.3	0.5	0.3
Er	1.1	1.3	1.0
Tm	0.1	0.2	0.1
Yb	0.9	1.1	0.8
Lu	0.1	0.2	0.1
La/Yb_{cn}	9.93	16.78	12.58

(*continued on next page*)

Table 2 (*continued*)

Samples	Metadiorites		Metatonalite
	TF14-XII-015A	PFG-CA-016B	TF14-XII-183
La/Sm_{cn}	4.13	4.18	2.91
Gd/Yb_{cn}	1.75	2.56	2.22
$(Eu/Eu)^*$	0.81	0.98	1.30
$(Ce/Ce)^*$	0.79	1.03	1.02
Nb/Th_{pm}	0.22	0.59	0.34
Ti/Sm_{pm}	0.43	0.39	0.45
Zr/Sm_{pm}	1.43	1.37	1.92
∑REE	49	113	67

minescence and back-scatter electron microscopes. The zircon crystals were dated by the LA-MC-ICP-MS method at the Geochronology Laboratory of the Universidade de Brasilia (UnB) and with the LA-SF-ICP-MS method at the Geochronology Laboratory of the Universidade Federal de Ouro Preto (UFOP). Sample TF14-XI-016 (chloritite) was dated using a laser ablation system (New Wave UP213) coupled to a MC-ICP-MS (Neptune) at the UnB. Isotope data were acquired using static mode with spot size of 30 μm. Samples TF14-I-099 (chloritite), TF14-XII-178 (amphibolite), PFG-CA-04A (metadiorite) and TF14-XI-183 (metatonalite) were dated by the SF-LA-ICP-MS method using a Thermo-Finnigan Element 2 sector field ICP-MS coupled to a CETAC213 ultraviolet laser system at the UFOP. Laser spot size of 20 μm was used and data were acquired in peak jumping mode during 20 s background measurement followed by 20 s sample ablation.

For both laboratories, raw data were corrected for background signal, and laser-induced elemental fractional and instrumental mass discrimination were corrected by the reference zircon (GJ-1) (Jackson et al., 2004). The common Pb correction was based on the Pb composition model (Stacey and Kramers 1975). To evaluate the accuracy and precision of the laser-ablation results, 91500 zircon (1065.4 ± 0.6 Ma; Wiedenbeck et al. 1995) was analyzed at the UnB laboratory, while at the UFOP laboratory, the Plešovice zircon (337 ± 1 Ma; Sláma et al. 2008), M127 zircon (524.35 ± 0.92 Ma; Klötzli et al. 2009) and 91500 zircon were analyzed. The external error is calculated after propagation error of the GJ-1 mean and the individual zircon sample (or spot). Bühn et al. (2009) and Santos (2015) described the detailed analytical methods and data treatment. The age calculation was carried out using Isoplot-Ex (Ludwig, 2003). The LA-MC-ICP-MS and LA-SF-ICP-MS U-Pb isotopic analytical data are listed in Tables 3.1–3.5.

3.4. Sm-Nd isotopes

The five selected samples for whole-rock Sm-Nd isotopic analyses were pulverized using an agate mill and analyzed at the Geochronology Laboratory of the Universidade de Brasilia (UnB). Whole-rock powders (~100 mg of sample powder) were spiked with a combined ^{150}Nd-^{149}Sm tracer and dissolved using a solution of 5:1 HF-HNO_3 in Savillex® tvials on a hot plate. After cooling and evaporation of the HF-HNO_3 solution, samples were re-dissolved in the Savillex® vials with 7 ml of 6 N HCl, evaporated, and then taken up in 3 ml of 2.5 N HCl. The chemical extraction of Sm and Nd follows the conventional chromatographic procedure described by Gioia and Pimentel (2000). Each sample was dried out to a solid and then loaded with 0.25 N H_3PO_4 on appropriated filament (Ta for Sm and Re for Nd). All samples were analyzed using a Thermo Scientific TRITON™ Plus Thermal Ionization Mass Spectrometer (TIMS) operating in the static multi-collector mode at the UnB. 100–120 ratios were collected with a 0.5 to 1-V ^{144}Nd beam. Nd ratios were normalized to $^{146}Nd/^{144}Nd = 0.7219$. All analyses were adjusted for variations in instrumental bias due to periodic adjustment of collector positions as monitored by measurements of our internal standards. Repeated measurements on the USGS BHVO-1 standard gave $^{143}Nd/^{144}Nd = 0.512996 \pm 0.000006$ (2SD; n = 7) during the course of this study. Average blank values were <100 pg for Sr and Sm, and <500 pg for Nd. Correction for blank was insignificant for Nd isotopic compositions and generally insignificant for Sm/Nd ratios. Sm-Nd isotopic data are listed in Table 4.

4. Field aspects and petrography

4.1. Ultramafic rocks and chloritites

The metavolcanic rocks of ultramafic composition are the most abundant in the Faina and Serra de Santa Rita greenstone belts. These rocks are predominantly ultramafic schists and fine- to medium-grained massive rocks. Primary igneous features are locally preserved and comprise pillow lavas and cumulate-textured zones. The pillow lavas occur in massive fine-grained rocks in the southern portion of the Serra de Santa Rita greenstone belt and attest the subaqueous volcanic character of these ultramafic rocks (Fig. 3A). The ultramafic schists are composed of variable quantities of chlorite, talc and tremolite, which mark the tectonic foliation of these rocks. Magnetite, chromite and apatite occur as accessory minerals. Syn- to post-tectonic euhedral tremolite porphyroblasts and post-tectonic magnetite porphyroblasts are common (Fig. 4A).

The rocks with preserved cumulate textures are massive and characterized by pseudomorphs of cumulus olivine totally replaced by serpentine. The olivine pseudomorphs are encompassed by tremolite, Mg-hornblende and talc that substituted the original igneous intercumulus minerals, characterizing mesocumulate and orthocumulate reliquiar textures (Fig. 4B). Similar cumulate textures are recognized at the base of thick komatiite lava flows of several worldwide greenstone belts (Arndt et al., 2008). However, the texture variations observed in the classical layered komatiite flow occurrences, such as spinifex-textured horizons, were not recognized in ultramafic rocks of the Faina and Serra de Santa Rita greenstone belts.

Some centimeter- to meter-thick irregular chloritite layers are interleaved with ultramafic schists and cumulate-textured rocks. The chloritites are composed mainly of Mg-chlorite (>95%) in a diablastic texture or rarely oriented according to the tectonic foliation. Apatite, magnetite and zircon are accessory minerals in these rocks.

4.2. Amphibolites

The mafic metavolcanic rocks are restricted to the Serra de Santa Rita greenstone belt and are represented by fine- to medium-grained amphibolites (Fig. 3B). These rocks are composed

Table 3.1
U-Pb zircon in situ data from sample TF14-I-099 (chloritite of the Faina greenstone belt) (LA-MC-ICP-MS).

Spot number	f_{206}[a]	Pb (ppm)	Th (ppm)	U (ppm)	Th/U[b]	Isotope ratio[c]							Ages (Ma)						Conc (%)[f]
						$^{207}Pb/^{235}U$	1 s (%)	$^{206}Pb/^{238}U$	1 s (%)	Rho[d]	$^{207}Pb/^{206}Pb$[e]	1 s (%)	$^{206}Pb/^{238}U$	1 s abs	$^{207}Pb/^{235}U$	1 s abs	$^{207}Pb/^{206}Pb$	1 s abs	
Std 15-Pleisovice	0.0051	38.4	34.2	708.4	0.05	0.3925	3.39	0.0535	1.95	0.58	0.0532	2.77	336.1	6.6	336.2	11.4	337.3	9.3	99.6
Std 16-Pleisovice	0.0028	74.0	115.6	1324.6	0.09	0.3948	3.13	0.0538	1.89	0.60	0.0532	2.50	337.9	6.4	337.9	10.6	337.7	8.4	100.1
Std 18	0.0056	137.0	116.0	419.6	0.28	8.8437	1.91	0.3207	1.55	0.81	0.2000	1.12	1793.2	27.8	2322.0	44.5	2826.1	31.7	63.5
Std 19	0.0017	165.4	107.1	317.2	0.34	13.1206	3.52	0.4559	3.28	0.93	0.2087	1.28	2421.3	79.3	2688.4	94.6	2895.8	37.2	83.6
Std 20	0.0015	183.1	101.9	332.4	0.31	12.9103	3.54	0.4492	3.30	0.93	0.2085	1.28	2391.5	79.0	2673.1	94.7	2893.6	37.0	82.6
Std 21	0.0064	113.2	60.9	289.2	0.21	16.0711	2.62	0.5407	2.33	0.89	0.2156	1.20	2786.2	65.0	2881.0	75.5	2948.0	35.3	94.5
Std 22	0.0017	109.3	37.0	234.7	0.16	12.6174	1.53	0.4476	1.31	0.85	0.2045	0.79	2384.5	31.2	2651.5	40.5	2862.1	22.7	83.3
Std 23	0.0048	117.7	80.5	291.9	0.28	8.3358	2.37	0.3136	2.08	0.88	0.1928	1.13	1758.4	36.6	2268.2	53.7	2766.1	31.3	63.6
Std 24	0.0080	138.8	152.8	315.2	0.49	10.9635	1.46	0.3994	1.22	0.83	0.1991	0.81	2166.2	26.4	2520.0	36.8	2818.8	22.7	76.8
Std 26	0.0024	135.6	67.4	225.7	0.30	16.6505	1.30	0.5605	1.08	0.83	0.2155	0.72	2868.6	31.1	2914.9	37.9	2947.1	21.3	97.3
Std 27	0.0028	128.5	144.7	289.6	0.50	10.5008	2.40	0.3896	1.65	0.69	0.1955	1.74	2120.8	35.0	2480.0	59.4	2789.0	48.4	76.0
Std 40-Pleisovice	0.0036	53.1	58.4	964.4	0.06	0.3948	3.19	0.0538	1.96	0.61	0.0532	2.52	337.8	6.6	337.9	10.8	338.0	8.5	100.0
Std 41-Pleisovice	0.0031	71.3	111.6	1284.4	0.09	0.3937	3.27	0.0537	2.12	0.65	0.0532	2.48	337.1	7.2	337.1	11.0	336.8	8.4	100.1

[a] Fraction of the non-radiogenic ^{206}Pb in the analyzed zircon spot, where $f_{206} = [^{206}Pb/^{204}Pb]c/[^{206}Pb/^{204}Pb]s$ (c = common; s = sample).
[b] Th/U ratios and amount of Pb, Th and U (in ppm) are calculated relative to 91500 reference zircon.
[c] Corrected for background and within-run Pb/U fractionation and normalized to reference zircon GJ-1 (ID-TIMS values/measured value); $^{207}Pb/^{235}U$ calculated using $(^{207}Pb/^{206}Pb)/(^{238}U/^{206}Pb * 1/137.88)$.
[d] Rho is the error correlation defined as the quotient of the propagated errors of the $^{206}Pb/^{238}U$ and the $^{207}/^{235}U$ ratio.
[e] Corrected for mass-bias by normalising to GJ-1 reference zircon and common Pb using the model Pb composition of Stacey and Kramers (1975).
[f] Degree of concordance = $(^{206}Pb/^{238}U \text{ age} * 100/^{207}Pb/^{206}U \text{ age})$.

mainly of Mg-hornblende and plagioclase (albite), with subordinate epidote, actinolite, chlorite and biotite. Magnetite, titanite and apatite are accessory minerals. Tectonic foliation is well marked by the preferential orientation of amphiboles and chlorite. The primary igneous texture is rarely preserved; it is characterized by subhedral plagioclase phenocrysts composing reliquiar porphyritic texture and minor intergranular texture domains. The mineral assemblage includes hornblende + plagioclase (albite) ± epidote and indicates that the metamorphic peak reached amphibolite facies. Nonetheless, retrometamorphic processes under greenschist facies are evidenced by the presence of chlorite, actinolite and biotite, which substitute in several degrees the hornblende crystals, predominantly at the edges (Fig. 4C and D). The plagioclase is partially replaced by epidote and has a sodic composition (An_{1-3}). The albitic composition of the plagioclase must be related to retrometamorphic processes under greenschist facies, but can also be result of late hydrothermal alteration processes.

4.3. Metandesites

Metandesite lenses occur among the amphibolites in the southern portion of the Serra de Santa Rita greenstone belt. The metandesites are interlayered with metavolcaniclastic rocks, metapelites, carbonaceous schists and metacherts with sulfide dissemination (Fig. 3C and D). Normally, the metamorphism and deformation obliterate the primary structures making it difficult to recognize the protoliths of these rocks. In the less deformed regions, the metandesites present preserved igneous texture and consist of euhedral to subhedral plagioclase (albite) phenocrysts embedded in a fine-grained groundmass of quartz, plagioclase (albite), muscovite and biotite (Fig. 4E). The plagioclase is partially replaced by epidote and the biotite is partially or fully substituted by chlorite. The strongly albitic composition of the plagioclase ($An_{0.1-0.4}$) may reflect the superimposed greenschist facies retrometamorphism and hydrothermal alteration. In the most deformed rocks, the original porphyritic texture is obliterated; the plagioclase phenocrysts are less preserved and highly saussuritized and the biotite is fully replaced by chlorite. Carbonate-rich veinlets oriented according to the foliation of the rocks are common.

4.4. Metadiorites and metatonalites

Dioritic intrusions also metamorphosed under amphibolite facies occur among the amphibolites of the Serra de Santa Rita greenstone belt. At the edges of these intrusions occur angular enclaves of fine-grained amphibolites that are possibly xenoliths of the greenstone belt's metavolcanic rocks (Fig. 3E and F). Mafic microgranular xenoliths are locally observed which may represent mingling features. The metadiorites are medium- to coarse-grained rocks composed of Mg-hornblende, plagioclase (albite) and quartz. Titanite, magnetite and zircon are accessory minerals. Hornblende may be partially substituted by actinolite and very often encompassed by films of chlorite related to the greenschist facies retrometamorphism. Plagioclase is highly replaced by epidote and has an albitic composition ($An_{0.7-2.4}$) that is probably also a result of the greenschist facies retrometamorphism and hydrothermal alteration. The least deformed rocks present original subhedral granular texture and minor intergranular texture domains (Fig. 4F). In the deformed rocks, the foliation is well marked by the preferential orientation of amphiboles and chlorite. In narrow shear zones, milonites are formed and the hornblende and plagioclase are fully substituted by actinolite and epidote, respectively. Subordinated to the metadiorites occur highly deformed tonalitic intrusions composed of quartz, plagioclase (albite) and Mg-hornblende. In these rocks, the hornblende is replaced by actinolite and chlorite, and the plagioclase is strongly saussuritized.

5. Whole rock geochemistry

5.1. Major and trace elements

5.1.1. Ultramafic rocks and chloritites

The ultramafic rocks of the Faina and Serra de Santa Rita greenstone belts are characterized by SiO_2 = 45–55 wt.%, MgO = 20–32 wt.%, Fe_2O_3 = 9–16 wt.%, Al_2O_3 = 3–8 wt.%, TiO_2 = 0.1–0.6 wt.%, P_2O_5 = 0.01–0.06 wt.%, Ni = 905–2560 ppm, Cr = 1320–2910 ppm and Mg# = 75–87 (Table 2). The ultramafic rocks have low absolute REE contents (∑REE = 5–43 ppm) and on chondrite-normalized diagram show flat to enriched LREE patterns (La/Sm_{cn} = 1.01–4.27, La/Yb_{cn} = 0.61–6.36) and flat to slightly fractionated HREE patterns (Gd/Yb_{cn} = 0.59–1.94). Slightly U-shaped REE patterns, marked by MREE depletion relative to LREE and HREE (La/Sm_{cn} = 1.05–1.88, Sm/Yb_{cn} = 0.59–0.73), are observed in two samples (TF14-075B and TF14-II-125A). Negative Ce anomalies are presented in some samples (Ce/Ce* = 0.24–0.77), while a pronounced negative Eu anomaly (Eu/Eu* = 0.55) is only observed in the sample TF14-00 (Fig. 5A). On primitive mantle-normalized diagram, these rocks show variable negative Nb, Ti and Zr anomalies (Fig. 5B).

The chloritites of the Faina and Serra de Santa Rita greenstone belts are characterized by high MgO = 28–31 wt.% and Mg# = 77–82 and differ from the other ultramafic rocks by the lower contents of SiO_2 (31–32 wt.%), Ni (110–410 ppm) and Cr (80–940 ppm), and by higher contents of Al_2O_3 (21–23 wt.%), TiO_2 (1.0–1.4 wt.%), P_2O_5 (0.1–0.4 wt.%) and REE (∑REE = 93–303 ppm) (Table 2). On chondrite-normalized diagram, the chloritites show LREE enrichment (La/Sm_{cn} = 3.91–4.97, La/Yb_{cn} = 11.12–27) and HREE depletion (Gd/Yb_{cn} = 1.60–3.58), with negative to positive Eu anomalies (Eu/Eu* = 0.72–1.40) (Fig. 5C). On primitive mantle-normalized diagram, the chloritites present pronounced negative Nb anomalies (Nb/Th_{pm} = 0.09–0.41) and negative to positive Zr (Zr/Sm_{pm} = 0.79–2.14) and Ti (Ti/Sm_{pm} = 0.24–0.60) anomalies (Fig. 5D).

5.1.2. Amphibolites

The amphibolites of the Serra de Santa Rita greenstone belt are characterized by SiO_2 = 53–55 wt.%, Al_2O_3 = 9–16 wt.%, Fe_2O_3 = 9–12 wt.%, MgO = 7–15 wt.%, CaO = 6–13 wt.%, TiO_2 = 0.4–1.2 wt.% and Mg# = 56–72 (Table 2). These rocks are classified as basalts on Nb/Y vs. Zr/Ti diagram and only one sample (TF14-XII-178) plots in the limit of the alkali basalts field due to the high Nb content (Fig. 6A). Based on the trace-elements behavior, the amphibolites can be subdivided into two groups: type 1 basalts and type 2 basalts. The type 1 basalts are characterized by the highest contents of MgO (9–15 wt.%), Mg# (60–72), Cr (570–1280 ppm) and Ni (191–384 ppm), show a toleiitic magmatic affinity on Y vs. Zr and Yb vs. La diagrams (Fig. 6B and C), and have the lowest absolute REE contents (∑REE = 15–28 ppm). On chondrite-normalized diagram, the type 1 basalts have relatively flat REE patterns marked by La/Sm_{cn} = 0.94–1.14, La/Yb_{cn} = 0.75–1.53 and Gd/Yb_{cn} = 1.00–1.67. Slightly positive Eu anomaly (Eu/Eu* = 1.24) is observed in one of the samples (PFG-CA-19A) (Fig. 7A). On

Table 3.2
U-Pb zircon in situ data from sample TF14-XI-016 (chloritite of the Serra de Santa Rita greenstone belt) (LA-MC-ICP-MS).

			Isotope ratios[c]							Ages (Ma)						Conc (%)[f]
Spot number	f_{206}[a]	Th/U[b]	$^{207}Pb/^{235}U$	1 s (%)	$^{206}Pb/^{238}U$	1 s (%)	Rho[d]	$^{207}Pb/^{206}Pb$[e]	1 s (%)	$^{206}Pb/^{238}U$	1 s abs	$^{207}Pb/^{235}U$	1 s abs	$^{207}Pb/^{206}Pb$	1 s abs	
003-91500	0.0273	0.17	1.8452	1.49	0.1784	1.09	0.72	0.0750	1.02	1058.0	10.6	1061.7	9.8	1069.5	20.4	98.9
004-Z01	0.0367	0.61	16.8171	2.26	0.5733	1.75	0.77	0.2128	1.43	2921.2	41.1	2924.5	21.7	2926.7	23.2	99.8
005-Z02	0.0350	0.70	16.6864	2.03	0.5448	1.49	0.73	0.2221	1.38	2803.6	34.0	2917.0	19.5	2996.2	22.2	93.6
006-Z03	0.0376	0.46	17.5235	2.47	0.5807	1.76	0.71	0.2189	1.74	2951.4	41.7	2963.9	23.7	2972.4	28.0	99.3
007-Z04	0.0409	0.52	17.2431	2.37	0.5748	1.81	0.76	0.2176	1.53	2927.5	42.5	2948.5	22.7	2962.8	24.6	98.8
008-Z05	0.0758	0.48	16.9752	3.55	0.5587	2.61	0.73	0.2203	2.41	2861.4	60.3	2933.4	34.0	2983.2	38.7	95.9
009-Z06	0.0530	0.59	17.7578	3.52	0.5805	2.55	0.72	0.2219	2.43	2950.6	60.3	2976.7	33.8	2994.4	39.1	98.5
010-Z07	0.0592	0.59	17.5012	4.85	0.5837	3.52	0.72	0.2175	3.34	2963.7	83.6	2962.7	46.6	2962.0	53.9	100.1
013-Z08	0.0089	0.50	17.9455	1.44	0.6022	1.03	0.70	0.2161	1.01	3038.7	24.9	2986.8	13.9	2952.0	16.3	102.9
014-Z09	0.0212	0.69	17.3373	2.21	0.5841	1.63	0.73	0.2153	1.48	2965.6	38.8	2953.7	21.2	2945.6	24.0	100.7
015-Z10	0.0379	0.51	17.0452	2.12	0.5570	1.59	0.74	0.2220	1.40	2854.2	36.7	2937.4	20.4	2994.9	22.5	95.3
016-Z11	0.0415	0.75	17.8992	1.51	0.5902	1.24	0.82	0.2200	0.86	2990.2	29.8	2984.3	14.5	2980.4	13.8	100.3
017-Z12	0.0193	0.71	17.6561	1.72	0.5879	1.49	0.86	0.2178	0.85	2980.9	35.6	2971.2	16.5	2964.6	13.7	100.6
018-Z13	0.0442	0.77	17.1755	1.14	0.5727	1.03	0.90	0.2175	0.47	2919.1	24.3	2944.7	10.9	2962.2	7.6	98.5
019-Z14	0.0289	0.62	17.4285	3.00	0.5923	2.49	0.83	0.2134	1.67	2998.8	59.7	2958.7	28.8	2931.6	27.0	102.3
020-Z15	0.0352	0.44	18.4853	4.36	0.6175	2.96	0.68	0.2171	3.21	3099.9	72.8	3015.3	42.0	2959.4	51.7	104.7
023-Z16	0.0118	0.72	17.8210	1.03	0.5881	0.81	0.76	0.2198	0.63	2981.8	19.3	2980.1	9.9	2979.0	10.2	100.1
024-Z17	0.1300	0.63	9.9515	0.91	0.3629	0.81	0.88	0.1989	0.41	1995.9	13.9	2430.3	8.4	2817.1	6.7	70.8
025-Z18	0.0203	0.49	17.1078	1.57	0.5740	1.32	0.83	0.2162	0.85	2924.1	31.0	2940.9	15.0	2952.4	13.7	99.0
026-Z19	0.0098	0.76	17.9487	1.06	0.6017	0.85	0.78	0.2163	0.63	3036.9	20.6	2987.0	10.2	2953.6	10.2	102.8
027-Z20	0.0106	0.76	17.6680	0.98	0.5894	0.82	0.82	0.2174	0.53	2987.0	19.7	2971.8	9.4	2961.6	8.5	100.9
028-Z21	0.0312	0.53	17.1737	1.56	0.5725	1.37	0.87	0.2176	0.76	2917.9	32.1	2944.6	15.0	2962.9	12.2	98.5
029-Z22	0.0057	1.05	18.6783	0.89	0.6194	0.79	0.87	0.2187	0.41	3107.5	19.4	3025.4	8.5	2971.2	6.6	104.6
030-Z23	0.0193	0.51	17.1492	1.23	0.5657	0.97	0.77	0.2199	0.75	2890.2	22.6	2943.2	11.8	2979.6	12.1	97.0
033-Z24	0.0090	0.62	18.7131	1.13	0.6240	1.01	0.88	0.2175	0.51	3125.9	24.9	3027.1	10.9	2962.2	8.2	105.5
034-Z25	0.0106	0.59	17.2298	1.26	0.5761	1.05	0.81	0.2169	0.71	2932.9	24.6	2947.7	12.1	2957.8	11.5	99.2
035-Z26	0.0098	0.70	17.6066	0.98	0.5868	0.74	0.72	0.2176	0.65	2976.5	17.7	2968.5	9.4	2963.0	10.4	100.5
036-Z27	0.0096	0.59	17.2983	1.16	0.5748	0.99	0.84	0.2183	0.60	2927.4	23.4	2951.5	11.2	2968.0	9.7	98.6
037-Z28	0.0150	0.54	16.9338	1.25	0.5756	1.07	0.85	0.2134	0.64	2930.8	25.3	2931.1	12.0	2931.3	10.4	100.0
038-Z29	0.0112	0.67	17.2196	1.26	0.5696	1.01	0.79	0.2193	0.75	2906.1	23.6	2947.1	12.1	2975.3	12.2	97.7
039-91500	0.0304	0.17	1.8632	1.65	0.1805	1.21	0.72	0.0749	1.13	1069.8	11.9	1068.1	10.9	1064.8	22.7	100.5

[a] Fraction of the non-radiogenic ^{206}Pb in the analyzed zircon spot, where $f_{206} = [^{206}Pb/^{204}Pb]c/[^{206}Pb/^{204}Pb]s$ (c = common; s = sample).
[b] Th/U ratios and amount of Pb, Th and U (in ppm) are calculated relative to 91500 reference zircon.
[c] Corrected for background and within-run Pb/U fractionation and normalized to reference zircon GJ-1 (ID-TIMS values/measured value); $^{207}Pb/^{235}U$ calculated using $(^{207}Pb/^{206}Pb)/(^{238}U/^{206}Pb * 1/137.88)$.
[d] Rho is the error correlation defined as the quotient of the propagated errors of the $^{206}Pb/^{238}U$ and the $^{207}/^{235}U$ ratio.
[e] Corrected for mass-bias by normalising to GJ-1 reference zircon and common Pb using the model Pb composition of Stacey and Kramers (1975).
[f] Degree of concordance = ($^{206}Pb/^{238}U$ age * 100/$^{207}Pb/^{206}U$ age).

Table 3.3
U-Pb zircon in situ data from sample TF14-XII-178 (amphibolite of the Serra de Santa Rita greenstone belt) (LA-SF-ICP-MS).

				Isotope ratios							Ages (Ma)						Conc (%)[b]
Spot number	CPS Pb206*	CPS Pb207*	Th/U	$^{207}Pb^*/^{206}Pb^*$	±1 s	$^{207}Pb^*/^{235}U$	±1 s	$^{206}Pb^*/^{238}U$	±1 s	Rho[a]	$^{206}Pb/^{238}U$	±1 s	$^{207}Pb/^{235}U$	±1 s	$^{206}Pb/^{207}Pb$	±1 s	
SMPABC011	100414	22722	0.19	0.2186	0.003	17.7502	0.21	0.5877	0.005	0.79	2980.0	22.2	2976.3	11.3	2970.7	21.5	100.3
SMPABC063	280691	62191	0.59	0.2202	0.004	17.5545	0.30	0.5781	0.005	0.54	2941.2	21.6	2965.6	16.3	2982.2	29.8	98.6
SMPABC056	128857	29079	0.63	0.2185	0.003	17.2997	0.24	0.5739	0.005	0.60	2924.0	19.6	2951.6	13.3	2969.8	25.3	98.5
SMPABC025	252520	55521	0.77	0.2167	0.002	17.1432	0.14	0.5732	0.004	0.88	2920.9	16.9	2942.9	7.9	2956.2	17.4	98.8
SMPABC024	68188	14928	0.40	0.2182	0.003	17.2408	0.19	0.5722	0.005	0.75	2916.8	19.1	2948.3	10.4	2967.8	21.0	98.3
SMPABC019	222119	49006	0.19	0.2183	0.002	17.2213	0.15	0.5713	0.004	0.84	2913.1	16.7	2947.2	8.1	2968.3	17.9	98.1
SMPABC023	191080	41762	0.60	0.2162	0.002	17.0349	0.14	0.5710	0.004	0.87	2911.8	17.0	2936.8	8.0	2952.2	17.7	98.6
SMPABC012	61517	13484	0.40	0.2161	0.002	16.9910	0.15	0.5696	0.004	0.88	2906.1	17.8	2934.3	8.3	2951.9	17.9	98.4
SMPABC026	252243	55750	0.71	0.2171	0.002	17.0458	0.14	0.5688	0.004	0.85	2902.8	16.8	2937.4	8.1	2959.3	17.7	98.1
SMPABC058	69504	15411	0.39	0.2158	0.004	16.9136	0.32	0.5682	0.006	0.55	2900.3	24.4	2929.9	18.1	2949.5	32.6	98.3
SMPABC015	237041	51859	0.68	0.2152	0.002	16.8400	0.13	0.5670	0.004	0.91	2895.7	16.9	2925.8	7.6	2944.7	17.0	98.3
SMPABC018	159286	35318	0.47	0.2187	0.002	17.0896	0.14	0.5661	0.004	0.89	2891.9	17.2	2939.9	7.9	2971.4	17.4	97.3
SMPABC042	175196	38670	0.72	0.2157	0.003	16.8162	0.18	0.5650	0.004	0.70	2887.3	17.5	2924.4	10.3	2948.6	21.0	97.9
SMPABC044	82064	18329	0.58	0.2166	0.003	16.8406	0.19	0.5634	0.004	0.71	2880.8	18.5	2925.8	10.7	2955.4	21.4	97.5
SMPABC031	181307	39902	0.80	0.2141	0.002	16.5418	0.14	0.5597	0.004	0.89	2865.2	16.9	2908.7	7.9	2937.0	17.3	97.6
SMPABC010	173935	37666	0.65	0.2138	0.002	16.5156	0.13	0.5596	0.004	0.91	2864.8	16.8	2907.1	7.7	2934.7	17.1	97.6
SMPABC062	262678	57858	0.18	0.2168	0.004	16.7027	0.26	0.5583	0.005	0.58	2859.5	20.5	2917.9	14.7	2956.8	27.4	96.7
SMPABC030	78242	17190	0.38	0.2146	0.002	16.5358	0.15	0.5582	0.004	0.87	2859.1	17.6	2908.3	8.4	2940.9	18.0	97.2
SMPABC046	76305	17081	0.52	0.2151	0.003	16.5606	0.19	0.5576	0.005	0.75	2856.6	19.5	2909.7	10.8	2944.6	21.3	97.0
SMPABC057	154804	34832	0.65	0.2147	0.002	16.4696	0.15	0.5558	0.004	0.82	2849.2	17.1	2904.5	8.6	2941.3	18.2	96.9
SMPABC027	66050	14523	0.55	0.2162	0.003	16.5275	0.15	0.5539	0.004	0.84	2841.4	17.5	2907.8	8.7	2952.3	18.6	96.2
SMPABC059	144695	32727	0.22	0.2151	0.003	16.1295	0.16	0.5435	0.004	0.78	2798.1	18.1	2884.5	9.8	2944.1	19.6	95.0
SMPABC054	45979	10237	0.22	0.2126	0.003	15.9042	0.18	0.5418	0.005	0.77	2790.9	19.3	2871.1	10.6	2925.7	20.9	95.4
SMPABC014	142119	31151	0.70	0.2111	0.002	15.7693	0.14	0.5414	0.004	0.86	2789.5	17.1	2862.9	8.4	2913.8	17.8	95.7
SMPABC049	137913	29913	0.24	0.2137	0.004	15.9377	0.30	0.5411	0.006	0.57	2787.9	24.4	2873.1	18.1	2933.9	32.8	95.0
SMPABC028	73187	15875	0.47	0.2131	0.002	15.6860	0.14	0.5333	0.004	0.84	2755.3	16.9	2857.9	8.6	2929.3	18.5	94.1
SMPABC055	89843	19860	0.23	0.2140	0.004	15.6906	0.26	0.5322	0.005	0.61	2750.7	22.8	2858.1	15.8	2936.3	29.1	93.7
SMPABC032	63837	13725	0.29	0.2112	0.003	15.4591	0.16	0.5302	0.004	0.75	2742.4	17.7	2844.0	10.1	2914.9	20.7	94.1
SMPABC016	38555	8274	0.19	0.2129	0.004	15.5149	0.26	0.5280	0.006	0.72	2733.1	26.6	2847.4	15.9	2927.8	29.1	93.4
SMPABC061	80408	17473	0.54	0.2141	0.004	15.5763	0.23	0.5271	0.005	0.64	2729.1	20.9	2851.2	14.0	2936.6	26.3	92.9
SMPABC043	35981	7622	0.58	0.2121	0.004	14.9376	0.28	0.5104	0.006	0.62	2658.5	24.8	2811.3	17.6	2921.8	32.0	91.0
SMPABC045	70647	15367	0.54	0.2108	0.003	14.6528	0.17	0.5038	0.004	0.70	2630.0	17.4	2793.0	10.9	2911.4	21.8	90.3
SMPABC060	355551	77115	0.81	0.2083	0.003	14.0180	0.15	0.4876	0.004	0.74	2560.1	16.7	2750.9	10.1	2892.4	20.4	88.5

[a] Rho is the error correlation defined as the quotient of the propagated errors of the $^{206}Pb/^{238}U$ and the $^{207}Pb/^{235}U$ ratio.
[b] Degree of concordance = ($^{206}Pb/^{238}U$ age * 100/$^{207}Pb/^{206}Pb$ age).

primitive mantle-normalized diagram, the type 1 basalts show relatively flat patterns without any significant anomalies (Fig. 7B).

The type 2 basalts are characterized by lower MgO (7–9 wt.%), Mg# (56–67), Cr (340–430 ppm) and Ni (110–237 ppm) and by higher REE contents (∑ETR = 60–82 ppm) compared to the type 1 basalts. Two samples (TF14-XII-015B and PFG-CA-16A) show a transitional sub-alkaline magmatic affinity and one sample (TF14-XII-178) show a calc-alkaline magmatic affinity according to Y vs. Zr and Yb vs. La diagrams (Fig. 6B and C). On chondrite-normalized diagram, the type 2 basalts have enriched LREE patterns and flat to slightly depleted HREE patterns marked by La/Sm_{cn} = 1.62–2.73, La/Yb_{cn} = 1.93–2.3 e Gd/Yb_{cn} = 1.31–1.95, without Eu anomalies (Fig. 7C). On primitive mantle-normalized diagram, the type 2 basalts show slightly negative to positive Nb anomalies (Nb/Th_{pm} = 0.68–1.27) and negative Ti anomalies (Ti/Sm_{pm} = 0.49–0.84) (Fig. 7D). The type 2 basalts are also characterized by high Nb contents (5–12 ppm), whereas the type 1 basalts present low values (1–2 ppm) (Table 2).

5.1.3. Metandesites

The metandesites of the Serra de Santa Rita greenstone belts are characterized by SiO_2 = 56–68 wt.%, Al_2O_3 = 16–20 wt.%, Fe_2O_3 = 5–8 wt.%, Na_2O = 4–6 wt.%, CaO = 3–6 wt.%, MgO = 3–6 wt.%, TiO_2 = 0.5–1.1 wt.%, K_2O = 0.1–1.4 wt.%, Cr = 60–240 ppm and Ni = 51–128 ppm (Table 2). These rocks are classified as andesites and basaltic andesites on Nb/Y vs. Zr/Ti diagram (Fig. 6A) and have a calc-alkaline magmatic affinity according to Y vs. Zr and Yb vs. La diagrams (Fig. 6B and C). On chondrite-normalized diagram, the metandesites have enriched LREE patterns and depleted HREE patterns marked by La/Sm_{cn} = 2.55–4.12, La/Yb_{cn} = 4.70–14.58 and Gd/Yb_{cn} = 1.66–2.34 (Fig. 8A). On primitive mantle-normalized diagram, the metandesites show pronounced negative Nb and Ti anomalies (Nb/Th_{pm} = 0.26–0.35; Ti/Sm_{pm} = 0.08–0.16), and slightly positive Zr anomalies (Zr/Sm_{pm} = 1.35–1.71) (Fig. 8B).

5.1.4. Metadiorites and metatonalites

The metadiorites of the Serra de Santa Rita greenstone belt are characterized by SiO_2 = 54–58 wt.%, Al_2O_3 = 13–15 wt.%, MgO = 9–15 wt.%, Fe_2O_3 = 7–10 wt.%, CaO = 5–7 wt.%, Na_2O = 1–5 wt.%, TiO_2 = 0.4–1.2 wt.% and K_2O = 0.1–1.4 wt.%. These rocks present unusual high Mg# (70–81), Cr (440–1060 ppm) and Ni (200–456 ppm) contents (Table 2). The only analyzed sample of metatonalite (TF14-XII-183) show higher SiO_2 (66 wt.%) and lower Fe_2O_3 (5 wt.%), MgO (1.7 wt.%), Mg# (42), Cr (330 ppm) and Ni (120 ppm) than the metadiorites (Table 2). On TAS classification diagram for plutonic rocks (Middlemost, 1994; not presented), the rocks plot predominantly in the field of quartz-diorites with the exception of the metatonalite sample, that plots consistently in the tonalite field. The metadiorites and metatonalite plot predominantly in the andesite and basaltic andesite field on Nb/Yb vs. Zr/Ti diagram (Fig. 6A), and show a calc-alkaline magmatic affinity on Y vs. Zr and Yb vs. La diagrams (Fig. 6B and C).

The metadiorites and metatonalites are characterized by ∑ETR = 50–162 ppm and on chondrite-normalized diagram they present enriched LREE patterns and depleted HREE patterns marked by La/Sm_{cn} = 2.91–4.18, La/Yb_{cn} = 8.49–18.61 and Gd/Yb_{cn} = 1.75–3.93. Only the metatonalite sample shows positive Eu anomaly (Eu/Eu* = 1.30) (Fig. 8C). On primitive mantle-normalized diagram the metadiorites present pronounced negative Nb and Ti anomalies (Nb/Th_{pm} = 0.22–0.84; Ti/Sm_{pm} = 0.24–0.45), and slightly negative Zr anomalies (Zr/Sm_{pm} = 0.83–0.92) (Fig. 8D).

6. Geochronology

6.1. U-Pb

LA-MC-ICP-MS and LA-SF-ICP-MS U-Pb zircon dating were conducted in five samples: a chloritite of the Faina greenstone belt (TF14-I-099), a chloritite of the Serra de Santa Rita greenstone belt (TF14-XI-016), an amphibolite that belong to the type 2 basalts group (TF14-XII-178), a metadiorite (PFG-CA-04A) and a metatonalite (TF1-XII-183). With the exception of the sample TF14-XI-016, the zircon crystals data of all dated samples provided discordia diagrams and ages defined by upper intercepts, interpreted as the magmatic crystallization ages of the protoliths.

The chloritite sample of the Faina greenstone belt yielded a discordia defining the upper intercept age of 2950 ± 37 Ma (Fig. 9A). The chloritite sample of the Serra de Santa Rita greenstone belt yielded the concordant age of 2960.3 ± 5.5 Ma (Fig. 9B). The amphibolite sample yielded a discordia defining the upper intercept age of 2968.3 ± 7.0 Ma (Fig. 9C). The metadiorite sample yielded a discordia defining the upper intercept age of 2922.8 ± 2.8 Ma (Fig. 9D). The metatonalite sample yielded a discordia defining the upper intercept age of 2809.3 ± 9.2 Ma (Fig. 9E). These ages mark two main periods of igneous activity: 2.96–2.92 Ga and 2.8 Ga.

6.2. Sm-Nd

The whole-rock Sm-Nd isotopic analyses were carried out in four samples: an amphibolite of the type 2 basalts group (TF14-XII-178), two metadiorites (PFG-CA-04A and PFG-CA-04E), and a metatonalite (TF14-XII-183). The amphibolite presented T_{DM} = 3.08 Ga and ε_{Nd} = +2.26 for the magmatic crystallization age of 2.96 Ga. The metadiorites PFG-CA-04A and PFG-CA-04E presented, respectively, T_{DM} of 3.03 and 2.99 Ga, and ε_{Nd} of +2.16 and +2.77 for the magmatic crystallization age of 2.92 Ga. The metatonalite presented T_{DM} = 3.13 Ga and ε_{Nd} = −0.15 for the magmatic crystallization age of 2.8 Ga (Table 4).

7. Discussion

7.1. Element mobility and crustal contamination

The recognition of the primary chemical composition of igneous rocks in Archean greenstone belts sometimes is difficult due to the effects of metamorphism, hydrothermal alteration and deformation. The metavolcanic and metaplutonic rocks of the Faina and

Table 3.4
U-Pb zircon in situ data from sample PFG-CA-04A (metadiorite of the Serra de Santa Rita greenstone belt) (LA-SF-ICP-MS).

				Isotope ratios							Ages (Ma)						Conc (%)[b]
Spot number	CPS Pb206*	CPS Pb207*	Th/U	$^{207}Pb^*/^{206}Pb^*$	±1 s	$^{207}Pb^*/^{235}U$	±1 s	$^{206}Pb^*/^{238}U$	±1 s	Rho[a]	$^{206}Pb/^{238}U$	±1 s	$^{207}Pb/^{235}U$	±1 s	$^{206}Pb/^{207}Pb$	±1 s	
SMPABC027a	56359	12769	0.34	0.2242	0.005	18.2854	0.35	0.5914	0.008	0.70	2994.9	32.3	3004.9	18.5	3011.4	32.3	99.5
SMPABC063a	119470	26325	0.57	0.2186	0.005	17.6110	0.37	0.5849	0.007	0.54	2968.9	27.3	2968.7	20.3	2970.5	36.6	99.9
SMPABC016	167243	39020	0.75	0.2085	0.003	16.9010	0.21	0.5869	0.006	0.78	2976.9	22.9	2929.2	11.8	2894.2	22.1	102.9
SMPABC023	234418	51869	0.35	0.2114	0.002	16.9661	0.16	0.5817	0.005	0.83	2955.6	18.7	2932.9	9.1	2915.9	18.5	101.4
SMPABC030	111939	24197	0.60	0.2122	0.002	17.0063	0.14	0.5808	0.004	0.88	2951.9	17.7	2935.2	8.2	2922.1	17.7	101.0
SMPABC019	323021	71801	0.72	0.2108	0.002	16.8867	0.16	0.5806	0.005	0.81	2951.2	18.6	2928.4	9.3	2911.5	18.7	101.4
SMPABC056	141358	31122	0.59	0.2113	0.002	16.9055	0.16	0.5796	0.004	0.79	2947.0	18.3	2929.5	9.3	2915.3	19.0	101.1
SMPABC043	179333	39313	0.52	0.2113	0.002	16.8806	0.15	0.5788	0.004	0.85	2943.8	18.0	2928.1	8.6	2915.6	18.0	101.0
SMPABC017	183086	39927	0.68	0.2113	0.002	16.8664	0.14	0.5787	0.004	0.91	2943.5	18.1	2927.3	8.1	2915.5	17.2	101.0
SMPABC026	75351	16825	0.36	0.2125	0.003	16.9655	0.17	0.5786	0.005	0.81	2942.9	19.6	2932.9	9.9	2924.6	19.5	100.6
SMPABC053	180479	39774	0.30	0.2116	0.002	16.8951	0.16	0.5782	0.004	0.80	2941.6	18.1	2928.9	9.1	2918.1	18.7	100.8
SMPABC032	55066	12069	0.42	0.2122	0.002	16.9206	0.16	0.5779	0.005	0.86	2940.2	18.7	2930.3	8.8	2922.3	18.3	100.6
SMPABC031	107057	23426	0.49	0.2118	0.002	16.8716	0.15	0.5774	0.004	0.87	2937.9	18.0	2927.6	8.4	2919.2	17.7	100.6
SMPABC040	77239	16515	0.52	0.2107	0.003	16.7685	0.16	0.5767	0.005	0.82	2935.2	19.0	2921.7	9.4	2910.9	19.2	100.8
SMPABC013	147178	31325	0.24	0.2112	0.002	16.7808	0.14	0.5761	0.004	0.89	2932.7	18.0	2922.4	8.2	2914.6	17.7	100.6
SMPABC050	131263	28656	0.63	0.2127	0.003	16.9151	0.18	0.5761	0.005	0.78	2932.7	19.6	2930.0	10.2	2926.3	20.2	100.2
SMPABC051	119760	26744	0.50	0.2125	0.003	16.8949	0.17	0.5760	0.005	0.79	2932.2	18.7	2928.9	9.7	2924.6	19.3	100.3
SMPABC060	95417	21064	0.23	0.2107	0.003	16.7432	0.17	0.5756	0.005	0.77	2930.8	18.8	2920.2	10.0	2910.9	19.8	100.7
SMPABC014	159013	34825	0.54	0.2133	0.002	16.8988	0.14	0.5744	0.004	0.92	2925.8	17.6	2929.1	7.8	2930.8	17.0	99.8
SMPABC055	112780	24767	0.25	0.2121	0.002	16.8190	0.16	0.5743	0.005	0.82	2925.4	18.5	2924.6	9.2	2922.0	18.8	100.1
SMPABC018	137756	29988	0.59	0.2121	0.002	16.7594	0.14	0.5729	0.004	0.91	2919.6	18.0	2921.2	8.0	2921.3	17.3	99.9
SMPABC042	184821	40698	0.66	0.2121	0.002	16.7558	0.15	0.5726	0.004	0.84	2918.3	18.0	2921.0	8.8	2921.3	18.2	99.9
SMPABC037	134293	29450	0.56	0.2118	0.002	16.7312	0.15	0.5723	0.004	0.87	2917.3	17.9	2919.6	8.4	2919.6	17.8	99.9
SMPABC054	96838	21047	0.30	0.2123	0.003	16.7474	0.17	0.5712	0.005	0.80	2912.7	18.7	2920.5	9.5	2923.3	19.4	99.6
SMPABC062	122549	27076	0.37	0.2116	0.003	16.6795	0.17	0.5710	0.004	0.76	2911.7	18.3	2916.6	9.8	2917.7	19.7	99.8
SMPABC044	62027	13442	0.34	0.2123	0.003	16.6563	0.16	0.5684	0.005	0.83	2901.1	19.0	2915.3	9.4	2923.2	19.1	99.2
SMPABC010	65629	14633	0.28	0.2139	0.003	16.6716	0.17	0.5648	0.005	0.83	2886.6	19.6	2916.1	9.7	2935.2	19.2	98.3
SMPABC052	57278	12364	0.32	0.2136	0.004	16.6045	0.25	0.5631	0.006	0.66	2879.5	22.7	2912.3	14.1	2933.4	26.4	98.2
SMPABC024	183989	40440	0.27	0.2133	0.002	16.5439	0.14	0.5623	0.004	0.90	2875.9	17.4	2908.8	8.0	2930.6	17.2	98.1
SMPABC061	234383	51927	0.71	0.2123	0.003	16.4671	0.16	0.5618	0.004	0.78	2874.1	17.9	2904.3	9.4	2923.1	19.0	98.3
SMPABC048	91054	20137	0.28	0.2129	0.002	16.4833	0.16	0.5610	0.004	0.83	2870.6	18.1	2905.3	9.0	2927.5	18.6	98.1
SMPABC039	258068	56986	0.61	0.2131	0.002	16.4617	0.14	0.5596	0.004	0.87	2865.1	17.4	2904.0	8.3	2929.5	17.7	97.8
SMPABC038	120773	26205	0.24	0.2129	0.002	16.3593	0.15	0.5568	0.004	0.86	2853.4	17.9	2898.0	8.7	2927.5	18.2	97.5
SMPABC028	46996	10145	0.27	0.2125	0.003	16.2974	0.16	0.5560	0.005	0.85	2849.9	19.2	2894.4	9.4	2924.4	19.1	97.5
SMPABC015	58499	12704	0.27	0.2135	0.002	15.6958	0.14	0.5331	0.004	0.88	2754.5	18.0	2858.5	8.7	2932.1	18.2	93.9
SMPABC036	89417	19300	0.30	0.2135	0.004	15.6561	0.24	0.5315	0.005	0.65	2747.7	22.3	2856.0	14.6	2932.5	27.4	93.7
SMPABC059	265489	57721	0.61	0.2121	0.002	15.4627	0.14	0.5281	0.004	0.80	2733.6	16.7	2844.2	8.9	2921.4	18.7	93.6
SMPABC011	108010	23299	0.31	0.2126	0.002	15.4727	0.14	0.5279	0.004	0.90	2732.5	17.6	2844.8	8.4	2925.3	17.8	93.4
SMPABC029	177148	38191	0.27	0.2114	0.002	15.3132	0.13	0.5251	0.004	0.89	2720.8	16.9	2834.9	8.1	2915.9	17.5	93.3
SMPABC025	169790	36479	0.33	0.2129	0.002	15.2695	0.14	0.5198	0.004	0.86	2698.2	16.9	2832.2	8.5	2928.0	18.1	92.2

[a] Rho is the error correlation defined as the quotient of the propagated errors of the $^{206}Pb/^{238}U$ and the $^{207}Pb/^{235}U$ ratio.
[b] Degree of concordance = ($^{206}Pb/^{238}U$ age * 100/$^{207}Pb/^{206}Pb$ age).

Table 3.5
U-Pb zircon in situ data from sample TF14-XII-183 (metatonalite of the Serra de Santa Rita greenstone belt) (LA-SF-ICP-MS).

				Isotope ratios							Ages (Ma)						Conc (%)[b]
Spot number	CPS Pb206*	CPS Pb207*	Th/U	$^{207}Pb^*/^{206}Pb^*$	±1 s	$^{207}Pb^*/^{235}U$	±1 s	$^{206}Pb^*/^{238}U$	±1 s	Rho[a]	$^{206}Pb/^{238}U$	±1 s	$^{207}Pb/^{235}U$	±1 s	$^{206}Pb/^{207}Pb$	±1 s	
SMPABC091	100676	20298	0.29	0.1900	0.002	10.6351	0.09	0.4073	0.003	0.91	2202.6	14.4	2491.8	7.9	2741.8	17.5	80.3
SMPABC090	122428	24939	0.30	0.1915	0.002	11.2708	0.09	0.4282	0.003	0.92	2297.7	14.8	2545.8	7.8	2755.1	17.3	83.4
SMPABC089	108908	22116	0.28	0.1912	0.002	12.3266	0.10	0.4689	0.004	0.92	2478.8	15.9	2629.6	7.9	2752.6	17.4	90.1
SMPABC087	116786	23344	0.34	0.1885	0.002	10.9607	0.09	0.4230	0.003	0.92	2274.0	14.7	2519.8	7.8	2728.9	17.3	83.3
SMPABC085	128882	23946	0.34	0.1750	0.002	6.9616	0.06	0.2892	0.002	0.92	1637.5	11.0	2106.5	7.4	2606.4	17.5	62.8
SMPABC083	106990	22101	0.29	0.1948	0.002	12.3217	0.10	0.4600	0.004	0.92	2439.5	15.6	2629.2	7.8	2782.8	17.2	87.7
SMPABC073	99876	19426	0.32	0.1834	0.002	8.7247	0.07	0.3455	0.003	0.93	1913.3	12.6	2309.7	7.5	2684.2	17.3	71.3
SMPABC072	102961	20612	0.26	0.1891	0.002	11.5509	0.09	0.4438	0.003	0.94	2367.5	15.2	2568.7	7.7	2734.2	17.1	86.6
SMPABC071	117121	24040	0.35	0.1937	0.002	13.3501	0.11	0.5006	0.004	0.94	2616.2	16.4	2704.7	7.7	2774.2	17.0	94.3
SMPABC070	119032	21828	0.41	0.1731	0.002	6.6858	0.05	0.2805	0.002	0.93	1593.9	10.7	2070.7	7.1	2588.1	17.3	61.6
SMPABC069	101828	20706	0.32	0.1919	0.002	11.5423	0.09	0.4369	0.003	0.94	2336.7	15.0	2568.0	7.6	2758.4	17.0	84.7
SMPABC067	126440	24116	0.26	0.1804	0.002	8.2655	0.07	0.3328	0.003	0.94	1851.9	12.2	2260.5	7.3	2656.1	17.1	69.7
SMPABC066	69594	13258	0.29	0.1798	0.002	8.8982	0.07	0.3593	0.003	0.93	1979.0	13.1	2327.6	7.6	2651.1	17.5	74.6
SMPABC064	113949	21796	0.36	0.1819	0.002	8.9111	0.07	0.3556	0.003	0.94	1961.4	12.8	2328.9	7.3	2670.4	17.1	73.5
SMPABC054	129686	24729	0.30	0.1801	0.002	8.5594	0.07	0.3448	0.003	0.96	1909.8	12.4	2292.3	7.1	2653.7	16.9	72.0
SMPABC052	112836	21987	0.32	0.1846	0.002	9.6959	0.08	0.3811	0.003	0.96	2081.3	13.4	2406.3	7.3	2694.3	16.9	77.2
SMPABC050	99432	20307	0.22	0.1934	0.002	12.2947	0.10	0.4611	0.004	0.96	2444.3	15.4	2627.2	7.5	2771.1	16.8	88.2
SMPABC048	63226	12110	0.27	0.1819	0.002	8.5723	0.07	0.3417	0.003	0.94	1894.8	12.6	2293.6	7.4	2670.4	17.3	71.0
SMPABC046	114264	21012	0.37	0.1748	0.002	7.2094	0.06	0.2990	0.002	0.96	1686.5	11.2	2137.7	7.0	2604.0	17.1	64.8
SMPABC037	76421	15493	0.28	0.1926	0.002	11.8672	0.09	0.4464	0.003	0.96	2379.3	15.2	2594.0	7.5	2764.5	16.9	86.1
SMPABC036	115181	22591	0.30	0.1863	0.002	9.5776	0.07	0.3725	0.003	0.96	2040.9	13.1	2395.0	7.1	2709.7	16.7	75.3
SMPABC035	133747	25888	0.34	0.1842	0.002	9.5264	0.07	0.3746	0.003	0.97	2051.0	13.1	2390.1	7.1	2691.2	16.7	76.2
SMPABC033	116514	21879	0.35	0.1782	0.002	7.7692	0.06	0.3157	0.002	0.97	1768.9	11.6	2204.6	7.0	2636.4	16.8	67.1
SMPABC032	101651	20364	0.29	0.1907	0.002	12.2015	0.09	0.4634	0.003	0.97	2454.4	15.4	2620.0	7.3	2748.3	16.7	89.3
SMPABC031	123307	22291	0.38	0.1722	0.002	6.8811	0.05	0.2895	0.002	0.97	1638.8	10.8	2096.2	6.9	2578.7	16.9	63.6
SMPABC030	127722	25582	0.26	0.1909	0.002	12.0961	0.09	0.4589	0.003	0.97	2434.6	15.2	2611.9	7.2	2749.8	16.6	88.5
SMPABC028	136278	25880	0.38	0.1804	0.002	7.9419	0.06	0.3188	0.002	0.97	1784.0	11.6	2224.5	6.9	2656.1	16.7	67.2
SMPABC019	115505	21829	0.35	0.1797	0.002	8.7231	0.07	0.3511	0.003	0.97	1940.0	12.5	2309.5	7.0	2650.5	16.8	73.2
SMPABC018	118076	22315	0.27	0.1798	0.002	8.0451	0.06	0.3237	0.002	0.97	1808.0	11.7	2236.1	6.9	2650.9	16.7	68.2
SMPABC017	100911	20846	0.25	0.1971	0.002	14.0354	0.11	0.5150	0.004	0.97	2678.1	16.5	2752.1	7.3	2802.7	16.5	95.6
SMPABC016	121428	23097	0.33	0.1815	0.002	8.8006	0.07	0.3508	0.003	0.97	1938.4	12.5	2317.6	7.0	2666.4	16.7	72.7
SMPABC015	117987	24206	0.28	0.1955	0.002	12.9292	0.10	0.4785	0.004	0.98	2520.7	15.6	2674.5	7.2	2788.6	16.5	90.4
SMPABC014	94046	19445	0.29	0.1969	0.002	13.7296	0.11	0.5043	0.004	0.97	2632.4	16.3	2731.2	7.4	2800.7	16.6	94.0
SMPABC013	87316	17283	0.44	0.1891	0.002	10.3309	0.08	0.3952	0.003	0.96	2147.0	13.8	2464.9	7.3	2734.0	16.8	78.5
SMPABC012	97015	19569	0.28	0.1931	0.002	12.9101	0.10	0.4835	0.004	0.97	2542.3	15.8	2673.1	7.3	2769.0	16.7	91.8
SMPABC011	81802	16856	0.27	0.1969	0.002	13.7502	0.11	0.5051	0.004	0.96	2635.7	16.4	2732.7	7.5	2800.3	16.8	94.1
SMPABC010	125017	23696	0.33	0.1792	0.002	7.9008	0.06	0.3189	0.002	0.95	1784.4	11.8	2219.8	7.1	2645.4	17.1	67.5

[a] Rho is the error correlation defined as the quotient of the propagated errors of the $^{206}Pb/^{238}U$ and the $^{207}Pb/^{235}U$ ratio.
[b] Degree of concordance = ($^{206}Pb/^{238}U$ age * 100/$^{207}Pb/^{206}Pb$ age).

Table 4
Sm-Nd isotopic data of metavolcanic and metaplutonic rocks of the Serra de Santa Rita greenstone belt.

Sample	Nd (ppm)	Sm (ppm)	$^{147}Sm/^{144}Nd$	$^{143}Nd/^{144}Nd \pm 2\sigma$	εNd (0)	t (Ma)	εNd (t)	T_{DM} (Ga)
TF14-XII-178 (Amphibolite)	3.751	17.629	0.1286	0.511418 ± 4	−23.80	2968	+2.26	3.08
PFG-CA-004A (Metadiorite)	7.380	38.469	0.1160	0.511192 ± 4	−28.22	2920	+2.16	3.03
PFG-CA-004E (Metadiorite)	4.654	25.205	0.1116	0.511137 ± 3	−29.27	2920	+2.77	2.99
TF14-XII-183 (Metatonalite)	2.729	14.023	0.1176	0.511164 ± 10	−28.74	2809	−0.15	3.13

Serra de Santa Rita greenstone belts were submitted to at least two thermal-tectonic events under greenschist to amphibolite conditions and to several phases of deformation. Nonetheless, several studies have demonstrated that in Archean volcanic rocks exposed to hydrothermal alteration and to greenschist to amphibolite facies metamorphism, the elements Al, Ti, Fe, P, HFSE (Th, Nb, Ta, Zr and Hf), REE and transition metals (Cr, Ni, Sc, V, Y e Co) are relatively immobile, while the elements Na, K, Ca, LILE (Cs, Rb, Ba e Sr) and Pb tend to be mobile (Hart et al., 1974; Condie et al., 1977; Kerrich and Fryer, 1979; Dostal et al., 1980; Ludden et al., 1982; Murphy and Hynes, 1986; Arndt, 1994; Polat et al., 2002; Polat and Hofmann, 2003). Therefore, in this study the geochemical data discussions are focused mainly on the elements that are relatively immobile during post-magmatic processes.

The ultramafic rocks of the Faina and Serra de Santa Rita greenstone belts are commonly associated with high loss on ignition (LOI = 4–11 wt.%) and four of these samples present pronounced negative Ce anomalies (Ce/Ce* = 0.24–0.77). Samples with Ce/Ce* < 0.9 and Ce/Ce* > 1.1 are considered "highly altered" and present LREE mobility (Polat and Hofmann, 2003). Thus, the ultramafic rocks with strong negative Ce anomalies must have undergone some kind of trace-element mobility. Three amphibolite samples (TF14-XII-015B, PFG-CA-19A e PFG-CA-19B) and one metadiorite sample (TF14-XII-015A) also present Ce/Ce* values lower than 0.9, although the chondrite- and primitive mantle-normalized patterns of these rocks are coherent with the other samples without Ce anomalies on the corresponding geochemical diagrams, therefore, we consider that their geochemical signatures might also be used in the interpretation of their original chemical composition.

The evaluation regarding crustal contamination in the precursor magma of the Faina and Serra de Santa Rita greenstone belts can be assessed on the basis of the pillow lava structures in ultramafic

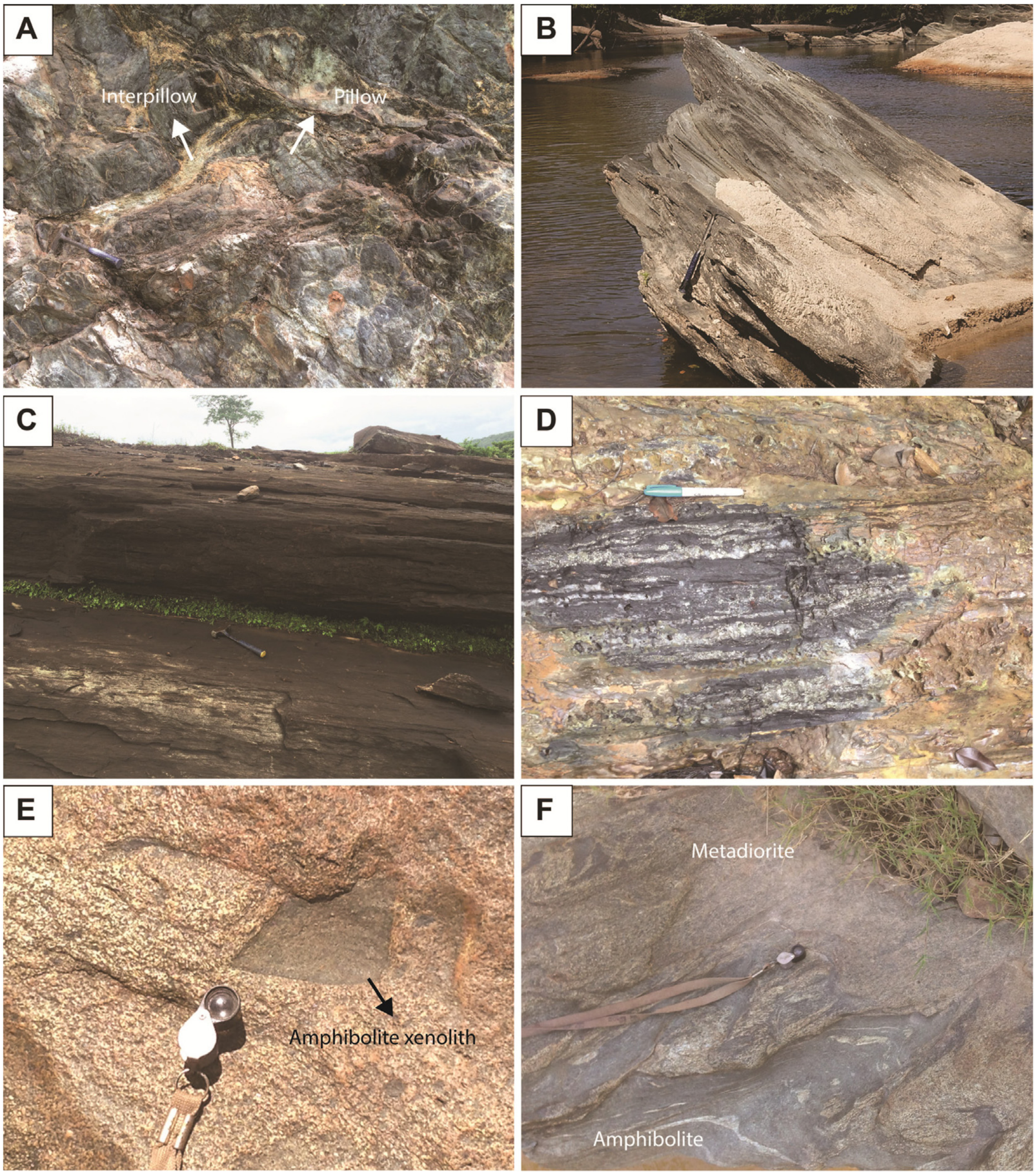

Fig. 3. Field characteristics of metavolcanic and metaplutonic rocks of the Faina and Serra de Santa Rita greenstone belts. (A) Pillow lavas in ultramafic rocks. (B) Foliated amphibolite outcrop. (C) Foliated metandesite outcrop. (D) Intercalation of metachert and carbonaceous schist that are associated with metandesites and metavolcanoclastic rocks. (E) Angular fine-grained amphibolite (metabasalt) xenolith in coarse-grained metadiorite. (F) Highly deformed irregular contact between metadiorite (upper) and amphibotite (lower).

rocks and the spatial association of metachert and carbonaceous schist interlayered with amphibolites and metandesites. Such characteristics are more consistent with an oceanic rather than a continental setting for the volcanism. The positive initial $_{\varepsilon Nd}$ values (+2.16 to +2.77) observed in the amphibolite and metadiorites with magmatic crystallization ages between 2.96 and 2.92 Ga are also not consistent with continental crust interaction in this period. The metatonalite that presented magmatic crystallization age of 2.8 Ga and initial $_{\varepsilon Nd}$ of $-0,15$ indicates that interaction with continental crust might have occurred in this second period.

7.2. Origin of the ultramafic rocks and similarities with boninites

Spinifex textures are well described in metakomatiites of the Crixás greenstone belt, in the northern portion of the Archean-Paleoproterozoic Terrane of Goiás (Sabóia and Teixeira, 1980; Teixeira, 1981; Teixeira et al., 1981; Kuyumjian and Teixeira, 1982), but textures of this kind are not yet recognized in the Faina and Serra de Santa Rita greenstone belts. However, the presence of pillowed structures in ultramafic rocks of the Serra de Santa Rita greenstone belt is extremely important because it indicates the subaqueous volcanic character of these sequences. Therefore, the ultramafic protoliths of the Faina and Serra de Santa Rita greenstone belts are correlated to komatiites.

The komatiites are traditionally divided into two groups: alumina depleted komatiites (ADK) and alumina undepleted komatiites (AUK) (Nestbitt et al., 1979; Arndt, 1994). The ADK are characterized by low Al_2O_3/TiO_2 ($\leq$10), high CaO/Al_2O_3 ($\sim$1.5) and Gd/Yb_{cn} = 1.1–1.7. The AUK have nearly chondritic Al_2O_3/TiO_2 ratios ($\sim$20), CaO/Al_2O_3 ($\sim$1) and flat chondrite-normalized HREE patterns. The ultramafic rocks of the Faina and Serra de Santa Rita greenstone belts are characterized by Al_2O_3/TiO_2 (12.3–44.8), CaO/

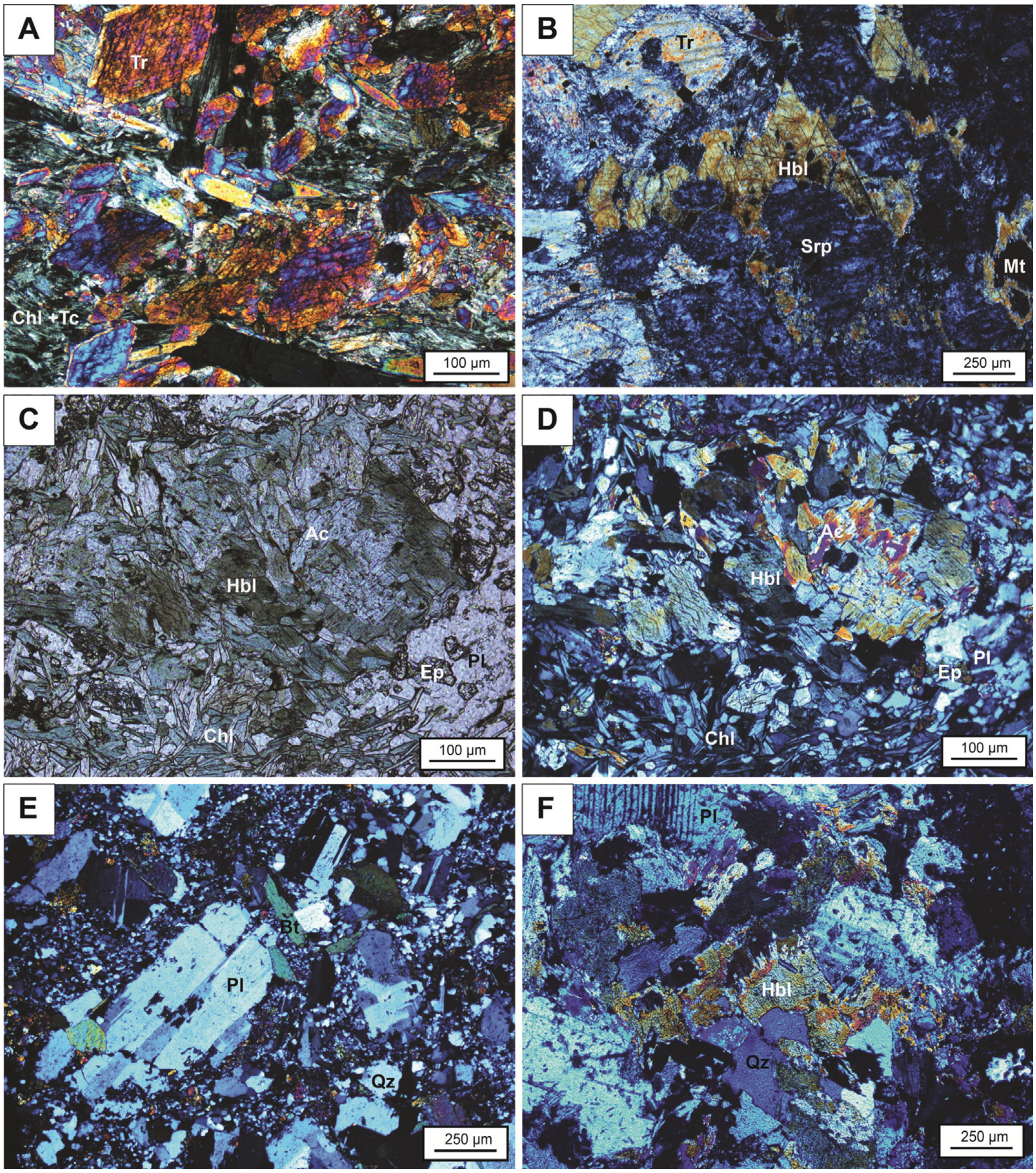

Fig. 4. Photomicrographs of metavolcanic and metaplutonic rocks of the Faina and Serra de Santa Rita greenstone belts. (A) Tremolite porphyroblasts in ultramafic schist composed of tremolite, chlorite and talc. (B) Pseudomorphs of olivine totally serpentinized and encompassed by Mg-hornblende and tremolite. (C-D) Amphibolite composed of Mg-hornblende partially substituted by actinolite and chlorite, and plagioclase replaced by epidote. (E) Metandesite with preserved plagioclase phenocrysts embedded in a fine-grained groundmass of quartz, plagioclase, muscovite and biotite. (F) Metadiorite composed of Mg-hornblende, plagioclase and quartz with original intergranular texture. Crossed polarized light: A, B, D, E and F. Plane polarized light: D. Abbreviations: Ac (actinolite); Chl (chlorite); Ep (epidote); Hbl (hornblende); Mt (magnetite); Pl (plagioclase); Qz (quartz); Tr (tremolite).

Al_2O_3 (0.6–1.1) and Gd/Yb_{cn} (0.7–1.9) ratios quite varied, which hinders their classification into one of the two komatiite groups, although they still present more similarity with AUK. This complexity may be related to different sources for komatiitic lava in the region, but the element mobility due to post-magmatic processes cannot be ruled out.

The origin of komatiites in greenstone belts has been commonly attributed to high-temperature mantle plumes generating a typical tholeiite-komatiite association (*e.g.* Campbell et al., 1989; Herzberg, 1992; Xie et al., 1993; Arndt, 1994; Condie, 1994; Dostal and Mueller, 1997, 2004; Puchtel et al., 1998; Polat, 2009). Nonetheless, studies have also suggested an origin related to subduction zones, in forearc environments, for some Archean komatiites and komatiitic basalts in analogy with Phanerozoic boninites (*e.g.* Barberton *greenstone belt*; Parman et al., 2001, 2004; Parman and Grove, 2004). The boninites are characterized by high SiO_2 (>53 wt.%) and Mg# (>60), and low TiO_2 (<0.5 wt.%) and are exclusive of subduction zones. The boninitic magmas are generated by hydrous melting of a refractory mantle at shallow depths (Crawford et al., 1989). The boninites are normally associated to forearc regions in the initial stages of subduction in intraoceanic arcs (Pearce et al., 1992). According to experimental data, komatiitic magma can also be produced by mantle hydrous melting at relatively low temperatures, between 1500 and 1600 °C. These temperatures are significantly cooler than estimates of mantle temperatures assuming an anhydrous plume origin for komatiites (>1900 °C) (Parman et al., 2001).

The ultramafic rocks of the Faina and Serra de Santa Rita greenstone belts have some chemical characteristics comparable to boninites, such as low TiO_2 (0.1–0.6 wt.%), negative Nb and Ti

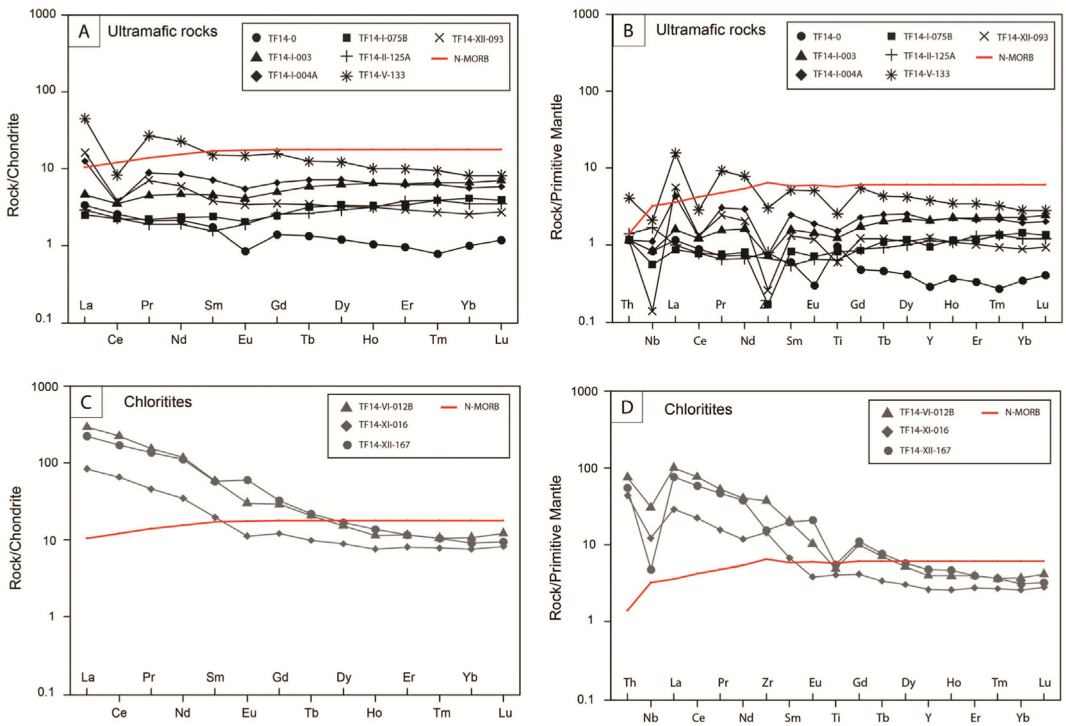

Fig. 5. Chondrite- and primitive mantle-normalized diagrams for ultramafic rocks and chloritites of the Faina and Serra de Santa Rita greenstone belts. (A–B) Ultramafic schists and cumulate-textured rocks. (C-D) Chloritites. Normalization values and N-MORB composition are those of Sun and McDonough (1989).

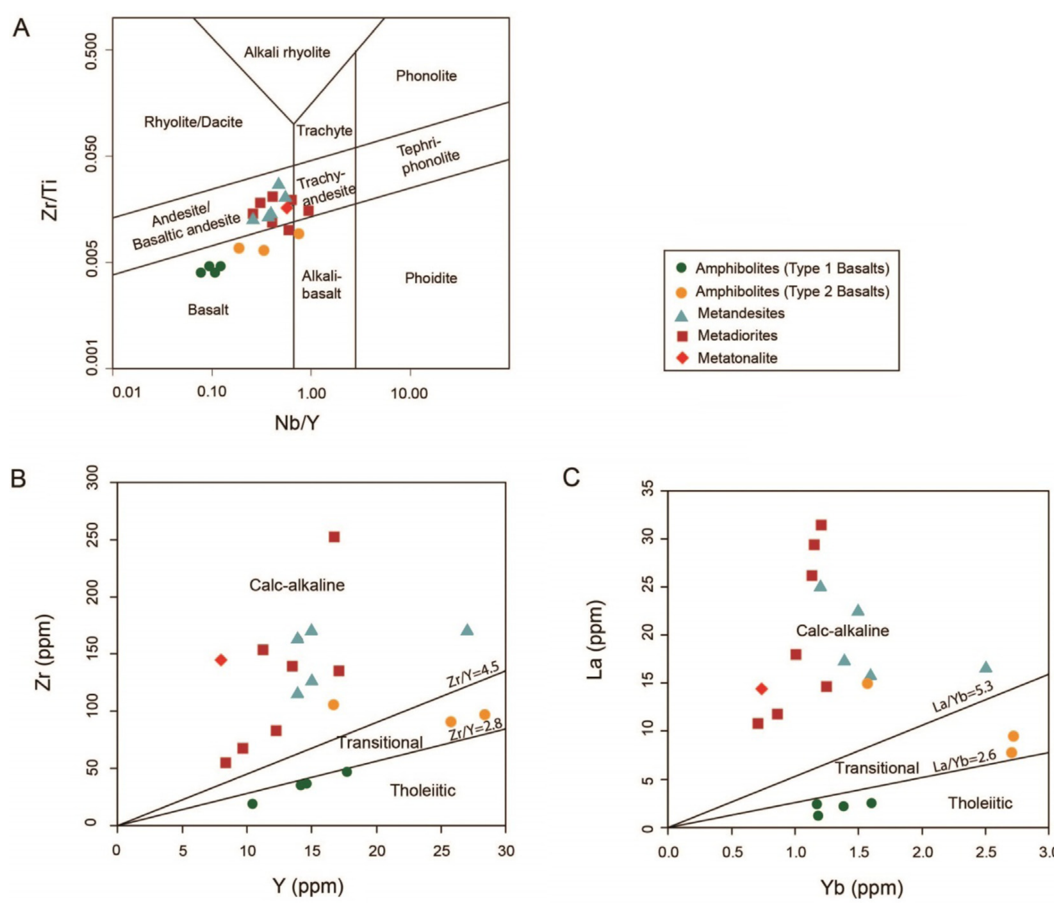

Fig. 6. Classification diagrams for metavolcanic and metaplutonic rocks of the Faina and Serra de Santa Rita greenstone belts. (A) Nb/Y vs. Zr/Ti classification diagram (Winchester and Floyd, 1977). (B–C) Y vs. Zr and Yb vs. La discriminant diagrams of magmatic affinity (Ross and Bédard, 2009).

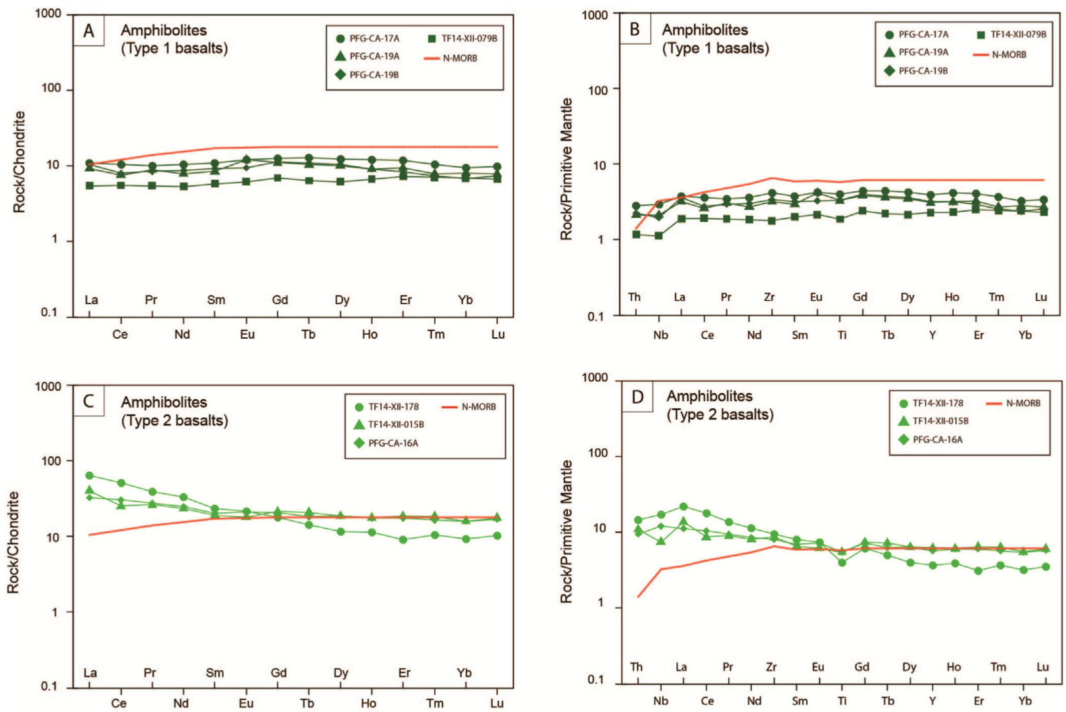

Fig. 7. Chondrite- and primitive mantle-normalized diagrams for amphibolites of the Faina and Serra de Santa Rita greenstone belts. (A–B) Amphibolites of the type 1 basalts group. (C–D) Amphibolites of the type 2 basalts group. Normalization values and N-MORB composition are those of Sun and McDonough (1989).

anomalies observed in some samples (Fig. 5B), and the slightly U-shaped REE patterns, which are observed in two samples (TF14-I-075B and TF14-II-125A) (Fig. 5A). Based on these chemical characteristics and also on the context of the other metavolcanic and metaplutonic rocks associated with the ultramafic rocks of the Faina and Serra de Santa Rita greenstone belts, as will be discussed that are related to subduction zones, we suggest that the komatiites of the Faina and Serra de Santa Rita greenstone belts were generated by hydrous melting of a depleted mantle in a forearc setting, as analogous to boninites. The Mesoarchean high geothermal gradient favored the production of komatiitic magma in these environments.

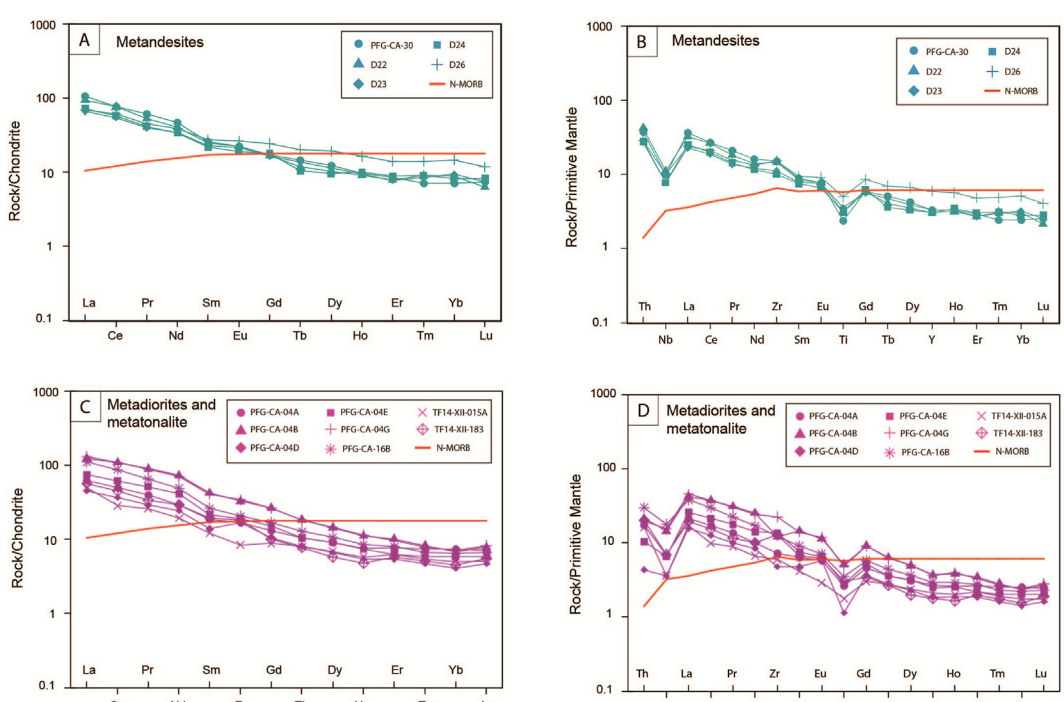

Fig. 8. Chondrite- and primitive mantle-normalized diagrams for metandesites, metadiorites and metatonalites of the Faina and Serra de Santa Rita greenstone belts. (A–B) Metandesites. (C–D) Metadiorites and metatonalites. Normalization values and N-MORB composition are those of Sun and McDonough (1989).

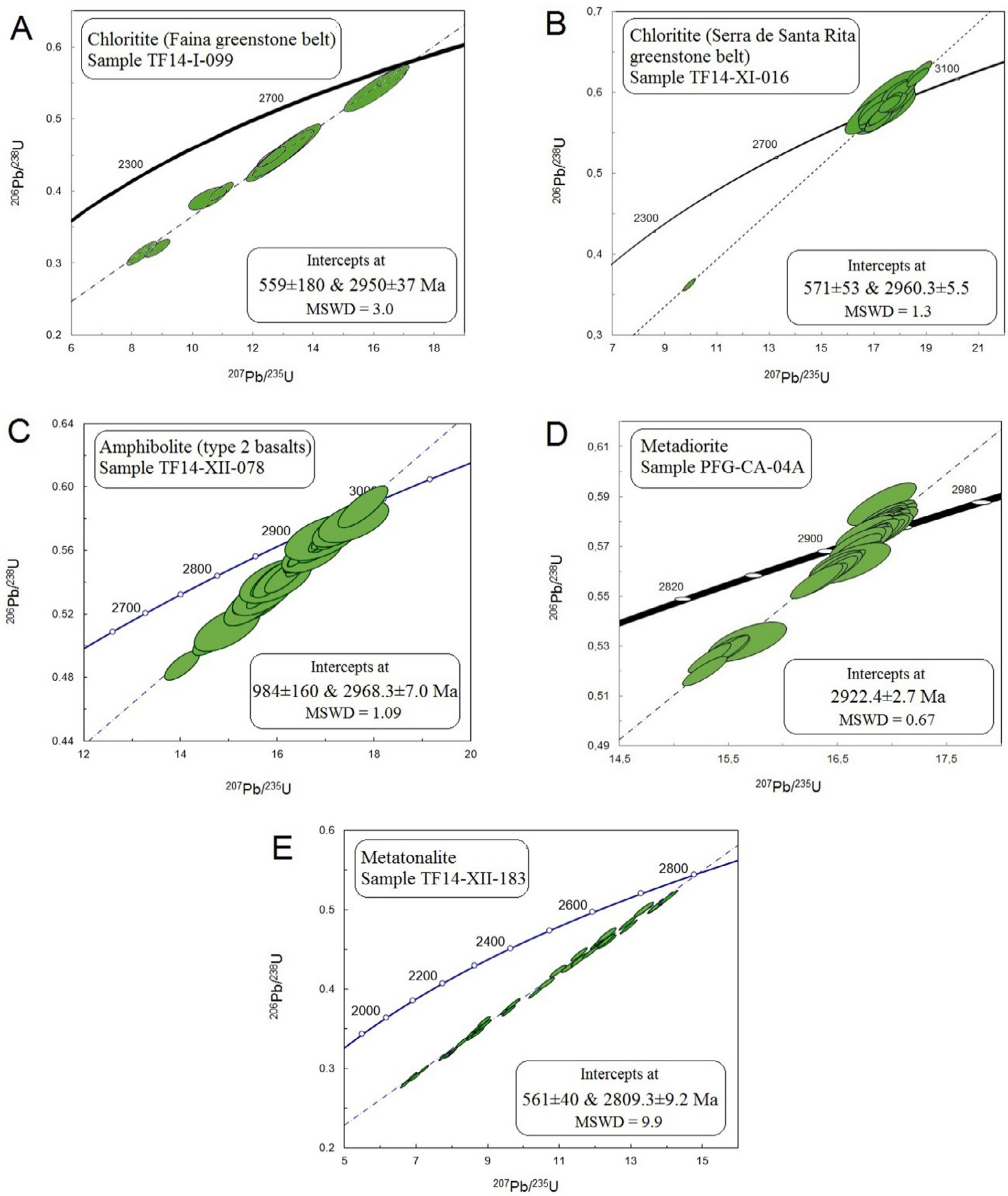

Fig. 9. LA-ICP-MS U-Pb zircon ages of metavolcanic and metaplutonic rocks of the Faina and Serra de Santa Rita greenstone belts. (A) TF14-I-099 (chloritite of the Faina greenstone belt). (B) TF14-XI-016 (chloritite of the Serra de Santa Rita greenstone belt). (C) TF14-XII-178 (amphibolite of the type 2 basalts group). (D) PFG-CA04A (metadiorite) and (E) TF14-XII-183 (metatonalite).

7.3. Origin of the chloritites

The mineralogy and chemical composition of the chloritites indicate that these rocks underwent intense hydrothermal alteration that resulted in the extremely low SiO_2 (31–32 wt.%) and high Al_2O_3 (21–23 wt.%). Even with the high values of loss on ignition (LOI = 11 wt.%), the chloritites do not show Ce anomalies (Ce/Ce* = 0.98–1.06) like some of the Faina and Serra de Santa Rita ultramafic rocks. The chloritites present chemical characteristics characterized by enriched LREE patterns and negative Nb and Ti anomalies, typical features of subduction-related magmas (Perfit et al., 1980; Saunders et al., 1991; Hawkesworth et al., 1993; Pearce and Peate, 1995; Kelemen et al., 2003; Pearce, 2008). At subduction zones, the mantle wedge is metasomatized by slab-derived fluids produced by dehydration of the subducting oceanic crust. These fluids do not transport Nb and Ta (Tatsumi et al., 1986; Tatsumi and Nakamura, 1986), which are concentrated in the subducting slab and gives origin to the Nb and Ta depletion of arc magmas generated by fluid-induced melting of the mantle wedge. The magmas with subduction signature are also enriched in LILE and LREE, while the residual slab is recycled into the mantle (McCulloch and Gamble, 1991). Considering that the trace-element composition of the chloritites can be used to interpret the primary composition of their protoliths, it is likely that those protoliths are subduction-related.

The chloritites are spatially associated to ultramafic schists and cumulate-textured rocks, which may suggest that their protoliths could also be komatiites that were quite submitted to hidrotermal alteration. However, although the ultramafic rocks of the Faina and Serra de Santa Rita greenstone belts are here interpreted as

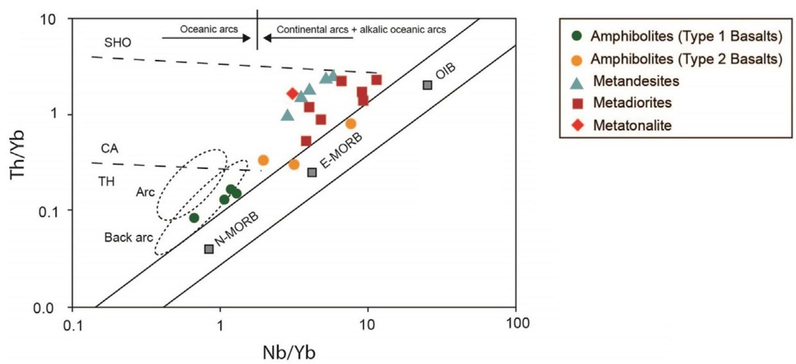

Fig. 10. Nb/Yb vs. Th/Yb discriminant diagram (Pearce, 2008) for metavolcanic and metaplutonic rocks of the Faina and Serra de Santa Rita greenstone belts. Dotted fields represent tholeiitic (TH), calc-alkaline (CA) and shoshonitic (SHO) rocks of convergent margins. Phanerozoic arc and back-arc fields are from Metcalf and Shervais (2008).

komatiites erupted in a forearc setting, similar to modern boninites, the chloritites differ from them by much higher TiO_2 (1.0–1.4 wt.%), P_2O_5 (0.1–0.4 wt.%) and LREE enrichment. On the other hand, the chondrite- and primitive mantle-normalized patterns of the chloritites (Fig. 5C and D) are also similar to the amphibolites (type 2 basalts group) patterns (Fig. 7C and D); and these rocks present geochemical characteristics consistent with subduction zones. Moreover, the two chloritite samples that were dated presented U-Pb zircon ages of 2.96 Ga and 2.95 Ga, similar to the obtained age for the amphibolite sample (2.96 Ga). Thus, it is more likely that the chloritites are also metabasalts that were intensely hydrothermalized and share the same protolith with the amphibolites of the type 2 basalts group.

7.4. Type 1 basalts: back-arc basin basalts (BABB)

The amphibolites corresponding to the type 1 basalts of the Serra de Santa Rita greenstone belt are characterized by tholeiitic magmatic affinity and flat chondrite-normalized REE patterns (Fig. 7A). These characteristics are similar to transitional MORB type basalts (T-MORB), but are also related to Phanerozoic oceanic plateau basalts (OPB) (*e.g.* Mahoney et al., 1995; Kerr et al., 1997) and to Archean intra-oceanic tholeiitic flows (*e.g.* Polat and Kerrich, 2000). Several of the Archean oceanic plateau tholeiitic basalts are interlayered with komatiites in a typical plume-related tholeiite-komatiite association (*e.g.* Campbell et al., 1989; Herzberg, 1992; Xie et al., 1993; Arndt, 1994; Condie, 1994; Dostal and Mueller, 1997, 2004; Puchtel et al., 1998; Polat, 2009). In general, the Phanerozoic OPB are chemically uniform, with La/Sm_{cn} = 0.6–0.7, Ce/Yb_{cn} = 0.8–0.9 and low Zr/Nb (10–16), Zr/Ta (260–275) and La/Ta (15–17) ratios (Floyd, 1989). However, the type 1 basalts of the Serra de Santa Rita greenstone belt are characterized by higher La/Sm_{cn} = 0.9–1.1 and Ce/Yb_{cn} = 0.8–1.2, and different Zr/Nb = 22–27, Zr/Ta = 180–235 and La/Ta = 11–13 ratios than the average values of OPB.

On Nb/Yb vs. Th/Yb diagram, mantle plume-derived intraplate basalts and MORB without relation to subduction zones plot in the MORB-OIB field, while volcanic rocks related to subduction zones and crustal contamination plot obliquely and subparallel to the MORB-OIB field. This indicates addition of Th relatively to Yb by subduction processes or crustal assimilation. On this diagram, the Serra de Santa Rita greenstone belt plot above the MORB-OIB field, in the region of the Phanerozoic back-arc basin basalts (BABB) (Fig. 10). The Nb/Yb ratio of most of the type 1 basalts samples (Nb/Yb = 1.1–1.3) are higher than average for the N-MORB (Nb/Yb = 0.76; Sun and McDonough, 1989), which indicates that the mantle source of these basalts is more enriched in Nb relatively to the N-MORB, but similar to some back-arc basin basalts (*e.g.* Pearce et al., 2005; Khanna et al., 2015).

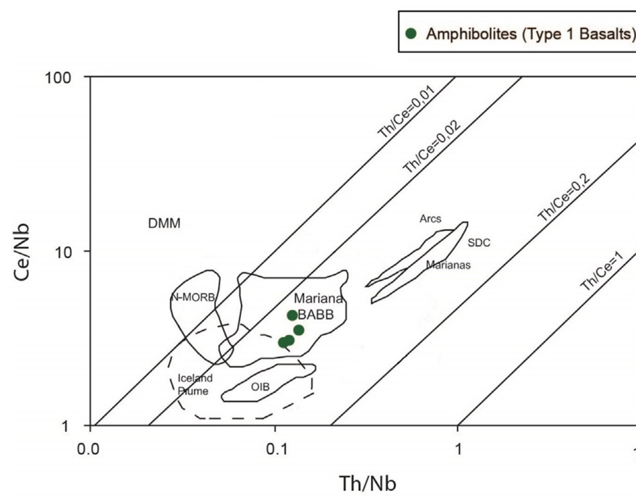

Fig. 11. Th/Nb vs. Ce/Nb discriminat diagram (modified after Saunders et al., 1988 and Khanna et al., 2015) for amphibolites of the type 1 basalts group of the Serra de Santa Rita greenstone belt; these rocks plot in the Phanerozoic Mariana back-arc basalts field (BABB; Pearce et al., 2005). Abbreviations: DMM (depleted MORB mantle component); SDC (subduction zone component).

The discriminant diagram Tb/Nb vs. Ce/Nb (Fig. 11) can be used to test the magmatic source in oceanic basins. In this model, the compositional heterogeneity of basaltic lava flow in oceanic basins is due to the variable mixture of three basic components: (1) a depleted mantle (MORB) with low Th/Nb ratio and high Ce/Nb ratio; (2) a subduction zone component with high Th/Nb and Ce/Nb ratios; and (3) a residual plate component. On this diagram, the type 1 basalts of the Serra de Santa Rita greenstone belt plot between the MORB and arc fields, and in the region where the composition of the Phanerozoic Mariana back-arc basin basalts concentrate (Pearce et al., 2005). Thus, the type 1 basalts of the Serra de Santa Rita greenstone belt have chemical characteristics that are similar to modern back-arc basin basalts (BABB) and are here interpreted as tholeiite flows originated by shallow decompression mantle melting related to the opening of a back-arc basin in the Mesoarchean.

7.5. Type 2 basalts: Nb-enriched basalts (NEB)

The amphibolites corresponding to the type 2 basalts of the Serra de Santa Rita greenstone belt are characterized by subalkaline transitional to calc-alkaline magmatic affinity, enriched chondrite-normalized LREE patterns, slightly negative to positive

Nb anomalies, and negative Ti anomalies (Fig. 7C and D). The LREE enrichment and negative Ti and Nb anomalies are typical features of intraoceanic arc basalts (Perfit et al., 1980; Tatsumi et al., 1986; Tatsumi and Nakamura, 1986; Saunders et al., 1991; Hawkesworth et al., 1993; Pearce and Peate, 1995; Kelemen et al., 2003; Pearce, 2008).

The type 2 basalts are also characterized by high Nb contents (5.3–12.2 ppm), higher than in typical intraoceanic arc basalts (~3 ppm) and comparable to Nb-enriched basalts (NEB; 7 < Nb < 20 ppm; Regan and Gill, 1989; Defant et al., 1992). The NEB were first documented in hot Cenozoic intraoceanic arcs, associated with high-Mg andesites and adakites, characterized by the subduction of young oceanic plate (<20 Ma). Sajona et al. (1996) proposed that the NEB are genetically linked to adakites and were generated by melting of a mantle wedge that had been previously metasomatized by adakitic melt. The adakitic melt originated by oceanic slab melting percolates through the mantle wedge and hybridize with it. In this mantle/melt interaction, the original peridotite mineralogy (olivine, orthopyroxene, clinopyroxene and spinel) is destabilized and substituted by new mineral phases, such as pargasitic amphibole, garnet, phlogopite, Na-clinopyroxene and Fe-orthopyroxene (Carroll and Wyllie, 1989; Johnston and Wyllie, 1989; Adam et al., 1993; Sen and Dunn, 1994; Kepezhinskas et al., 1995; Rapp et al., 1999; Prouteau et al., 2001). Subsequent melting of this Nb-enriched metasomatized mantle generates the NEB magma.

Nb-enriched basalts characterized by LREE enrichment and negative to positive Nb anomalies have been recognized in some Phanerozoic island arc volcanic associations, showing that some volcanic rocks with chemical characteristics similar to ocean island basalts (OIB) can also originate in subduction zones. (Defant et al., 1992; Kepezhinskas et al., 1996; Sajona et al., 1996; Aguillón-Robles et al., 2001; Wang et al., 2007).

On Nb/Yb vs. Th/Yb discriminant diagram, two samples of type 2 basalts of the Serra de Santa Rita greenstone belt plot in the MORB-OIB field, next to E-MORB, but almost in the boundary with the subduction-related volcanic rocks field, and one sample plot in the subduction zone field (Fig. 10). The Nb contents of these rocks are "anomalous" and cause the higher Nb/Yb. On MgO vs. Nb/La (Fig. 12A) and Nb vs. Nb/U (Fig. 12B) diagrams, the type 2 basalts plot consistently in the NEB field. The exception is the TiO_2 vs. P_2O_5 diagram, where the samples share lower TiO_2 and P_2O_5 contents than NEB (Fig. 12C).

In the Serra de Santa Rita greenstone belt, the type 2 basalts are spatially associated with the metandesites and metadiorites that have clear geochemical affinity with magmatic arcs, as enhanced by the Nb/Yb vs. Th/Yb discriminat diagram (Fig. 10). The metandesites and metadiorites also share some similarities with adakites and high-Mg andesites (HMA), respectively, as will be discussed. Thus, these rocks must represent an association between NEB, HMA and adakites. This association has also been recognized in several Archean greenstone belts (*e.g.* Hollings and Kerrich, 2000; Wyman et al., 2000; Polat and Kerrich, 2001; Hollings, 2002; Shchinpasky et al., 2004; Manikyamba and Khanna, 2007; Manikyamba et al., 2007; Kerrich and Manikyamba, 2012), in which petrogenesis has been interpreted as analogous to the modern equivalents, therefore being extremely important for the understanding of the Archean geodynamics.

7.6. Correlations between the metandesites, metadiorites and metatonalies with adakites and high-Mg andesites

As originally defined by Defant and Drummond (1990), adakites are a suite of intermediate to felsic rocks with $SiO_2 \geq 56$ wt.%, $Al_2O_3 \geq 15$ wt.%, high Na_2O contents (Na_2O = 3.5–7.5 wt.%), low K_2O/Na_2O ratio (~0.42), MgO usually < 3 wt.% and high contents of Sr

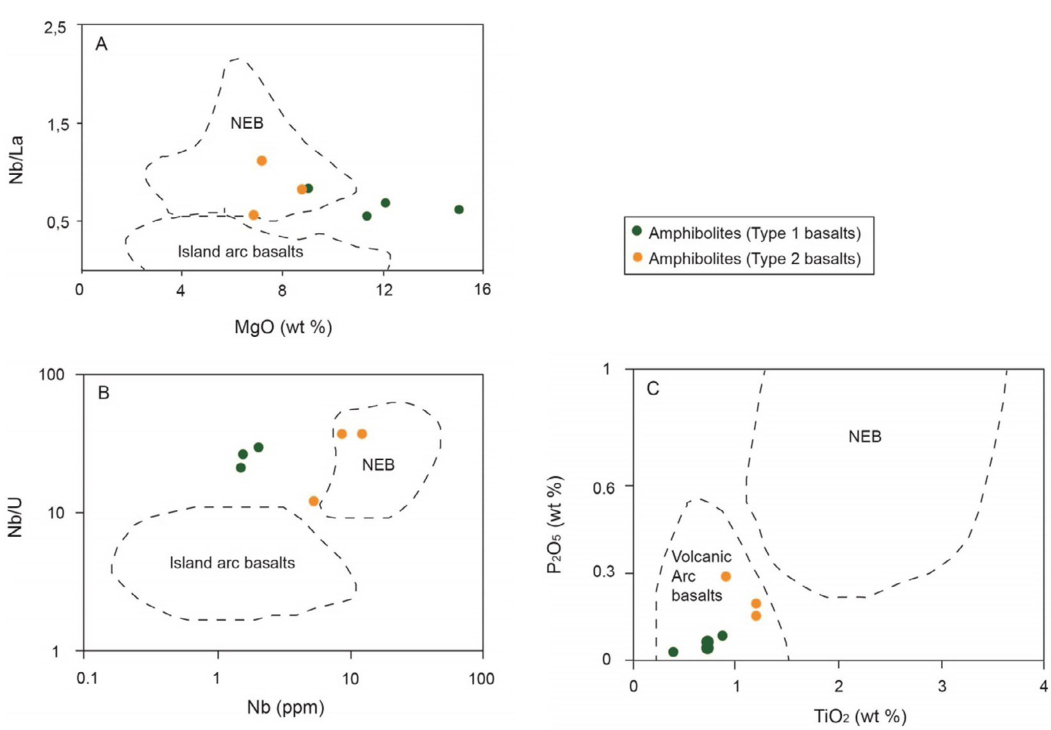

Fig. 12. Discriminant diagrams distinguishing Nb-enriched basalts (NEB) from classical volcanic arc basalts for the amphibolites of the Serra de Santa Rita greenstone belt. (A) Nb vs. Nb/U diagram (Kepezhinskas et al., 1996). (B) MgO vs. Nb/La diagram (Kepezhinskas et al., 1996). (C) TiO_2 vs. P_2O_5 diagram (Defant et al., 1992). The amphibolites of the type 2 basalts group plot in the NEB field on MgO vs. Nb/La and Nb vs. Nb/U diagrams, while on TiO_2 vs. P_2O_5 diagram these rocks plot outside. The amphibolites of the type 1 basalts group plot outside the NEB field on all diagrams.

(≥400 ppm). Adakites are also characterized by strongly fractionated REE patterns ($La/Yb_{cn} > 10$) and low contents of $Y \leq 18$ ppm and $Yb \leq 1.9$ ppm. They were initially introduced as Na-rich volcanic and plutonic rocks formed in Cenozoic magmatic arcs associated with subduction of young (≤25 Ma) and hot oceanic lithosphere. Based on SiO_2 and MgO contents, Martin et al. (2005) divided the adakites into two broad groups: the high-silica adakites (HSA; $SiO_2 > 60$ wt.%, $MgO \leq 4$ wt.% and $Mg\# \leq 50$) and the low silica-adakites (LSA; also referred as high-Mg andesites; $SiO_2 < 60$ wt.%, MgO = 4–9 wt.% and $Mg\# \geq 60$). The LSA are also characterized by higher Sr contents (>1000 ppm) than HSA (<1100 ppm).

The metandesites of the Serra de Santa Rita greenstone belt have fractionated REE patterns (La/Yb_{cn} = 7–15) and low contents of Yb (1.2–1.6 ppm) and Y (14–15). The only exception is one metandesite sample (D26) that exhibits values of La/Yb_{cn}, Yb and Y (5, 2.5 and 27 ppm, respectively) contrasting from the other samples. The metadiorites and the analyzed metatonalite sample have higher REE fractionated patterns (La/Yb = 8–19) and lower contents of Yb (0.7–1.2 ppm) and Y (8–17 ppm) than the metandesites. On Sr/Y vs. Y (Fig. 13A) and $(La/Yb)_{cn}$ vs. Yb_{cn} (Fig. 13B) discriminant diagrams, most of the metandesite, metadiorite and metatonalite samples plot in the adakite field.

The above characteristics show that the metandesites, metadiorites and metatonalites of the Serra de Santa Rita greenstone belt present some of the typical diagnostic features of adakites. However, it is important to point out that adakites are characterized by high Sr contents and related high Sr/Y ratio (>50), which is not observed in the metandesites and metadiorites, in which Sr/Y ratios are lower and quite variable (12–44 for the metandesites and 5–38 ppm for the metadiorites) than those of adakites. The metatonalite sample, otherwise, have very high Sr/Y ratio (114), consistent with adakites. Adakitic magmas with high Sr contents are produced by partial melting of Sr-rich eclogite in a descending slab (as there is no plagioclase in the restite). Fractional crystallization of these magmas at shallower depths could reduce the Sr contents by plagioclase removal (Kamber et al., 2002; Samaniego et al., 2002). Thus, the metandesites, metadiorites and metatonalites of the Serra de Santa Rita greenstone belt are adakite-like rocks that were possibly affected by different degrees of fractional crystallization processes.

The metandesites are characterized by relative high contents of MgO (2–6 wt.%) and Mg# (51–61), values near to those of LSA, otherwise, their SiO_2 contents (56–68 wt.%) show that some of the samples are more consistent with HSA. The metatonalite sample have lower contents of MgO (2 wt.%) and Mg# (42), and higher contents of SiO_2 (66 wt.%), also consistent with HSA. On SiO_2 vs. MgO and SiO_2 vs. Nb diagrams, most of the metandesite samples and the metatonalite sample plot in the HSA field (Fig. 13C and D), and some of the metandesite samples plot in

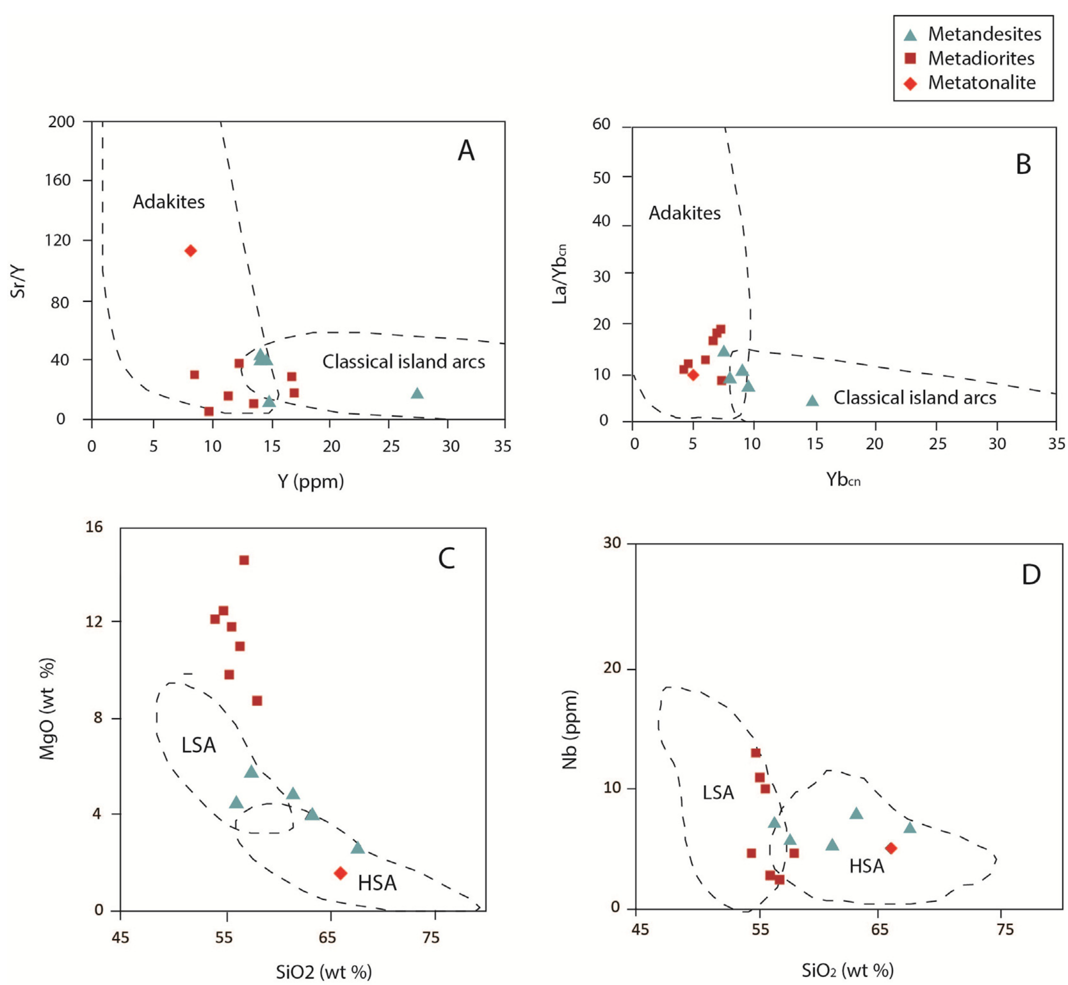

Fig. 13. Discriminant diagrams distinguishing adakites from classical calc-alkaline island arc volcanic rocks (A-B) and high-SiO_2 adakites from low-SiO_2 adakites (C-D) for the metandesites, metadiorites and metatonalites of the Serra de Santa Rita greenstone belt. (A) Y vs. Sr/Y diagram (Defant and Drummond, 1990). (B) Y_{cn} vs. La/Yb_{cn} diagram (Martin, 1987, 1999). (C) SiO_2 vs. MgO diagram (Martin et al., 2005). (D) SiO_2 vs. Nb diagram (Martin et al., 2005). The rocks plot predominantly in the adakite fields on Y vs. Sr/Y and Y_{cn} vs. La/Yb_{cn} diagrams. The metandesites and metatonalite plot predominantly in the HSA fields on SiO_2 vs. MgO and SiO_2 vs. Nb diagrams, while the metadiorites plot in the LSA field on SiO_2 vs. Nb diagram and extrapolates the LSA field on SiO_2 vs. MgO diagram due to their very high MgO contents.

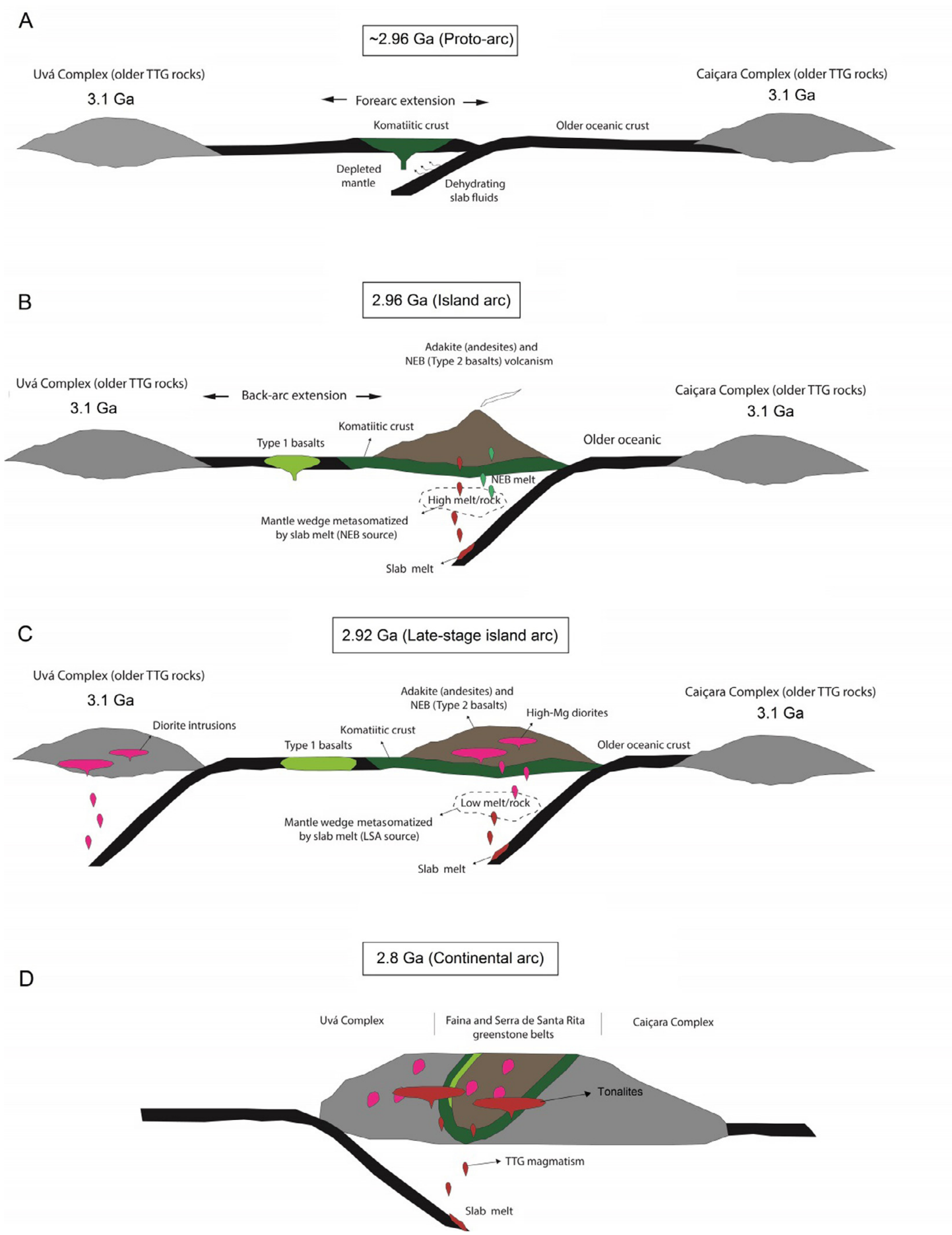

Fig. 14. Geodynamic setting evolution stages proposed for the Faina and Serra de Santa Rita greenstone belts. The volcanic and plutonic rocks are inserted into an island arc evolution at 2.96–2.92 Ga and continental arc at 2.8 Ga. The Uvá and Caiçara complexes are represented by their oldest TTG rocks (~3.1 Ga).

the LSA field on SiO_2 vs. MgO diagram (Fig. 13C). The metadiorites are characterized by very high contents of MgO (9–15%) and Mg# (70–81), and low contents of SiO_2 (54–58 wt.%), being comparable to LSA. All metadiorite samples plot in the LSA field on SiO_2 vs. Nb diagram (Fig. 13D), and extrapolate the LSA field on SiO_2 vs. MgO diagram due to their extremely high MgO contents (Fig. 13C).

Although modern adakites occur in subduction zones that show unusually high heat-flow, which is the case of young oceanic slab subduction, several other mechanisms have also been proposed to account for the origin of specific adakite-like rocks in different tectonic settings. Some of these mechanisms include: crustal assimilation and fractional crystallization from basaltic magmas (*e.g.* Castillo et al., 1999); partial melting of hydrated mafic rocks in the base of thickened crust (*e.g.* Atherton and Petford, 1993; Condie, 2005); and partial melting of delaminated lower crust (Gao et al., 2004; Wang et al., 2006). However, apparently there is no evidence of any older continental crust contamination in the metandesites and metadiorites of the Faina and Serra de Santa Rita greenstone belts. Moreover, the adakites which are generated from crustal melting processes have relatively high K and Th contents (K_2O ~3 wt/% and Th = 10–20 ppm), due to the greater involvement with felsic crustal material (Condie, 2005), which is clearly not the case of the metandesites, metadiorites and metatonalites of the Serra de Santa Rita greenstone belt (K_2O = 0.1–1.4 wt.%; Th = 0.4–3.2 ppm). Thus, these rocks were probably not derived from melting processes of lower thickened crust; and it is more likely that they were produced by partial melting of subducting oceanic slab.

In this subduction-related context, the difference between HSA and LSA is not simply a subtle difference in chemistry or an artefact of classification. Rather, it reflects a fundamental difference in petrogenesis, and specifically in different sources (Martin et al., 2005). The HSA are generated by direct melting of subducted oceanic crust transformed into garnet-bearing amphibolite or eclogite (Defant and Drummond, 1990; Martin, 1999; Gutscher et al., 2000; Martin et al., 2005). Those slab-melts are variably contaminated by peridotite assimilation as they ascend through the mantle wedge (Martin et al., 2005). The LSA (or high-Mg andesites; HMA) are generated in two distinct episodes; complete consumption of slab-melt during melt-peridotite interaction, followed by melting of this metasomatized mantle source (Rapp et al., 1999; Martin et al., 2005). The unifying petrogenetic feature of the HSA and LSA magmas is that both are directly or indirectly linked to slab-melts (Martin et al., 2005).

The adakitic melt not only assimilates the peridotite during its ascent, but also hybridize with the mantle wedge, being progressively consumed. When the melt/rock (adakitic melt/peridotite) is high, not all adakitic melt is consumed during the mantle metasomatism, and the melt can erupt as adakitic lavas. When the melt/rock is low, all adakitic melt is consumed in the metasomatic reaction with the mantle. Melting of this metasomatized mantle also produces magma that preserves strong adakite-like signatures (Rapp et al., 1999).

The metandesites and metatonalites of the Serra de Santa Rita greenstone belt have more similarities with HSA and, attributing a similar petrogenesis, these rocks may represent melting of subducting oceanic slab that variably interacted with the mantle during its ascent, thus explaining the MgO, Cr and Ni enrichment in the metandesites. The metadiorites are more similar to LSA or high-Mg andesites, although these rocks have lower Sr (167–616 ppm) than the common high Sr contents of LSA (>1000 ppm). The high contents of MgO, Cr and Ni of the metadiorites indicate presumably that these magmas were in equilibrium with the peridotite mantle (Tatsumi and Ishizaka, 1982; Yogodzinski et al., 1994). The origin of these magmas is interpreted as melting of mantle wedge that was previously metasomatized by adakitic melt, similar to the petrogenesis assigned to LSA.

8. Geodynamic setting

Discussions of the presented data indicate that the protoliths of the metavolcanic and metaplutonic rocks of the Faina and Serra de Santa Rita greenstone belts are related to subduction zones. The komatiites, basalts, andesites and diorites constitute a Mesoarchean intraoceanic forearc-arc-back-arc assembly, formed between 2.96 and 2.92 Ga. These ages were obtained by U-Pb zircon dating of the amphibolite (type 2 basalts group) and chloritite samples (2.96 Ga), and the metadiorite sample (2.92 Ga). Positive and homogeneous values of initial $_{\varepsilon Nd}$ (+2.16 to +2.77) suggest that these rocks were derived from a juvenile arc. The system later progressed to a continental arc setting with tonalitic magmatism at around 2.8 Ga. This age was obtained by U-Pb zircon dating of the metatonalite sample that presented slightly negative initial $_{\varepsilon Nd}$ of −0.15, indicating a crustal contribution to this magmatism.

Therefore, the evolution model of the Faina and Serra de Santa Rita greenstone belts' igneous protoliths proposed in this study is summarized in four main stages:

1. The initial stage is represented by ultramafic volcanism in a forearc setting under shallow hydrous high melting degrees of the refractory mantle in the early stages of an island arc formation, at around 2.96 Ga (Fig. 14A);
2. The subduction progression led to subducting slab melting and adakite production. The high-SiO_2 adakitic melt hybridized with the peridotite mantle during its ascent, variably increasing the MgO, Cr and Ni contents; the high melt/rock ratio allowed the magma to reach the surface as adakitic lavas that are now represented by the metandesites of the Serra de Santa Rita greenstone belt. Melting of the residual mantle that was previously metasomatized by adakitic melt led to Nb-enriched basalts formation, that are now represented by the amphibolites of the type 2 basalts group of the Serra de Santa Rita greenstone belt. Decompression mantle melting in the back-arc region led to the generation of tholeiitic basalt flows that are now represented by the amphibolites of the type 1 basalts group of the Serra de Santa Rita greenstone belt (Fig. 14B);
3. The low melt/rock ratio, at around 2.92 Ga, led to the consumption of all adakitic melt by the peridotite mantle in the metasomatic reaction. Melting of this hybridized mantle, that preserves the chemical imprint of the slab-melt, generated high-Mg andesitic magma with very high contents of MgO, Cr and Ni, comparable to low-SiO_2 adakites or high-Mg andesites. The magma did not reach the surface as new andesitic lava flows, and lodged as dioritic plutons that intruded the volcanic sequences (Fig. 14C);
4. The final stage, at around 2.8 Ga, is related to the generation of tonalitic magma in a continental arc setting in the late Mesoarchean and early Neoarchean. This stage corresponds to the initial agglutination and cratonization of the Archean substrate of the southern portion of the Archean-Paleoproterozoic Terrane of Goiás and is also recorded in the Caiçara and Uvá complexes by TTG magmatism with ages at around 2.8 Ga (Jost et al., 2005, 2013; Beghelli Junior, 2012) (Fig. 14D).

9. Conclusions

The petrographic, geochemical and isotopic studies of the metavolcanic and metaplutonic rocks of the Faina and Serra de Santa Rita greenstone belts presented in this study allowed the following conclusions:

1. The basal metavolcanic sequences of the Faina and Serra de Santa Rita greenstone belts are composed mainly of ultramafic rocks. The mafic rocks correspond to amphibolites restricted to the Serra de Santa Rita greenstone belt and are associated with metandesite lenses and dioritic to tonalitic poly-deformed intrusions. These rocks were metamorphosed under amphibolite facies and are overlain by Paleoproterozoic metasedimentary sequences metamorphosed under greenschist facies;
2. The geochemical signatures of the ultramafic rocks have some similarities with boninites. The amphibolites can be divided into two groups based on their trace-element behavior: type 1 basalts and type 2 basalts. The type 1 basalts are similar to back-arc basin basalts, while the type 2 basalts are similar to Nb-enriched basalts. The metandesites, metadiorites and metatonalites are adakite-like rocks; the metandesites and metatonalites have some similarities with high-SiO_2 adakites, while the metadiorites are characterized by very high MgO, Cr and Ni contents, being similar to low-silica adakites or high-Mg andesites. The association between adakites, high-Mg andesites and Nb-enriched basalts occur in some hot Cenozoic subduction zones and is also described in several Archean greenstone belts;
3. The chloritites are spatially associated to the ultramafic schist and cumulate-textured rocks but they have different geochemical signatures from them. On the other hand, the trace-elements features and U-Pb zircon ages of the chloritites are

more consistent with the amphibolites of the type 2 basalts group. Thus, these rocks are probably metabasalts that were strongly hydrothermalized;

4. LA-ICP-MS U-Pb zircon dating were conducted in five samples: a chloritite of the Faina greenstone belt, a chloritite of the Serra de Santa Rita greenstone belt, an amphibolite of the type 2 basalts group, a metadiorite and a metatonalite. With the exception of the chloritite of the Serra de Santa Rita greenstone belt sample, the zircon crystals data of all dated samples provided discordia diagrams and ages defined by upper intercepts. The chloritite sample from the Faina greenstone belt yielded the age of 2950 ± 37 Ma. The chloritite sample from the Serra de Santa Rita greenstone belt yielded the concordant age of 2960.3 ± 6 Ma. The amphibolite sample yielded the age of 2968.3 ± 7 Ma. The metadiorite sample yielded the age of 2922.8 ± 3 Ma. The metatonalite sample yielded the age of 2809.3 ± 9.2 Ma. These results are interpreted as the best approximations of the protoliths' crystallization ages and mark two main periods of igneous activity: 2.96–2.92 Ga and 2.8 Ga;
5. Isotopic Sm-Nd analyses were carried out in four samples: an amphibolite of the type 2 basalts group, two metadiorites and a metatonalite. The amphibolite presented T_{DM} of 3.08 Ga and initial $_{\varepsilon Nd}$ of +2.26. The metadiorites presented T_{DM} of 3.03 and 2.99 Ga, and initial $_{\varepsilon Nd}$ of +2.16 and +2.77. These data indicate juvenile magmatic signatures and absence of older sialic crust contamination for the rocks crystallized in the first period (2.96–2.92 Ga). The metatonalite sample crystallized at 2.8 Ga shows T_{DM} of 3.13 Ga and initial $_{\varepsilon Nd}$ of -0.15, indicanting crustal contribution in this second period;
6. The geodynamic model for the volcanic and plutonic protoliths that constitute the Faina and Serra de Santa Rita greenstone belts is inserted into an intraoceanic forearc-arc-back-arc setting. The initial stage corresponds to eruption of ultramafic lavas in the forearc region of a proto-island arc, at around 2.96 Ga. The evolution of the island arc and subduction progression led to oceanic slab-melting and generation of adakites (metandesites of the Serra de Santa Rita greenstone belt). Melting of the enriched residual mantle that was metasomatized with adakitic melt generated Nb-enriched basalts (amphibolites of the type 2 basalts group of the Serra de Santa Rita greenstone belt). Decompression mantle melting at the back-arc region generated tholeiitic basaltic flows (amphibolites of the type 1 basalts group of the Serra de Santa Rita greenstone belt). At around 2.92, the adakitic melt was totally consumed by peridotite mantle and the subsequent melting of these hybridized mantle wedge generated high-Mg andesites that lodged in the crust as dioritic intrusions with very high contents of MgO, Cr and Ni (metadiorites of the Serra de Santa Rita greenstone belt). The late stage corresponds to a continental arc formation at around 2.8 Ga, marked by tonalitic magmatism and amalgamation with other island arcs and continental arcs that constitute the TTG Uvá and Caiçara complexes to form the Archean substrate of the southern portion of the Archean-Paleoproterozoic Terrane of Goiás.

Acknowledgements

The authors acknowledge the support from the staff of the geochronology laboratories of the Universidade de Brasília and Universidade Federal de Ouro Preto. We are grateful to Prof. Guochun Zhao and Dr. Wilson Teixeira for the editorial handling of the manuscript. We sincerely thank two anonymous reviewers for their constructive comments and suggestions. A.M. Silva and F. Chemale Jr thank Conselho Nacional de Desenvolvimento Científico e Tecnológico-CNPq for their respective research grants. This work has been carried out from funds of CNPq (Project No. 474336/2013-1).

References

Adam, J., Green, T.H., Sie, S.H., 1993. Proton microprobe determined partitioning of Rb, Sr, Ba, Y, Zr, Nb and Ta between experimentally produced amphiboles and silicicate melts with variable F content. Chem. Geol. 109, 29–49.

Aguillón-Robles, A., Calmus, T., Benoit, M., Bellon, H., Maury, R.C., Cotton, J., Bourgois, J., Michard, F., 2001. Late Miocene adakites and Nb-enriched basalts from Vizcaino Peninsula, Mexico: indicators of East Pacific Rise subduction below Southern Baja California? Geology 29, 531–534.

Almeida, F.F.M., Hasui, Y., Brito Neves, B.B., Fuck, R.A., 1981. Brazilian structural provinces: an introduction. Earth Sci. Rev. 17 (1), 1–29.

Anhaeusser, C.R., 2014. Archaean greenstone belts and associated granitic rocks - A review. J. Afr. Earth Sc. 100, 684–732.

Araújo Filho, J.O., 2000. The Pirineus Syhntaxis: an example of the intersection of two Brasiliano foldthrust belts in central Brazil and its implications for the tectonic evolution of western Gondwana. Revista Brasileira de Geociências 30, 144–148.

Arndt, N.T., Lesher, C.M., Barnes, S.-J., 2008. Komatiite. Cambridge University Press. 465 pp. Nature 362, 144–146.

Arndt, N.T., 1994. Archaean komatiites. In: Condie, K.C. (Ed.), Archaean Crustal Evolution. Elsevier, Amsterdam, pp. 11–44.

Atherton, M.O., Petford, N., 1993. Generation of sodium-rich magmas from newly underplated basaltic crust. Nature 362, 144–146.

Baêta Júnior, J.D.A., Oliveira, C. C., Pinheiro, M. M., Andrade, R. S., Camargo, M. A., 2000. Programa Levantamentos Geológicos Básicos do Brasil – Escala 1:100,.000, Folha SD.22-Z-C-V, Goiás. CPRM.

Beghelli Junior, L.P., 2012. Charnockitos e ortognaisses da porção centro-oeste do Bloco Arqueano de Goiás: dados geoquímicos e isotópicos Dissertação de Mestrado. Instituto de Geociências, Universidade de Brasília, p. 87.

Brant, R.A.P., Souza, V.S., Dantas, E.L., Jost, H., Rodrigues, V.G., Carvalho, M.J., Araújo, K.C., 2015. Contribuição ao estudo de proveniência sedimentar com base em dados U-Pb para o greenstone belt de Faina, Goiás. In: SBG, XIV Simpósio de Geologia do Centro-Oeste, Brasília, Anais, pp. 30–33.

Bühn, B., Pimentel, M.M., Matteini, M., Dantas, E., 2009. High spatial resolution analysis of Pb and U isotopes for geochronology by laser ablation multi-collector inductively coupled plasma mass spectrometry (LA-MC-ICP-MS). Anais da Academia Brasileira de Ciências 81 (1), 99–114.

Campbell, I.H., Griffiths, R.W., Hill, R.L., 1989. Melting in an Archaean mantle plume: heads it's basalts, tails it's komatiites. Nature 369, 697–699.

Carroll, M.R., Wyllie, P.J., 1989. Experimental phase relations in the system tonalite-peridotite-H_2O at 15 kb: implications for assimilation and differentiation processes near the crust-mantle boundary. J. Petrol. 30, 1351–1382.

Carvalho, M.J., Rodrigues, V.G., Jost, H., 2013. Formação Arraial Dantas: Depósito aurífero detrítico glacígeno do greenstone belt de Faina, Goiás. In: UFRGS, Simpósio Brasileiro de Metalogenia, 3, Gramado.

Castillo, P.R., Janney, P.E., Solidum, R.U., 1999. Petrology and geochemistry of Camiguin island, southern Philippines: insights to the source of adakites and other lavas in a complex arc setting. Contrib. Mineral. Petrol. 134, 33–51.

Condie, K.C., Viljoen, M.J., Kable, E.J.D., 1977. Effects of alteration on element distributions in Archean tholeiites from the Barberton greenstone belt, South Africa. Contrib. Mineral. Petrol. 64, 75–89.

Condie, K.C., 1994. Greenstones through time. In: Condie, K.C. (Ed.), Archean Crustal Evolution. Elsevier, Amsterdam, pp. 85–121.

Condie, K.C., 2005. TTGs and adakites: are they both slab melts? Lithos 80, 33–34.

Corrêa da Costa, P.C., 2003. Petrologia, geoquímica e geocronologia dos diques máficos da região de Crixás-Goiás, porção centro-oeste do Estado de Goiás. Tese de Doutorado, Instituto de Geociências, Universidade de São Paulo, p. 151.

Crawford, A.J., Falloon, T.J., Green, D.H., 1989. Classification, petrogenesis and tectonic setting of boninites. In: Crawford, A.J. (Ed.), Boninites. Unwin Hyman, London, pp. 1–49.

Danni, J.C.M., Ribeiro, C.C., 1978. Caracterização Estratigráfica da Sequência Vulcanossedimentar de Pilar de Goiás e de Guarinos, Goiás. In: SBG, Congresso Brasileiro de Geologia, 30, Recife, Anais, vol. 2, pp. 582–596.

Danni, J.C.M., Dardenne, M.A., Fuck, R.A., 1981. Geologia da região da Serra da Santa Rita e Sequência Serra de Cantagalo. In: SBG, Simpósio de Geologia do Centro-Oeste, l, Goiânia, Anais, pp. 265–280.

Danni, J.C.M., Jost, H., Winge, M., Andrade, G.F., 1986. Aspectos da evolução dos terrenos granito-greenstone belt: exemplo da região de Hidrolina, Goiás. In: SBG, Congresso Brasileiro de Geologia, 35, Goiânia, Anais, vol. 2, pp. 570–584.

Defant, M.J., Drummond, M.S., 1990. Derivation of some modern arc magmas by melting of Young subducted lithosphere. Nature 347, 662–665.

Defant, M.J., Jackson, T.E., Drummond, M.S., De Boer, J.Z., Bellon, H., Feigenson, M.D., Maury, R.C., Stewart, R.H., 1992. The geochemistry of young volcanism throughout western Panama and southeastern Costa Rita: an overview. J. Geol. Soc. (London) 149, 569–579.

DellaGiustina, M.E.S., Oliveira, C.G., Pimentel, M., Buhn, B., 2009. Neoproterozoic magmatism and high-grade metamorphism in the Goiás Massif: new LA-MC-ICMPS U-Pb and Sm-Nd data and implications for collisional history of the Brasília Belt. Precambr. Res. 172, 67–79.

Dostal, J., Mueller, W.U., 1997. Komatiite flooding of rifted Archean rhyolite arc complex: geochemical signature and tectonic significance of Stoughton-Roquemaire Group, Abitibi greenstone belt, Canada. J. Geol. 105, 545–563.

Dostal, J., Mueller, W.U., 2004. Komatiite geochemistry. In: Eriksson, P.G., Altermann, W., Nelson, D.R., Mueller, W.U., Catuneamu, O. (Eds.), The Precambrian Earth: Tempos and Events. Elsevier, Amsterdam, pp. 290–298.

Dostal, J., Strong, D.F., Jamieson, R.A., 1980. Trace element mobility in the mylonite zone within the ophiolite aureole, St. Anthony Complex, Newfoundland. Earth Planet. Sci. Lett. 49, 188–192.

Ferreira Filho, C.F., Nilson, A.A., Naldrett, A.J., 1992. The Niquelândia mafic-ultramafic complex, Goiás, Brazil: a contribution to the ophiolite x stratiform controversy based on new geological and structural data. Precambr. Res. 59, 125–143.

Ferreira Filho, C.F., Kamo, S.L., Fuck, R.A., Krogh, T.E., Naldrett, A.J., 1994. Zircon and rutile U/Pb geochronology of the Niquelândia layered mafic and ultramafic intrusion, Brazil: constraints for the timing of magmatism and high grade metamorphism. Precambr. Res. 68 (3–4), 241–255.

Floyd, P.A., 1989. Geochemical features of intraplate oceanic plateau basalts. In: Saunders, A.D., Norry, M.J. (Eds.), Magmatism in the Ocean Basins. Geological Society Special Publications, London, 42, pp. 313–345.

Fortes, P.T.F.O., Pimentel, M.M., Santos, R.V., Junges, S., 2003. Sm-Nd study of the Crixás greenstone belt, Brazil: implications for the age of deposition of the upper sedimentary rocks and associated Au mineralization. J. S. Am. Earth Sci. 16, 503–512.

Fortes, P.T.F.O., 1996. Metalogênese Dos Depósitos Auríferos Mina III, Mina Nova E Mina Inglesa, Greenstone Belt De Crixás. Tese de Doutorado, Instituto de Geociências, Universidade de Brasília, GO, p. 176.

Gao, S., Rudnick, R.L., Yuan, H.L., Liu, X.M., Liu, Y.S., Xu, W.L., Lin, W.L., Ayers, J., Wang, X.C., Wang, Q.H., 2004. Recycling lower continental crust in the North China craton. Nature 432, 892–897.

Gioia, S.M.C.L., Pimentel, M.M., 2000. The Sm-Nd isotopic method in the geochronology laboratory of the University of Brasília. Anais da Academia Brasileira de Ciências 72 (2), 19–245.

Gutscher, M.-A., Spakman, W., Bijwaard, H., Engdahl, E.R., 2000. Geodynamics of flat subduction: seismicity and tomographic constraints from the Andean margin. Tectonics 19 (5), 814–833.

Hart, S.R., Erlank, A.J., Kable, E.J.D., 1974. Sea-floor basalt alteration: some chemical and isotopic effects. Contrib. Miner. Petrol. 44, 219–230.

Hawkesworth, C.J., Gallagher, K., Hergt, J.M., McDetmott, F., 1993. Mantle and slab contributions in arc magmas. Annu. Rev. Earth Planet. Sci. 21, 175–204.

Herzberg, C., 1992. Depth and degree of melting of komatiites. J. Geophys. Res. 97, 4521–4540.

Hollings, P., Kerrich, R., 2000. An Archean arc basalt-Nb-enriched basalt-adakite association: the 2.7 Ga confederation assemblage of the Birch-Uchi greenstone belt, superior province. Contrib. Miner. Petrol. 139, 208–226.

Hollings, P., 2002. Archean Nb-enriched basalts in the northern Superior Province. Lithos 64, 1–14.

Jackson, S.E., Pearsona, N.J., Griffina, W.L., Belousova, E.A., 2004. The application of laser ablation-inductively coupled plasma-mass spectrometry to in situ U-Pb zircon geochronology. Chem. Geol. 211, 47–69.

Johnston, A.D., Wyllie, P.J., 1989. The system tonalite-peridotite-H_2O at 30 kbar, with applications to hybridization in subduction zone magmatism. Contrib. Mineral. Petrol. 102, 257–264.

Jost, H., Oliveira, A.M., 1991. Stratigraphy of the greenstone belts, Crixás region, Goiás, Central Brazil. J. S. Am. Earth Sci. 4, 201–214.

Jost, H., Oliveira, A.M., Vargas, M.C., 1992. Petrography, geochemistry and structural control of trondhjemitic intrusions in greenstone belts of the Crixás region, Central Brazil. In: SBG, Congresso Brasileiro de Geologia, 37, São Paulo, Anais, vol. 1, pp. 43–44.

Jost, H., Pimentel, M.M., Fuck, R.A., Danni, J.C., Heaman, L., 1993. Idade U-Pb do Diorito Posselândia, Hidrolina, Goiás. Revista Brasileira de Geociências 23, 352–355.

Jost, H., Kuyumjian, R.M., Freitas, A.L.S., Costa, A.L.L., Nascimento, C.T.C., Vasconcelos, F.M., Galotti, L., Martins, M.C.A., Carvalho, M.N., Condé, V.C., 1995. Geologia da porção norte do Greenstone Belt de Guarinos, GO. Revista Brasileira de Geociências 25, 51–60.

Jost, H., Fuck, R.A., Dantas, E.L., Rancan, C.C., Rezende, D.B., Santos, E., Portela, J.F., Mattos, L., Chiarini, M.F.N., Oliveira, R.C., Silva, S.E., 2005. Geologia e geocronologia do Complexo Uvá, Bloco Arqueano de Goiás. Revista Brasileira de Geociências 35, 559–572.

Jost, H., Dussin, I.A., Chemale Jr., F., Tassinari, C.C.G., Junges, S., 2008. U-Pb and Sm-Nd constraints for the Paleoproterozoic age of the metasedimentary sequences of the Goiás Archean greenstone belts. South American Symposium on Isotope Geology, 6, San Carlos de Bariloche, Argentina, Proceedings, 4 pp.

Jost, H., Chemale Jr., F., Dussin, I.A., Tassinari, C.C.G., Martins, R., 2010. A U-Pb zircon Paleoproterozoic age for the metasedimentary host rocks and gold mineralization of the Crixás greenstone belt, Goiás, Central Brazil. Ore Geol. Rev. 37, 127–139.

Jost, H., Rodrigues, V.G., Carvalho, N.J., Chemale Jr., F., Marques, J.C., 2012. Estratigráfica e geocronologia do greenstone belt de Guarinos, Goiás. Geologia USP. Série Científica, São Paulo 12 (2), 3–48.

Jost, H., Chemale Jr., F., Fuck, R.A., Dussin, R.A., 2013. Uvá complex, the oldest orthogneisses of the Archean Paleoproterozoic terrane of central Brazil. J. S. Am. Earth Sci. 47, 201–212.

Jost, H., Carvalho, M.J., Rodrigues, V.G., Martins, R., 2014. Metalogênese dos greenstone belts de Goiás. In: Silva, M.G., Neto, M.B.R., Jost, H., Kuyumjian, R. M. (Orgs.), Metalogênese das províncias tectônicas brasileiras, Belo Horizonte, CPRM, pp. 141–168.

Junges, S.L., Dantas, E.L., Pimentel, M.M., Laux, J.H., 2002. Idades U-Pb de granitos sin- a tardi-tectônicos do Arco Magmático de Mara Rosa, Goiás. SBG-Núcleo Nordeste, Congresso Brasileiro de Geologia, vol. 41, João Pessoa, Anais, pp. 312.

Junges, S.L., Pimentel, M.M., Dantas, E.L., Laux, J.H., 2003. New ID-TIMS U-Pb ages in the western portion of the Mara Rosa Arc: two hundred million years of arc building. South American Symposium on Isotope Geology, vol. 4, Salvador, Short Papers 1, pp. 198–201.

Kamber, B.S., Ewart, A., Collersin, K.D., Bruce, M.C., McDonald, G.D., 2002. Fluid-mobile trace element constraints on the role of slab melting and implications for Archean crustal growth models. Contrib. Miner. Petrol. 144, 38–56.

Kelemen, P.B., Hanghøj, K., Greene, A.R., 2003. One View of the Geochemistry of Subduction-Related Magmatic Arcs, with Emphasis on Primitive Andesite and Lower Crust. In: Treatise on Geochemistry, 3. Elsevier, pp. 593–659.

Kepezhinskas, P., Defant, M.J., Drummond, M.S., 1995. Na metasomatism in the island.-arc mantle by slab melt-peridotite interaction: evidence from mantle xenoliths in the North Kamchatka Arc. J. Petrol. 36, 1505–1527.

Kepezhinskas, P., Defant, M.J., Drummond, M.S., 1996. Progressive enrichment of island arc mantle by melt-peridotite interaction inferred from Kamchatka xenoliths. Geochim. Cosmochim. Acta 60, 1217–1229.

Kerr, A.C., Tarney, J., Marriner, G.F., Nivia, A., Saunders, A.D., 1997. The Caribbean-Columbian cretaceous igneous province: the internal anatomy of an oceanic plateau. In: Mahoney, J.J., Coffin, M. (Eds.), Large Igneous Provinces: Continental, Oceanic, and Planetary Flood Volcanism. AGU Geophysical Monographs, vol. 100, pp. 123–144.

Kerrich, R., Fryer, B.J., 1979. Archean precious metal hydrothermal systems Dome Mine, Abitibi greenstone belt. II. REE and oxygen isotope relations. Can. J. Earth Sci. 16, 440–458.

Kerrich, R., Manikyamba, C., 2012. Contemporaneous eruption of Nb-enriched basalts-K-adakites-Na-adakites from the 2.7 Ga Penakacherla terrane: implications for the subduction zone processes and crustal growth in the eastern Dharwar craton. India. Canadian Journal of Earth Sciences 49, 615–636.

Kerrich, R., Wyman, D.A., Fan, J., Bleeker, W., 1998. Boninite series: low-Ti tholeiite associations from the 2.7 Ga Abitibi greenstone belt. Earth Planet. Sci. Lett. 164, 303–316.

Khanna, T.C., Sesha Sai, V.V., Bizimis, M., Krishna, A.K., 2015. Petrogenesis of basalt-high-Mg andesite-adakite in the Neoarchean Veligallu greenstone terrane: Geochemical evidence for a rifted back-arc crust in the eastern Dharwar craton, India. Precambr. Res. 258, 260–277.

Klötzli, U., Klötzli, E., Günes, Z., Košler, J., 2009. Accuracy of Laser Ablation U-Pb Zircon Dating: Results from a Test Using Five Different Reference Zircons. Geostand. Geoanal. Res. 33, 5–15.

Kuyumjian, R.M., Teixeira, N.A., 1982. Um novo tipo de estrutura em lavas ultramáficas: greenstone belt de Crixás, GO. Revista Brasileira de Geociências 12, 572–577.

Laux, J.H., Pimentel, M.M., Dantas, E.L., Armstrong, R., Junges, S.L., 2005. Two neoproterozoic crustal accretion events in the Brasília Belt, central Brazil. J. S. Am. Earth Sci. 18, 183–198.

Ludden, J.N., Gélinas, L., Trudel, P., 1982. Archean metavolcanic from the Rouyn-Noranda district, Abitibi greenstone belt, Québec. 2. Mobility of trace elements and petrogenetic constraints. Can. J. Earth Sci. 19, 2276–2287.

Ludwig, K.R., 2003. User's Manual for Isoplot/Ex Version 3.00-A Geochronology Toolkit for Microsoft Excel, No. 4. Berkeley Geochronological Center Special Publication, p. 70.

Mahoney, J.J., Jones, W.B., Freu, F.A., Salters, V.J.M., Pyle, D.G., Davies, H.L., 1995. Geochemical characteristics of lavas from Broken Ridge, the Naturaliste Plateau and southernmost Kerguielen Plateau: Cretaceous plateau volcanism in the southeast India Ocean. Chem. Geol. 120, 315–345.

Manikyamba, C., Khanna, T.C., 2007. Crustal growth processes as illustrated by the Neoarchaean intraoceanic magmatism from Gadwal greenstone belt, Eastern Dhawar Craton, India. Gondwana Res. 11, 476–491.

Manikyamba, C., Kerrich, R., Khanna, T.C., Subba Rao, D.V., 2007. Geochemistry of adakites and rhyolites from Gadwal greenstone belt, India: implications on their tectonic setting. Can. J. Sci. 44, 1517–1535.

Manikyamba, C., Kerrich, R., Khanna, T.C., Satyanarayanan, M., Krishna, A.K., 2009. Enriched and depleted arc basalts, with high-Mg andesites and adakites: a potential paired arc-backarc of the 2.7 Ga Hutti greenstone terrane, India. Geochim. Cosmochim. Acta 73, 1711–1736.

Martin, H., Smithies, R.H., Rapp, R., Moyen, J.-F., Champion, D., 2005. An overview of adakite, tonalite-trondhjemite-granodiorite (TTG), and sanukitoid: relationships and some implications for crustal evolution. Lithos 79, 1–24.

Martin, H., 1987. Petrogenesis of Archaean trondhjemites, tonalites and granodiorites from eastern Finland: major and trace element geochemistry. J. Petrol. 28 (5), 921–953.

Martin, H., 1999. The adakitic magmas: modern analogues of Archaean granitoids. Lithos 46 (3), 411–429.

McCulloch, M.T., Gamble, A.J., 1991. Geochemical and geodynamical constraints on subduction zone magmatism. Earth Planet. Sci. Lett. 102, 358–374.

Melezhik, V.A., Huhma, H., Condon, D.J., Fallick, A.E., Whitehouse, M.J., 2007. Temporal constraints on the Paleoproterozoic Lomagundi-Jatuli carbon isotopic event. Geology 35, 655.

Metcalf, R.V., Shervais, J.W., 2008. Suprasubduction-zone ophiolite: is there really an ophiolites conundrum? In: Wright, J.E., Shervais, J.W. (Eds.), Ophiolites, Arcs, and Batholiths: A tribute to Cliff Hopson, Geological Society of America Special Paper 438, pp. 191–222.

Middlemost, E.A.K., 1994. Naming materials in magma/igneous rock system. Earth-Sci. Rev. 37, 215–224.

de Moraes, R., Fuck, R.A., 2000. Ultra-high-temperature metamorphism in Central Brazil: the Barro Alto complex. J. Metamorph. Geol. 18 (4), 345–358.
Murphy, J.B., Hynes, A.J., 1986. Contrasting secondary mobility of Ti, P, Zr, Nb and Y in two metabasaltic suites in the Appalachians. Can. J. Earth Sci. 23, 1138–1144.
Nestbitt, R.W., Sun, S.S., Purvis, A.C., 1979. Komatiites: Geochemistry and Genesis. Can. Mineral. 17, 165–186.
Parman, S.W., Grove, T.L., 2004. Petrology and geochemistry of Barberton komatiites and basaltic komatiites: evidences of Archean fore-arc magmatism. In: Kusky, T. M. (Ed.), Precambrian Ophiolites and Related Rocks. Developments in Precambrian Geology, vol. 13, pp. 539–565.
Parman, S.W., Grove, T.L., Dann, J.C., 2001. The production of Barberton komatiites in an Archean subduction zone. Geophys. Res. Lett. 28, 2513–2516.
Parman, S.W., Grove, T.L., Dann, J.C., De Wit, M.J., 2004. A subduction origin for komatiites and cratonic lithospheric mantle. S. Afr. J. Geol. 107, 107–118.
Pearce, J.A., Peate, D.W., 1995. Tectonic implications of the composition of volcanic arc magmas. Annu. Rev. Earth Planet. Sci. 23, 251–285.
Pearce, J.A., Thirlwall, M.F., Ingram, G., Murton, B.J., Arculus, R.J., Van der Laan, S.R., 1992. Isotopic evidence for the origin of boninites and related rocks drilled in the Izu-Bonin (Ogasawara) foreac, Leg 125. In: Fryer, P., Pearce, J.A., Stokking, L. B. et al. Proceedings of the Ocean Drilling Program, Scientific Results 125, 237–261.
Pearce, J.A., Sterm, R.J., Bloomer, S.H., Fryer, P., 2005. Geochemical mapping of the Mariana arc-basin system: implications for the nature and distribution of subduction components. Geochem. Geophys. Geosyst. 6, Q07006. http://dx.doi.org/10.1029/2004GC000895.
Pearce, J.A., 2008. Geochemical fingerprinting of oceanic basalts with applications to ophiolite classification and the search for Archean oceanic crust. Lithos 100, 14–48.
Pearce, J.A., 2014. Geochemical fingerprinting of the Earth's oldest rocks. Geology 42, 175–176. Geological Society of America Special Paper 373, pp. 269–293.
Percival, J.A., Stern, R.A., Rayner, N., 2003. Archean adakites from the Ashuanipi complex, eastern Superior Province, Canada: geochemistry, geochronology, and tectonic significance. Contrib. Mineral. Petrol. 145, 265–280.
Perfit, M.R., Gust, D.A., Bence, A.E., Arculus, R.J., Taylor, S., 1980. Geochemical characteristics of island.-arc basalts: implications of mantle sources. Chem. Geol. 30, 227–256.
Pimentel, M.M., Fuck, R.A., 1992. Neoproterozoic crustal accretion in Central Brazil. Nature 20 (4), 375–379.
Pimentel, M.M., Heaman, L., Fuck, R.A., 1991. U-Pb zircon and sphene geochronology of late Proterozoic volcanic arc rock units from southwestern Goiás, central Brazil. J. S. Am. Earth Sci. 4, 329–339.
Pimentel, M.M., Whitehouse, M.J., Vianna, M.G., Fuck, R.A., Machado, N., 1997. The Mara Rosa arc in the Tocantins Province: further evidence for Neoproterozoic crustal accretion in central Brazil. Precambr. Res. 81, 299–310.
Pimentel, M.M., Fuck, R.A., Jost, H., Ferreira Filho, C.F., Araújo, S.M., 2000. The basement of the Brasilia Fold Belt and Goiás Magmatic Arc. In: Cordani, U.G., Milani, E.J., Thomaz Filho, A., Campos, D.A. (Eds.), Tectonic Evolution of South America, 31st International Geological Congress, pp. 195–230.
Pimentel, M.M., Jost, H., Fuck, R.A., Armstrong, R.A., Dantas, E.L., Potrel, A., 2003. Neoproterozoic anatexis of 2.9 Ga old granitoids in the Goiás-Crixás block, Central Brazil: evidence from new SHRIMP U-Pb data and Sm-Nd isotopes. Geologia 3, 1–12. USP, Série Científica.
Pimentel, M.M., Jost, H., Fuck, R.A., 2004. O embasamento da Faixa Brasília e o Arco Magmático de Goiás. In: Mantesso-Neto, V., Bartorelli, A., Carneiro, C.D.R., Neves, B.B.B. (Eds.), Geologia do Continente Sul-Americano: evolução da obra de Fernando Fávio Marques de Almeida. Beca Produções Culturais Ltda, São Paulo, pp. 356–368.
Piuzana, D., Pimentel, M.M., Fuck, R.A., Armstrong, R., 2003. Neoproterozoic magmatism and high-grade metamorphism in the Brasília Belt, central Brazil: regional implications of SHRIMP U-Pb and Sm-Nd geochronological studies. Precambr. Res. 125, 245–273.
Polat, A., Hofmann, A.W., 2003. Alteration and geochemical patterns in the 3.7–3.8 Ga Isua greenstone belt, West Greenland. Precambr. Res. 126, 197–218.
Polat, A., Kerrich, R., 2000. Archean greenstone magmatism and the continental growth-mantle evolution connection: constraints from Th-U-Nb-LREE systematics of the 2.7 Ga Wawa subprovince, Superior Province, Canada. Earth Planet. Sci. Lett. 175, 41–54.
Polat, A., Kerrich, R., 2001. Magnesian andesites, Nb-enriched basalt-andesites, and adakites from late Archean 2.7 Ga Wawa greenstone belts, Superior Province, Canada: implications for late Archean subduction zone petrogenetic processes. Contrib. Mineral. Petrol. 141, 36–52.
Polat, A., Kerrich, R., 2004. Precambrian arc associations: boninites, adakites, magnesian andesites, and Nb-enriched basalts. In: T.M. Kusky (Ed.), Precambrian Ophiolites and Related Rocks, Amsterdam, pp. 567–597.
Polat, A., Kerrich, R., 2006. Reading the geochemical fingerprints of Archean hot subduction volcanic rocks: evidence for accretion and crustal recycling in a mobile tectonic regime. In: Benn, K., Mareschal, J.C., Condie, K.C. (Eds.), Archean Geodynamics and Environments. AGU Geophysics Monograph Series, 164. Pp. 189–213.
Polat, A., Hofmann, A.W., Rosing, M., 2002. Boninite-like volcanic rocks in the 3.7–3.8 Ga Isua greenstone belt, West Greenland: Geochemical evidence for intra-oceanic subduction zone processes in the early Earth. Chem. Geol. 184, 231–254.
Polat, A., 2009. The geochemistry of Neoarchean (ca. 2700 Ma) tholeiitic basalts, transitional to alcaline basalts, and gabbros, Wawa Subprovince, Canada: Implications for petrogenetic and geodynamic processes. Precambr. Res. 168, 83–105.
Profumo, J.J.L., 1993. Alteração hidrotermal das rochas ultramáficas e máficas do greenstone belt de Goias Velho (GO) Dissertação de Mestrado. Instituto de Geociências, Universidade de Brasília, p. 143.
Prouteau, G., Scaillet, B., Pichavant, M., Maury, R., 2001. Evidence for mantle metasomatism by hydrous silicic melts derived from subducted oceanic crust. Nature 410, 197–200.
Puchtel, I.S., Hofmann, A.W., Mezger, K., Jochum, P.K., Scipansky, A.A., Samsanov, A. V., 1998. Oceanic plateau model for continental crustal growth in the Archean: a case study from the Kostomuksha greenstone belt, NW Baltic Shield. Earth Planet. Sci. Lett. 155, 57–74.
Queiroz, C.L., Jost, H., Silva, L.C., McNaughton, N.J., 2008. U-Pb SHRIMP and Sm-Nd geochronology of granite-gneiss complexes and implications for the evolution of the central Brazil Archean terrain. J. S. Am. Earth Sci. 26, 100–124.
Queiroz, C.L., 2000. Evolução Tectono-Estrutural dos Terrenos Granito-Greenstone Belt de Crixás, Brasil Central. Tese de Doutorado, Instituto de Geociências, Universidade de Brasília, p. 209.
Rapp, R.P., Shimizu, N., Norman, M.D., Applegate, G.S., 1999. Reaction between slab-derived melts and peridotite in the mantle wedge: experimental constraints at 3.8 GPa. Chem. Geol. 160, 335–356.
Regan, M.K., Gill, J.B., 1989. Coexisting calc-alkaline and high-niobium basalts from Turrialba volcano, Costa Rita: implications for residual titanates in arc magma sources. J. Geophys. Res. 94, 4619–4633.
Resende, M.G., Jost, H., 1994. Redefinição da Formação Aimbé, greenstone belt de Guarinos, Goiás, e sua interpretação paleogeográfica e paleotectônica. Boletim de Geociências do Centro-Oeste 17, 49–56.
Resende, M.G., Jost, H., 1995a. Petrogênese de formações ferríferas e metahidrotermalitos da Formação Aimbé, Grupo Guarinos (Arqueano), Goiás. Revista Brasileira de Geociências 25, 41–50.
Resende, L., Jost, H., 1995b. Características estratigráficas e petrográficas da sequência metassedimentar do greenstone belt de Pilar de Goiás. SBG Goiânia. Revista Brasileira de Geociências do Centro-Oeste 18 (1/2), 66–83.
Resende, M.G., Jost, H., Osborne, G.A., Mol, A.G., 1998. Stratigraphy of the Goiás and Faina greenstone belts, Central Brazil: a new proposal. Revista Brasileira de Geologia 28, 77–94.
Resende, M.G., Jost, H., Lima, B.E.M., Teixeira, A.A., 1999. Proveniência e idades-modelo Sm-Nd de rochas siliciclásticas arqueanas dos greenstone belts de Faina e Santa Rita, Goiás. Revista Brasileira de Geologia 29, 281–290.
Rodrigues, V.G., 2011. Geologia do depósito aurífero do Caiamar, greenstone belt de Guarinos: um raro depósito associado a albitito sódico Dissertação de Mestrado. Instituto de Geociências, Universidade de Brasília, Brasília, p. 79.
Ross, P.-S., Bédard, J.H., 2009. Magmatic affinity of modern and ancient subalkaline volcanic rocks determined from trace-element discriminant diagrams. Can. J. Earth Sci. 46, 823–839.
Sabóia, L.A., Teixeira, N.A., 1980. Lavas ultrabásicas da unidade basal do greenstone belt de Crixás, Goiás: uma nova classe de rochas ultrabásicas no Estado de Goiás. Revista Brasileira Geociências 10, 28–42.
Sajona, F.G., Maury, R.C., Bellon, H., Cotton, J., Defant, M.J., 1996. High field strength elements enrichment of Pliocene-Pleistocene island arc basalts, Zamboanga Peninsula, Western Mindanao (Philippines). J. Petrol. 37, 693–726.
Samaniego, P., Martin, H., Robin, C., Monzier, M., 2002. Transition from calc-alkalic to adakitic magmatism at Cayambe volcano, Ecuador: insights into slab melts and mantle wedge interactions. Geology 30, 967–970.
Santos R.V., Oliveira C.G., Souza V.H.V., Carvalho M.J., Andrade T.V., Souza H.G.A. 2008. Correlação isotópica baseada em isótopos de Carbono entre os greenstone belts de Goiás. In: SBG, Congresso Brasileiro de Geologia, 44, Curitiba, Volume de Resumos, p. 52.
Santos, M, M., 2015. Deesenvolvimento de padrões de zircão para geocronologia U-Pb e análises isotópicas de Hf por Laser Abaltion ICP-MS. Dissertação de Mestrado, Universidade Federal de Ouro Preto, 115 p.
Saunders, A.D., Norry, M.J., Tarney, J., 1988. Origin of MORB and chemically-depleted mantle reservoirs: trace element constraints. J. Petrol. (Special Lithosphere Issue), 415–445.
Saunders, A.D., Norry, M.J., Tarney, J., 1991. Fluid influence on the trace element compositions of subduction zone magmas. Philosophical transactions: physical sciences and engineering. R. Soc. London 335, 377–392.
Seer, H.J., Brod, A.J.A., Fuck, R.A., Pimentel, M.M., Boaventura, G.R., Dardenne, M.A., 2001. Grupo Araxá em sua área tipo: um fragmento de crosta oceânica neoproterozóica na Faixa de Dobramentos Brasília. Revista Brasileira de Geociências 31 (3), 385–396.
Sen, C., Dunn, T., 1994. Experimental modal metasomatism of a spinel lherzolite and the production of amphibole-bearing peridotite. Contrib. Mineral. Petrol. 119, 422–432.
Shchinpasky, A.A., Samsonov, A.V., Bibikova, E.V., Babarina, I.I., Konilov, A.N., Slabunov, A.I., Bogina, M.M., 2004. Boninite hosting partial subduction zone ophiolite sequences from the north Karelian greenstone belt, NE Baltic Shield, Russia. In: Kusky, T.M. (Ed.), Precambrian Ophiolites and Related Rocks. Elsevier, Amsterdam, pp. 425–486.
Sláma, J., Košler, J., Condon, D.J., Crowley, J.L., Gerdes, A., Hanchar, J.M., Horstwood, M.S.A., Morris, G.A., Nasdala, L., Norberg, N., Schaltegger, U., Schoene, B., Tubrett, M.N., Whitehouse, M.J., 2008. Plešovice zircon – a new natural reference material for U-Pb and Hf isotopic microanalysis. Chem. Geol. 249, 1–35.
Stacey, J.S., Kramers, J.D., 1975. Approximation of Terrestrial Lead Isotope Evolution by a 2-stage Model. Earth Planet. Sci. Lett. 26 (2), 207–221.

Strieder, A., Nilson, A.A., 1992. Melange Ofiolítica nos Metassedimentos Araxá de Abadiânia (GO) e Implicações Tectônicas Regionais. Revista Brasileira de Geociências 22 (2), 204–215.
Sun, S.S., McDonough, W.F., 1989. Chemical and Isotopic systematics of oceanic basalts, implications for mantle composition and processes. In: Saunders, A.D., Norry, M.J. (Eds.), Magmatism in the Ocean Basins. Geological Society of London Special Publication 42. Blackwell Scientific Publication, UK, pp. 313–345.
Tassinari, C.C.G., Jost, H., Santos, J.C., Nutman, A.P., Bennell, M.R., 2006. Pb and Nd isotope signatures and SHRIMP U-Pb geochronological evidence of paleoproterozoic age for Mina III gold mineralization, Crixás District, Central Brazil. 5th South American Symposium on Isotope Geology, Punta Del Este, Uruguay, Short Papers Volume, pp. 527–529.
Tatsumi, Y., Ishizaka, K., 1982. Magnesian andesite and basalt from Shodo-Shima Island, southwest Japan, and their bearing on the genesis of calc-alkaline andesites. Lithos 15, 161–172.
Tatsumi, Y., Nakamura, N., 1986. Composition of aqueous fluid from serpentinite in the subducted lithosphere. Geochem. J. 20, 191–196.
Tatsumi, Y., Hamilton, D.L., Nesbitt, R.W., 1986. Chemical characteristics of fluid phase released from a subducted lithosphere and origin of arc magmas: evidence from high-pressure experiments and natural rocks. J. Volcanol. Geoth. Res. 29, 293–309.
Taylor, S.R., McLennan, S.M., 1985. The Continental Crust: Its Composition and Evolution. Blackwell, Oxford, p. 312.
Teixeira, N.A., Sabóia, L.A., Ferreira, M.C.B., Teixeira, A.S., Castro, J.H.G., 1981. Estruturas e texturas das lavas ultrabásicas e básicas do greenstone belt de Crixás, Goiás, Brasil. SBG, Núcleo do Centro-Oeste, Boletim Informativo 10, 33–87.
Teixeira, A.S., 1981. Geologia da região de Goiás-Faina. SBG, Simpósio Geologia Centro-Oeste, Atas, Goiânia, pp. 344-360.
Toledo, C.L.B., Silva, A.M. et al., 2014. Trabalho Final de Graduação em Geologia da Universidade de Brasília (Projeto Faina-Goiás): Mapeamento geológico em escala 1:25.000 dos greenstone belts Faina e Serra de Santa Rita.
Ujike, O., Goodwin, A.M., Shibata, T., 2007. Geochemistry and origin of Archean volcanic rocks from the Upper Keewantin assemblage (ca. 2.7 Ga), Lake of the Woods Greenstone Belt, Western Wabigoon Subprovince, Superior Province. Canada. Island Arc 16, 191–207.
Wang, Q., Xu, J.F., Jian, P., Bao, Z.W., Zhao, Z.H., Li, C.F., Xiong, X.L., Ma, J.L., 2006. Petrogenesis of adakitic porphyries in an extensional tectonic setting, Dexing, South China: implications for the genesis of porphyry copper mineralization. J. Petrol. 47, 119–144.
Wang, Q., Wyman, D.A., Xu, J.F., Jian, P., Zhao, Z.H., Li, C.F., Xu, W., Ma, J.L., He, B., 2007. Early Cretaceous adakitic granites in the Northern Dabie Complex, central China: implications for partial melting and delamination of thickened lower crust. Geochim. Cosmochim. Acta 71, 2609–2636.
Wiedenbeck, M., Allé, P., Corfu, F., Griffin, W.L., Meier, M., Oberli, F., Von Quadt, A., Roddick, J.C., Spiegel, W., 1995. Three natural zircon standards for U-Th-Pb, Lu-Hf, trace element and REE analyses. Geostand. Newsl. 19, 1–23.
Winchester, J.A., Floyd, P.A., 1977. Geochemical discrimination of different magma series and their differentiation products using immobile elements. Chem. Geol. 20, 325–343.
Wyman, D.A., Ayer, J.A., Devaney, J.R., 2000. Niobium-enriched basalts from the Wabigoon subprovince, Canada: evidence for adakitic metasomatism above na Archean subduction zone. Earth Planet. Sci. Lett. 179, 21–30.
Xie, Q., Kerrich, R., Fan, J., 1993. HFSE/REE fractionations recorded in the three komatite-basalt sequence, Archean Abititi belt: implications for multiple plume sources and depth. Geochim. Cosmochim. Acta 57, 4111–4118.
Yogodzinski, G.M., Volynets, O.N., Koloskov, A.V., Matvenkov, V.V., 1994. Magnesian andesites and subduction component in a strongly calc-alkaline series at Piip volcano, far western Aleutians. J. Petrol. 35, 163–204.